NTNU
Norwegian University of Science and Technology

Material and Fatigue Life Investigation of a Lead Alloy used as Sheathing in Subsea Power Cables

Gaute Fotland

Abstract

Subsea power cables are used to transport electricity offshore. They consist of several layers, where a lead sheathing is used as the water barrier layer. From reeling and installation, in addition to daily cycles from thermo-mechanical expansion, a subsea power cable is subjected to fatigue, where the lead sheathing is the component failing. Fatigue failure of the lead sheathing could cause complete system failure in a subsea power cable, but still there is no framework for advanced fatigue calculation. It is known that previous fatigue testing of the lead sheathing has provided over-conservative results due to the test specimen geometry used. This thesis was carried out to obtain material characteristics for lead to better understand the failure mechanisms at strain rates from $\dot{\epsilon} = $ 1E-8 s^{-1} to $\dot{\epsilon} = $ 1E-2 s^{-1}. Furthermore an analysis to find the most suitable test specimen geometry for fatigue testing is done. Laboratory experiments have been conducted with a tension test configuration, together with digital image correlation for strain measurement. Numerical simulations have been performed to predict the strain field to decide for the most suitable test specimen geometry. A curved specimen with a short distance between the grips, and interaction between tension and shear forces is found to be favorable. From laboratory testing, it is found that load controlled tests are better when working with lead. Lead is strongly dependent on strain rate, where the stress, in a tension test, decreases with decreasing strain rate. Three different thicknesses of the lead sheathing have been investigated, where a thickness effect has been observed. Furthermore creep is found to strongly affect the material. For the strain rates used in this thesis, there are interaction between creep and fatigue, which causes a severe state in the material. Since creep is temperature dependent, temperature will strongly affect the material behavior. This study will allow for a comparison of different lead alloys, and for less conservative fatigue tests.

Sammendrag

Blydekket brukt som vannbarriere i en undersjøisk strømkabel er utsatt for utmattingsbrudd fra opprulling og installering, i tillegg til daglige svingninger gjennom termisk ekspansjon. Det er kjent at tidligere utmattingstester har gitt konservative resultat på grunn av prøvegeometrien benyttet til testing. Dette studiet ble gjennomført for å erverve mer kunnskap rundt material egenskapene til bly, og for å bedre forstå brudd hva som forårsaker brudd for tøyningshastigheter mellom $\dot{\epsilon}$ = 1E-8 s^{-1} og $\dot{\epsilon}$ = 1E-2 s^{-1}. Videre vil ulike prøvegeometrier bli analysert for å finne den mest passende å bruke til utmattingstesting. Et utmattingsbrudd i blydekket kan forårsake fullstendig svikt i en undersjøisk strømkabel, men fortsatt finnes det ikke noe rammeverk for avanserte beregninger av utmatting. Strekktester har blitt gjennomført i laboratoriet, sammen med "digital image correlation" for å finne tøyningsbildet. Numeriske simuleringer har blitt gjort for å forutsi hvilken prøvegeometri som er mest passende. En kurvet prøvegeometri, med kort avstand mellom grepet og samspill mellom skjær- og strekkrefter er funnet å være bra. Erfaring fra laboratorietesting viser at bly lettest lar seg teste i kraftkontrollerte tester. Tøyningshastighet i en strekktest påvirker belastningen drastisk, hvor en lavere tøyningshastighet gir laverer belastning. Tre ulike tykkelser på blydekket har blitt undersøkt, og en tykkelseseffekt er observert. Testing viste at siging i aller høyeste grad påvirket materialet. For alle tøyningshastighetene brukt i dette studiet er det samspill mellom siging og utmatting, noe som fører til en alvorlig tilstand i materialet. Siging er temperaturavhening, noe som gjør temperatur til en viktig parameter for egenskapene til bly. Dette studiet gjør det mulig å sammenligne ulike blylegeringer, samt at den sørger for at fremtidig utmattingstesting blir mindre konservativ.

Project Desciption

This page is intentionally left blank.

NTNU

Avtale om gjennomføring av masteroppgave

Denne avtalen bekrefter at masteroppgavens tema er godkjent, at et veilederforhold er etablert, og at partene (student, veileder og institutt) er kjent med og har akseptert gjeldende retningslinjer for gjennomføring av masteroppgaven. Avtalen er videre regulert av lovverk, studieforskrift og studieplanen for masterprogrammet.

1. Personopplysninger

Etternavn, fornavn **Fotland, Gaute**	Fødselsdato **01. desember 1989**
E-post **gautefo@stud.ntnu.no**	Telefon **45103394**

2. Institutt og studieprogram

Fakultet **Fakultet for ingeniørvitenskap**	
Institutt **Institutt for maskinteknikk og produksjon**	
Studieprogram **Master i produktutvikling og produksjon**	Studieretning **Produkters integritet**

3. Avtalens varighet

Oppstartsdato **25. januar 2017**	Innleveringsfrist* **21. juni 2017**
Hvis avtale om deltidsstudier, angi prosent:	

* Inkludert 1 uke ekstra p.g.a påske
All veiledning må være gjennomført innenfor avtaleperioden.

4. Arbeidstittel for oppgaven

Low Cycle Fatigue of Alloy for Cable Sheathing

5. Veiledning

Veileder **Odd Magne Akselsen**
Medveiledere: **Antonio Alvaro** (SINTEF Materials and Chemistry), **Bård Nyhus** (SINTEF Materials and Chemistry)

Normert veiledningstid er **25 timer** for 30 studiepoengs (siv.ing) og **50 timer** for 60 studiepoengs (realfag) masteroppgaver.

6. Thematic description

The insulation system of high voltage subsea power cables are kept dry by a metallic water barrier. Both static and dynamic power cables will be subject to cyclic loading whereby fatigue failure of the sheathing will cause complete system failure. The sheathing of static high voltage power cables are normally constructed from lead-based alloys. The objective of this study is to develop fatigue material data of ductile alloys which are most suitable candidates for cable sheathing and overcome the testing constraint with respect to the sheathing in a full cable cross section. The results will be applied to compare different sheathing materials and associated process. Tasks include the evaluation of testing geometry by both 3D FEM modelling and Digital Image Correlation (DIC) method. Different materials and thermo-mechanical histories will be investigated.

7. Andre avtaler

Tilleggsavtale	Ikke aktuelt
Søknad om godkjenninger (REK, NSD)	Ikke aktuelt
Risikovurdering (HMS) gjennomført	Ja

Vedlegg (oversiktsliste)

Risikovurdering

8. Underskrifter

Vilkår	Dato	Underskrifter
Jeg har lest og akseptert gjeldende retningslinjer for masteroppgaven	25/1- 17	*Gaute Fotland* Studenten
Jeg påtar meg ansvaret for veiledning av studenten etter gjeldende retningslinjer	25/1-17	*Odd M Andersen* Veileder
Jeg påtar meg ansvaret for medveiledning av studenten etter gjeldende retningslinjer	25/1-17	*Børel Nyhus* *Antaïo Alvero* Medveiledere
Institutt/Fakultet godkjenner opplegget for masteroppgaven		Fakultet/Institutt

Acknowledgment

First and foremost, I would like to thank the amazing team I got to be a part of at SINTEF. Thanks to: Supervisor Odd Magne Akselsen for your guidance during the work with this thesis. Co-supervisor Antonio Alvaro for constantly pushing me further. Co-supervisor Bård Nyhus for discussing observations, and for lending me some of your great wisdom. Also, thanks to: Vidar Hjelmen, Vidar Osen and Bjørnar Fugløy.

Thanks to Nexans and Audun Johanson for running the project.

With no previous experience in neither DIC nor *eCorr v4.0*, several questions and problems arose during my work with the software. I would like to thank Egil Fagerholt for technical support.

Mor and far, you have always believed in me, and for that I am forever thankful. For all the times I have called home, when going home from school. I am looking forward spend the summer together, where I do not have to sit in front of a computer for too many hours, but have fun outdoors.

Thanks to the proofreaders: Marta Fotland, you are a lyrical wordsmith genius. Leif Tore Larsen, Knut Bjørsvik, Eivind Rørvik and Jarand Nærland.

Jarand, how you have influenced my career is priceless. We have done high school together, served the army "together", bible school together, and you pulled me through though classes at NTNU, as you started two years ahead of me. I am grateful my friend!

A very special thanks to my dear friends in Fader Herons Sønner, Kølla and Lean Green Consulting. It has been an privilege an honor to do university together with you. You guys have done this time to the best of times! I am really looking forward to what is in store for us in the future. The launching of the broAPP prototype during the work with this thesis, has been very inspirational to me. Finally we will all be joining the fellowship of the precious rings. Let us become invincible (error#404 - spell check: invisible)!

Elisabeth, you are my absolute favorite <3, and I am so thankful and blessed that I have written you into my life.

"It is the glory of God to conceal a matter,
But the glory of kings is to search out a matter."
(Proverbs 25:2 NASB)

<div align="right">G.F.</div>

Abbreviations

AOI	=	Area of Interest
DIC	=	Digital Image Correlation
FEM	=	Finite Element Method
SPC	=	Subsea Power Cable
TSG	=	Test Specimen Geometry

Explanation of Symbols

ϵ	=	Strain
$\Delta\epsilon$	=	Strain range
$\dot{\epsilon}$, (sr)	=	Strain rate
$\dot{\epsilon}_{cr} =$	=	Creep rate
$\epsilon_{long-mid}$	=	Average of strain in the longitudinal mid plane
$\epsilon_{ref} =$	=	Reference strain
$\epsilon_{trans-mid}$	=	Average of strain in the transverse mid plan
$\epsilon_{yy} =$	=	Longitudinal strain, normal strain
F	=	Force
ht	=	Hold time
N_f	=	Cycles to failure
R-ratio (R)	=	$\sigma_{min}/\sigma_{max}$
sr, ($\dot{\epsilon}$)	=	Strain Rate
Stroke	=	Displacement of the crosshead in the test machine
σ	=	Stress
t	=	Thickness
T_m	=	Absolute melting temperature

Contents

List of Figures

Introduction

1.1   Background

Subsea Power Cables (SPCs) are used to transport electricity to such as offshore oil platforms and wind power plants. The cables vary in complexity, usually consisting of several layers protecting the conductor in the middle, as illustrated in figure 1.1. Static and dynamic are the two main types of SPCs, where static SPCs are placed on the seabed, while dynamic SPCs are used from the seabed to the installation. The insulation system in the SPCs are kept dry by a metallic water barrier layer, which for static SPCs are normally constructed from lead-based alloys. Nexans is a world leading producer of high voltage SPCs, having modern technology and manufacturing methods. This allows for better control over the thickness and quality of the lead sheathing, which will make the SPCs less expensive, lighter and more environmental friendly [Worzyk, 2009]. Usually a screw extruder is used, or some times a press, to apply a uniform thickness between $2\,\mathrm{mm}$ to $5\,\mathrm{mm}$ for the lead sheathing. Both static and dynamic SPCs will be subjected to cyclic loading, whereby fatigue failure of the water barrier will cause complete system failure. The service lifetime for static SPCs are 50 years, where a significant amount of damage is accumulated from reeling, installation and joining of cables. During service, the SPC undergoes a couple of daily cycles due to thermo-mechanical expansion. A challenge in lifetime modelling is that there is no framework for advanced fatigue calculation for the lead sheathing [Nexans, 2015].
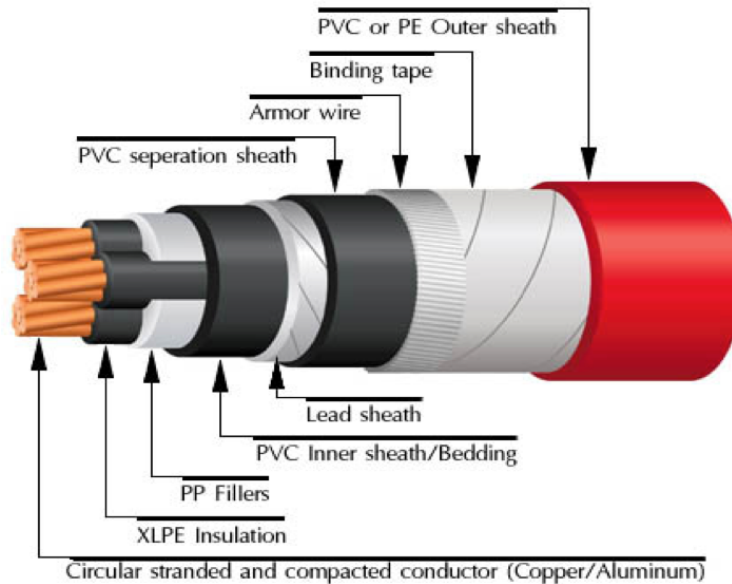
Figure 1.1: Illustration of a subsea power cable with three conductors in the middle and several layers for protection. The lead sheath is acting as the water barrier, [Corporation, 2015].

1.2 Objective

There are two main objectives for this thesis meant to lay the foundation for fatigue analysis of lead sheathings used in static SPCs. The first is to obtain material characteristics of lead since this has only been done to a small extent, and achieve a better understanding of important and controlling parameters such as load time, load level, strain level and strain rate. This will allow for a comparison of different lead alloys. Unfortunately the second alloy was not supplied from customer, and a comparison of alloys will therefore not be included in this thesis. All experiments were conducted at ambient temperature, to reduce the complexity of the test results.

Lead behaves differently than other common engineering metals and is in many ways more comparable to a polymer. This also makes the laboratory testing complex. Due to high ductility and plasticity in lead, Digital Image Correlation (DIC) will be used for strain measurement. The material was supplied as a lead sheathing, see figure 3.6. This put certain limitations to what specimens could be used for testing, which became a hybrid between material and component testing.

The second objective is to evaluate different test specimen geometries (TSGs) and find the one that is best suited to use for fatigue testing and fatigue lifetime estimation for lead alloys. Four different TSGs have been considered. The analysis will be based on numerical simulations in Abaqus. For verification of the numerical simulations the results will be compared with laboratory experiments. Firstly the different specimens will be compared one to one with tension testing. Then a fatigue test will be performed on the best suited TSG. Previous fatigue testing has been conducted on strips which present obvious limitation and has given over-conservative results, which in turn would affect the estimation of the necessary thickness for the lead sheathing.

Theory and Background

2.1 Tension or Three Point Bending Test

A SPC will be subjected to severe strains when reeled up for transportation before installation. Moreover waves and currents can cause high strains during installation. If the SPC is laying on the seabed without being buried, tidal currents can cause strains. In addition the SPC will have daily cycles when operating caused by thermo-mechanical strains, due to the variation in power usage day and night time [Anelli et al., 1988].

When the SPC is reeled up for transportation there will be tension in the top and compression in the bottom. This can be represented as a pipe subjected to bending moment with a linear growing stress over the cross section, illustrated in figure 2.1. Even though there is a linear growing stress over the cross section, the stress will be approximately uniform over the relatively thin lead sheathing. During daily cycles caused by thermo-mechanical strains, the stress is expected to be either as in figure 2.1 or uniform. In both cases the stress field will be uniform in the marked areas displaying the approximate size for the TSG in the lead sheathing, see figure 2.2.
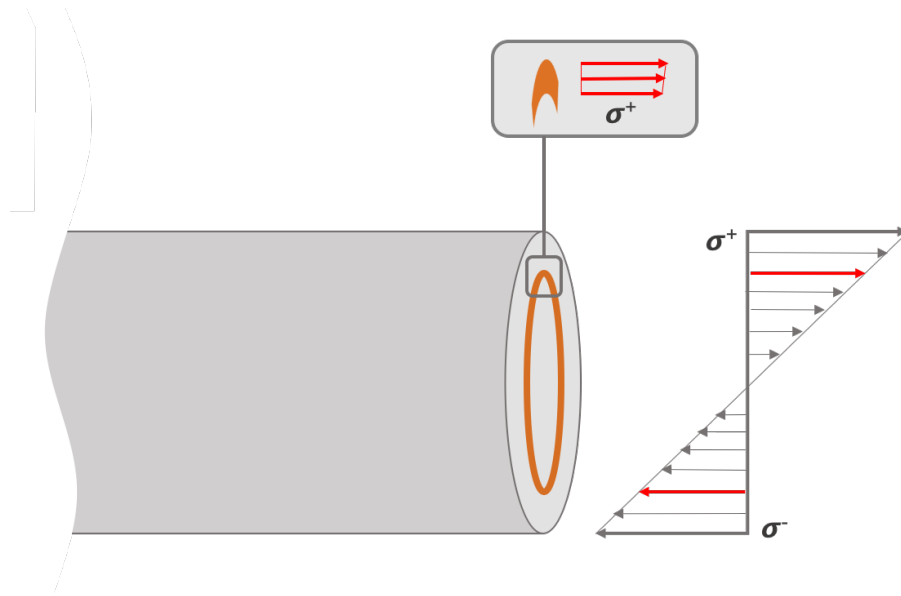
Figure 2.1: A bending moment in a pipe causes tension in top and compression in bottom with a linear growing stress over the cross section, smaller section of the lead sheathing will be subjected to a uniform stress.
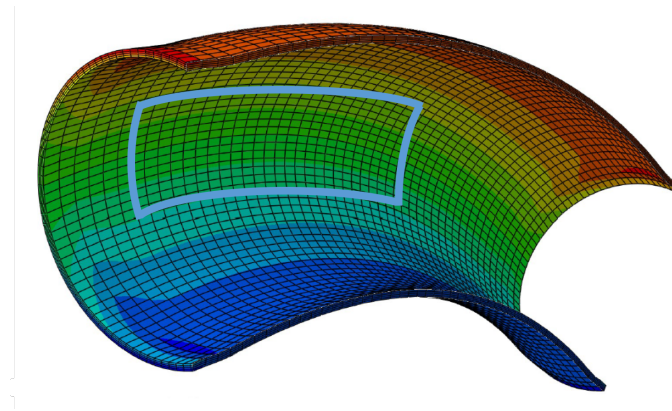
Figure 2.2: The lead sheathing subjected to a bending moment causes tension in top (red) and compression in bottom (blue), marked area displays approximate size for a TSG.

For a small scale test to be accurate, the stress field in the TSG should be similar to the stress field in the SPC during operation. In a three point bending test the stress field in the specimen will be a linear growing moment with opposing maximums in the top and bottom, illustrated in figure 2.3. In a tension test the stress field will be uniform, illustrated in figure 2.4. The stress field is therefore best represented by the tension test, which is the suggested test configuration for small scale fatigue testing of a lead sheathing.
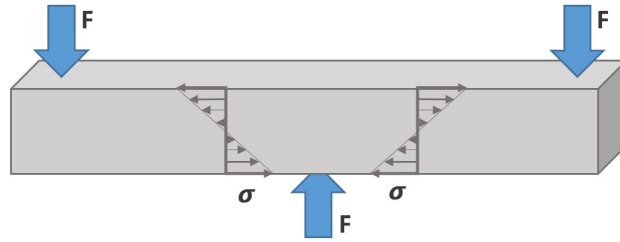
Figure 2.3: A three point bending test causes a linear growing stress over the cross section of the TSG with opposing stress in top and bottom.
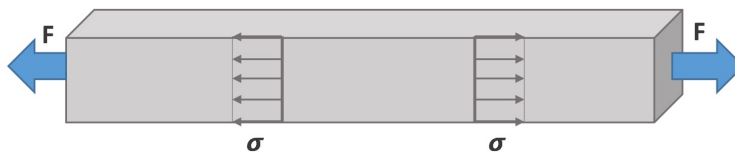
Figure 2.4: A tension test causes a uniform stress field over the cross section of the TSG.

2.2   Stress and Strain

Engineering strain is defined as the deformation normalized by the initial length, see equation (2.1). Measurements from extensometers are defined to be engineering strain. True strain, also known as logarithmic strain, is the exact strain and is calculated based on incremental displacements, see equation (2.2).

$$\epsilon_{eng} = \frac{L_i - L_0}{L_0} = \frac{\Delta L}{L_0} \tag{2.1}$$

$$\epsilon_{true} = \int_{L_0}^{L_i} \frac{1}{L} \, \mathrm{d}L = \ln\left(\frac{L_i}{L_0}\right) = \ln\left(1 + \epsilon_{eng}\right) \tag{2.2}$$

For small deformations the difference between true strain and engineering strain is considered neglectable. This can be seen in figure 2.5 where true strain and engineering strain is plotted against engineering strain. The plot is equal for compression, as in tension. Tension tests in this thesis is run at a strain level where the difference in true and engineering strain is negligible.
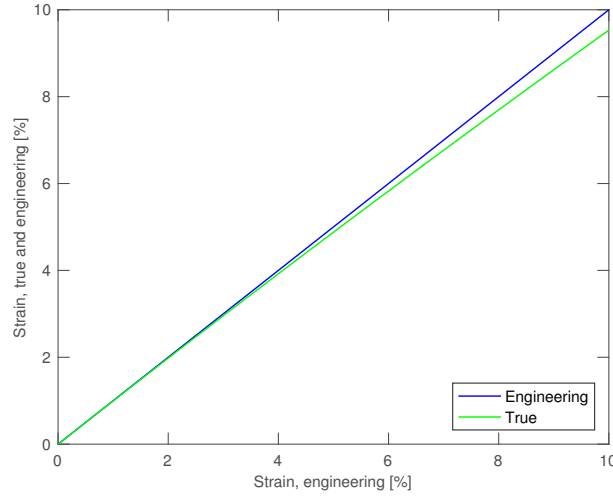
Figure 2.5: True strain and engineering strain compared.

Strain rate is the change in strain with respect to time. In other words, it is the speed the material is deformed by. This is described in equation (2.3).

$$\dot{\epsilon}(t) = \frac{\mathrm{d}\epsilon}{\mathrm{d}t} = sr \tag{2.3}$$

Engineering stress is defined as instantaneous load action on the original cross-sectional area, see equation (2.4). True stress is defined as instantaneous load action on the instantaneous cross-sectional area, see equation (2.5). All stress calculated in this thesis are calculated from the original cross-section area of the specimen, and are therefore engineering stress.

$$\sigma_{eng} = \frac{F}{A_0} \tag{2.4}$$

$$\sigma_{true} = \frac{F}{A_i} \tag{2.5}$$

2.3   Test Specimen Geometries

Many standardized TSGs exist. For low cycle fatigue it is recommended to use a cylindrical specimen, where different kinds of end connections are suggested in "Standard Test Method for Strain-Controlled Fatigue Testing" [AST, 2012]. For fatigue testing of the lead sheathing the TSGs are machined out of the sheathing. This limits the range of geometries that could possibly be obtained, and a cylindrical TSG would be difficult to make. Standardized fatigue testing errors, such as

precracks, can be introduced in the TSG, see figure 2.6.
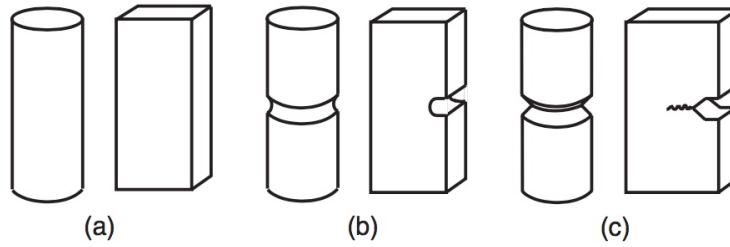
Figure 2.6: Three classes of test specimen: (a) smooth or unnotched, (b) notched, and (c) precracked [Dowling et al., 2013].

If the TSG has a stress raiser, illustrated in figure 2.7, then the stress and the strain will be highest at the edges prior to yielding. The radius of the stress raiser governs the level of stress concentration in the elastic region of the material. When full yielding has taken place for a perfectly plastic material, the whole cross section will be subjected to the same stress.
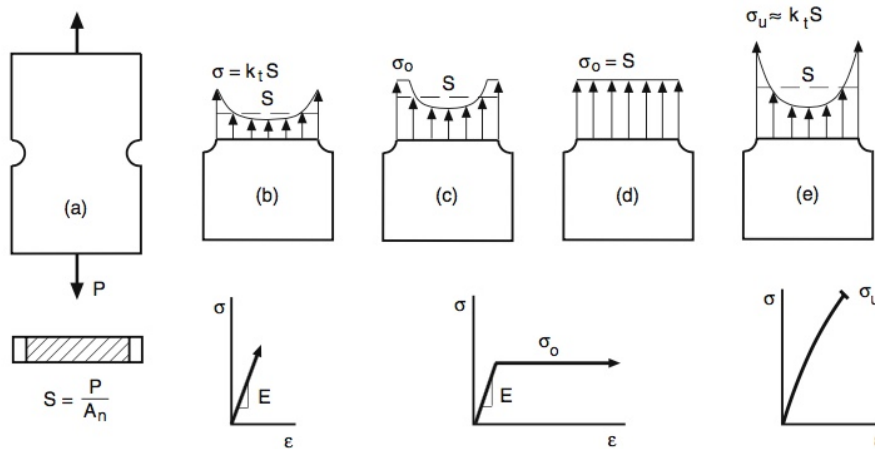
Figure 2.7: (a) Component with a stress raiser and stress distributions for various cases, (b) linear-elastic deformation, (c) local yielding for a ductile material, (d) full yielding for a ductile material, and (e) brittle material at fracture [Dowling et al., 2013].

2.4   DIC - Digital Image Correlation

Several different techniques could be used for strain measurement. From previous tests conducted by Alvaro in [Alvaro, 2016], both extensometers and strain gauges have been used. Alvaro found

extensometers to be insufficient as they introduce strain concentrations where fastened, which initiates cracks in the specimen. Strain gauges are difficult to place correctly, as it is unknown when and where localization can happen in the specimen. DIC (Digital Image Correlation) is another method used for surface deformation and strain measurement. The technique rely on comparing images of the deformation taking place in the object studied, with a reference image where the object is undeformed. DIC is based on image processing and numerical computing. It can measure both in-plane and out-of-plane, respectively 2D and 3D, but not through-thickness deformation.

The specimen that is to be measured by DIC has to be prepared with a white surface with a black and random speckle pattern, as seen in figure 2.8. This so that the computing software can recognize the movement of the speckles and by numerical computing post-processing find the deformation and strain in the specimen. The speckle pattern is commonly made by spray paint, other methods are described in appendix section D. A camera is used to capture deformation, and should be placed with the optical axis normal to the specimen surface, see figure 2.9.

Figure 2.8: Test specimen with speckle pattern sprayed on.

2D-DIC is easier to set up and post-process, but for numerical calculations to be valid in 2D-DIC the specimen must be flat and remain in the same plane parallel to the camera during deformation. Out-of-plane movement will introduce errors with a misconception between the actual displacement the specimen has undergone, and the displacement captured by the camera. For out-of-plane movement 3D-DIC has to be used.

3D-DIC is more demanding than 2D-DIC where two cameras with a stereo set up has to be used, as displayed in figure 2.10. The cameras must be calibrated to create a common virtual 3D mesh. A calibration target with a known pattern, displayed in figure **??**, is used to create individual meshes

that are merged with a common reference point, illustrated in figure 2.11a. Several photos are taken of the calibration target in the area the specimen will be tested, allowing the computing software to calculate where the two cameras are placed according to each other, and to create the virtual 3D-mesh.

For curved specimens it could be difficult to have the whole specimen in focus. The camera lens decides the focal point of the photo, and the focus area will be in this plane. The focal area will have a tolerance distance depth wise, which is known as deep focus or depth of field. The depth of field is increased by having a large aperture (f-number) on the camera lens, which demands sufficient background lights. The images are further post-processed in a numerical computing software. For each test it is suggested to have between a total of 500 to 1,000 images per test. Also it is suggested to have a higher acquisition rate if there are some parts of the test that runs with a different speed.

DIC calculates the true strain, described in section 2.2, by the displacement field. The displacement field is used to find the deformation gradient and the deformation tensor. This allows for the principal strains to be found for the individual elements, and by the use of a rotation matrix the true logarithmic strains in X and Y-direction are found. The full derivation can be found in [Sutton et al., 2009] and [Fagerholt, 2011].
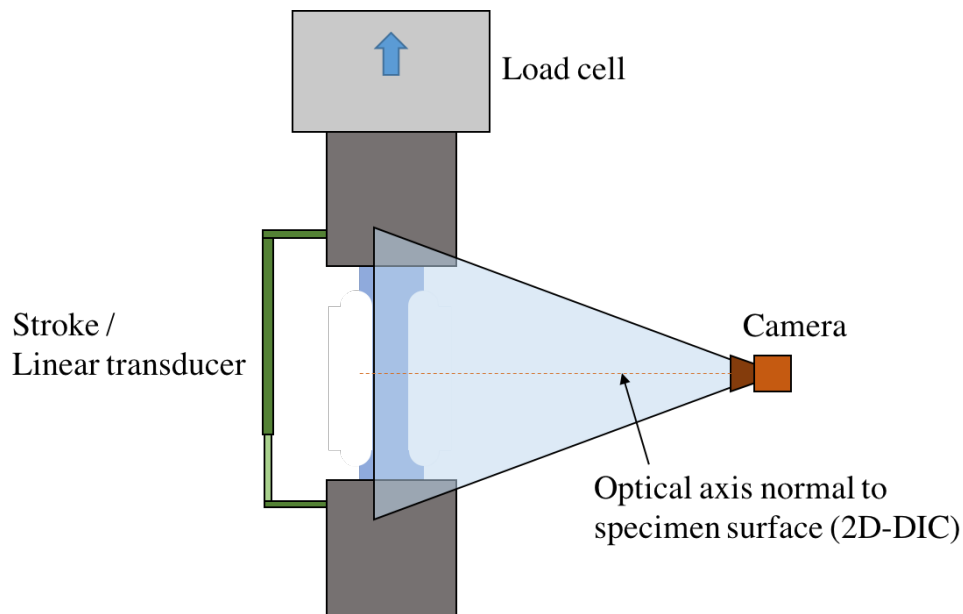
Figure 2.9: Basic principle of DIC for tension test configuration.

Straight specimen

Curved specimen

Y X
Z
Target coordinates

2D- DIC
Single camera

3D-DIC
Two cameras
Stereo vision
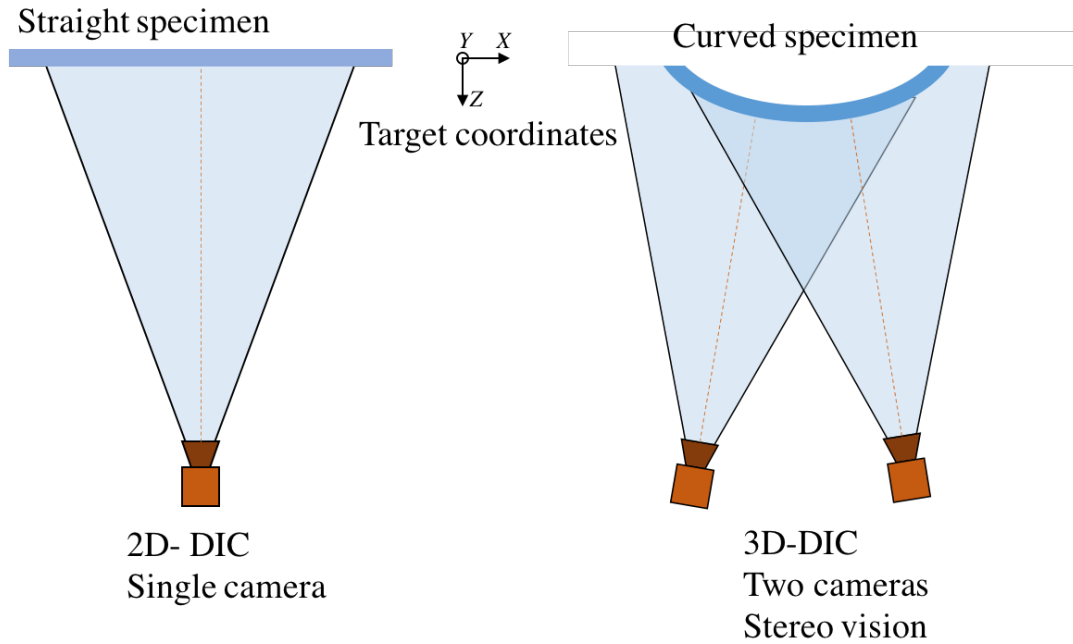
Figure 2.10: 2D-DIC set up with one camera, 3D-DIC set up with two cameras in stereo vision.

(a)

(b)
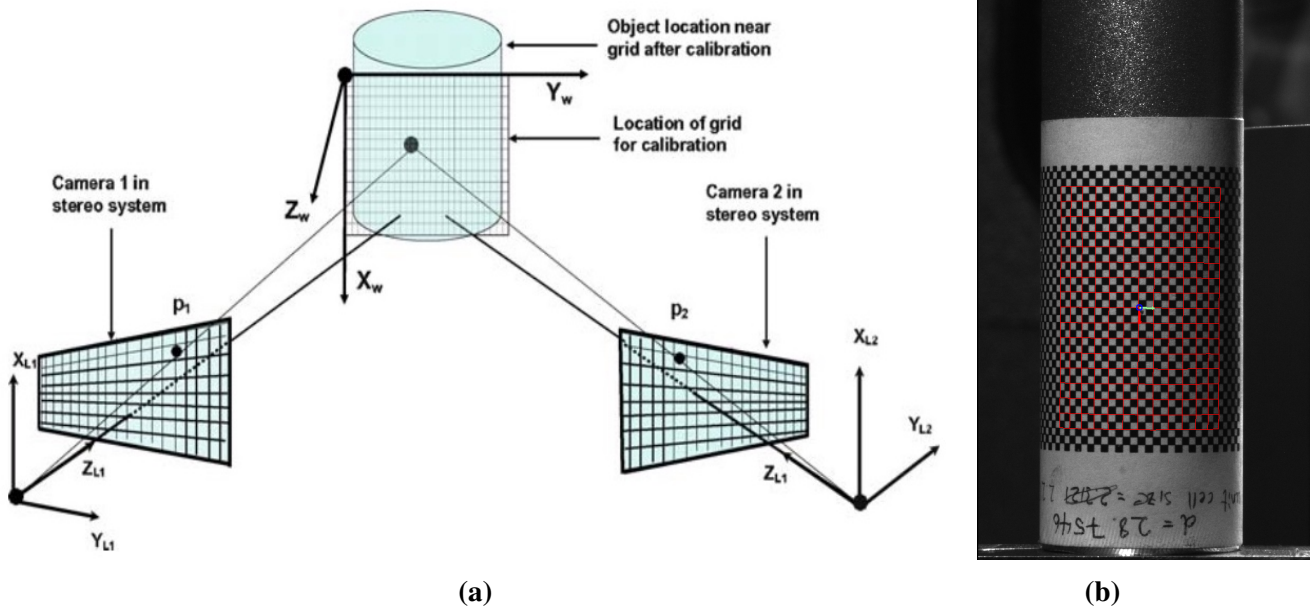
Figure 2.11: (a) Schematic of two camera stereo-vision system during imaging of a target grid. World system is generally aligned with the first grid location. Origin is at an arbitrary grid intersection point [Sutton et al., 2009], and (b) the calibration target used as reference to create a common 3D virtual mesh for 3D-DIC analysis.

2.4.1   Errors in DIC

Both the experimental setup and the numerical computation are of importance for reducing the noise in the DIC results. The numerical computation can filter the noise, but this can affect the accuracy. The experimental set up is strongly influenced by the equipment used, the light setting, heat waves and other factors that vary during the experiment. Low strain levels are more vulnerable, as the ratio between displacement and unavoidable noise is high. Below is an overview commenting on issues based on findings by Bing Pan in [Pan et al., 2009].

- **Element size**

  Bigger elements will decrease noise, but provide less possibilities for outputting localization in the specimen.

- **Greyscale correction**

  Greyscale correction ON can in some cases make the calculation more stable, but in general it will also introduce more noise.

- **DIC filter - additional software tool**

  It is not recommended to use filters additional to default settings in the numerical computing software.

- **Output elements**

  Boundary elements usually have more trouble describing the movement in the speckled pattern, and will therefore have more noise.

- **Number of images**

  If more images are used, the results will be more stable.

- **Reference image**

  The reference image can be updated to reduce noise, but will then cancel out information. The challenge with choosing a reference image is pointed out in [Fagerholt, 2011]. If there are large displacement gradients between current and reference image, a first order shape function might have problem describing the displacement field. The reference image can be updated to an image later in the series so that high correlation residuals are canceled. But this will also include measurement errors in the new reference image.

2.5   Lead as an Engineering Material

A variety of different lead alloys are used as engineering materials. They are mechanically soft and ductile with melting temperature as low as $T_m = 327\,°C$, [Callister and Rethwisch, 2009]. The yielding takes place between $1\,MPa$ and $12\,MPa$ depending on temperature and strain rate. Lead has good resistance toward corrosive environments. With a recrystallization temperature at T = $-4\,°C$, recrystallization will take place during service in most application. The density is considerably high with $11.34\,g/cm^3$ compared to iron with $7.87\,g/cm^3$. Some common applications for lead are x-ray shields, sheathing and batteries.

2.6   Creep and Relaxation

Creep is a deformation mechanism on a level with elastic and plastic deformation. Both plastic and creep deformation forms an irreversible strain. While plastic deformation happens instantaneously by shear forces causing atoms to dislocate and create slip bands; creep is time and temperature dependent occurring from $0.3T_m$ to $0.6T_m$ (absolute melting temperature), [Dowling et al., 2013], depending on metal. Creep can lead to failure, just like fatigue, but is not dependent on cyclic behavior. According to Dieter there are four governing creep mechanisms which is dependent on stress and temperature presented in [Dieter, 1988]:

- *Dislocation glide* - involves dislocations moving along slip planes and overcoming barriers by thermal activation.
- *Dislocation creep* - involves the movement of dislocations which overcome barriers by thermal assisted mechanisms involving the diffusion of vacancies or interstitials. Here dislocation climb plays a major role.
- *Diffusion creep* - involves the movement of vacancies and interstitials through a crystal under the influence of applied stress, including Nabarro-Herring and Coble creep, illustrated in figure 2.12.
- *Grain boundary sliding* - involves the sliding of grains past each other.

Drury discovers in [Drury et al., 1989] that there is a transition from dislocation creep to grain boundary sliding, which is a form of diffusion flow, due to dynamic recrystallization. "Recrystallization is the formation of a new set of strain-free and equiaxed grains (i.e., having approximately equal dimensions in all directions) that have low dislocation densities and are characteristic of the

precold-worked condition" [Callister and Rethwisch, 2009]. Dynamic recrystallization is expected to allow for more creep, as they accommodate each other. Voids are then "repaired" and the failure happens by necking. Hotta showed in [Hotta et al., 2007] that pure lead has complete static recrystallization after 600 second at $0\,°C$, however for lead alloys it can take up to 100 times longer. According to [Callister and Rethwisch, 2009] recrystallization causes the material to become softer and more ductile.
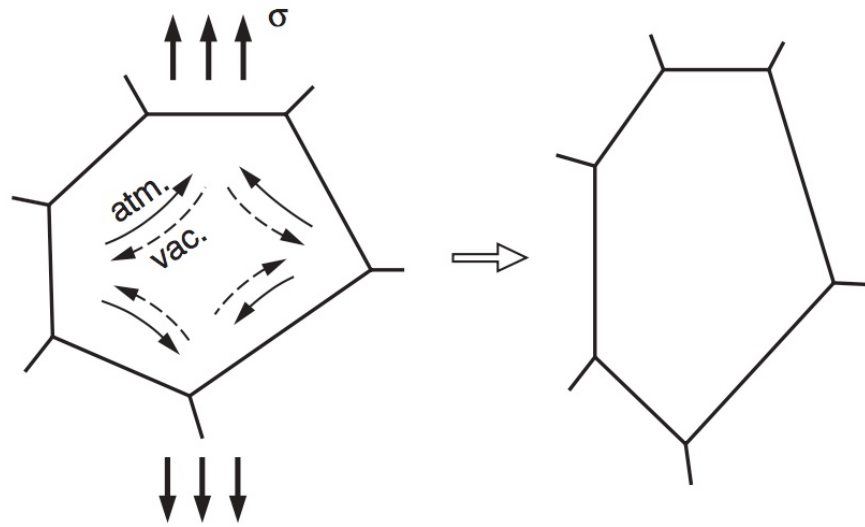
Figure 2.12: Mechanism of creep by diffusion of vacancies within a crystal grain [Dowling et al., 2013].

The schematic creep behavior of a material subjected to constant stress is illustrated in figure 2.13. The primary creep stage, also called transient creep, goes on for a short time before the secondary creep stage, also called steady state creep, occurs. According to [Hofmann, 1970] the instantaneous and transient creep in lead should be distinguished as the time to steady state takes several days. Tertiary creep happens before fracture. Creep rate, $\dot{\epsilon}_{cr}$, is defined as the steady state creep in the secondary area. The creep rate is expected to increase as the grain size decreases. Creep limit is the lowest stress that causes creep to take place. According to [Blaskett and Boxall, 1990] pure lead has an elongation of $0.06\,\%$ after 500 days at $30\,°C$ subjected to $0.7\,MPa$, and $2\,\%$ if the stress is doubled.
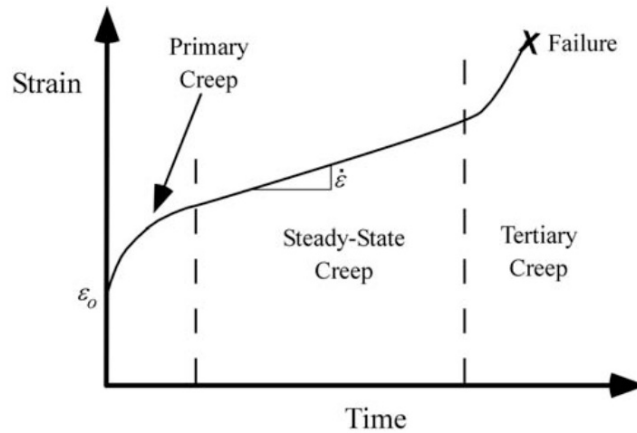
Figure 2.13: Schematic creep behavior of a material subject to a constant stress [Anderson and Anderson, 2005].

While creep is happening at a constant stress, relaxation is the same phenomenon happening at a constant strain. Relaxation can be observed by the stress decreasing during constant strain. According to [Brinson and Brinson, 2015] it is normal to make a relaxation test history less: "In a relaxation test, it is also normal to assume that the material has no previous stress or strain history or if one did exist, the effect has been nullified in some way."
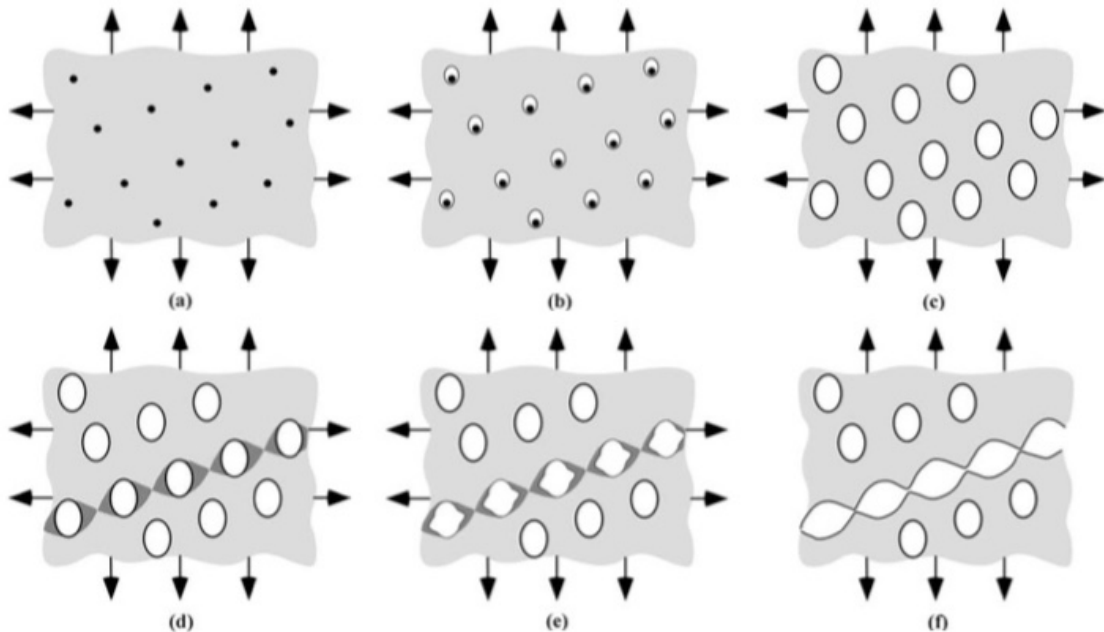
Figure 2.14: Void nucleation, growth, and coalescence in ductile metals: (a) inclusions in a ductile matrix, (b) void nucleation, (c) void growth, (d) strain localization between voids, (e) necking between voids, and (f) void coalescence and fracture [Anderson and Anderson, 2005].

Crack growth in a ductile material will follow the schematic representation in figure 2.14. When the material is stressed small voids will start to form around inclusions. Stress concentration will take place at the void edges the same way as in figure 2.7, causing the voids to grow. When the voids grow into each other small pores are created. The pores start to form cracks and eventually it ends up fracturing.

2.7   Fatigue

Fatigue is crack growth due to repeated or cyclic loading or strain where the material gets a plastic zone at the crack tips during loading, illustrated in figure 2.15. Plastic deformation is caused by atoms moving and creating edge, screw and mixed dislocations along slip planes like in figure 2.16. As the dislocation comes to a free surface during loading, it creates a step. When the loading is reversed the dislocations can move in opposite direction, but also on other slip planes. After a number of cycles persistent slip bands are formed, which is where fatigue cracks are initiated, figure 2.17. The material is weakened, and eventually it will lose its load bearing capacity.

To find the number of cycles to failure, fatigue testing is performed on a test specimen at an elevated frequency. This allows for a test fail after a couple of days, instead of a couple of years. Temperature, frequency and strain range are all parameters that can influence the result. The goal is to find an equation where this is accounted for, to predict the lifetime of the component. Fatigue testing is divided into high cycle and low cycle fatigue, where low cycle indicates a relatively low number of cycles before failure. The governing equation for low cycle fatigue is the Coffin-Manson's law, equation (2.6), where full plasticity is assumed. N is the number of cycles to failure and ϵ'_f and c are constants. Due to the plastic behavior in lead it will be low cycle fatigue.

$$\epsilon_{amp} = \epsilon^{pl}_{amp} = \epsilon'_f (2N)^c \tag{2.6}$$

A limiting factor for the strain range in a fatigue test is, by Antonio in [Alvaro, 2016], found to be bifurcation, better known as buckling. Buckling can happen in any sufficiently thin structures that experience compression. For simplified linearized prebuckling the design criteria are geometry, E-module and boundary conditions. Eigenanalysis can be calculated by FEM, providing the magnitude of the loads which buckling is expected to occur [Felippa, 2016]. To avoid buckling issues the strain range should be below $\Delta\epsilon = 0.3\,\%$. As the lead sheathing is stabilized by several layers

and the conductor in the SPC, buckling can not occur in the sheathing during operation.

Alvaro found in [Alvaro, 2016] that there were a detrimental effect observable on lead when increasing the test frequency for the fatigue test. The number of cycles to failure will go down as the test frequency goes up.
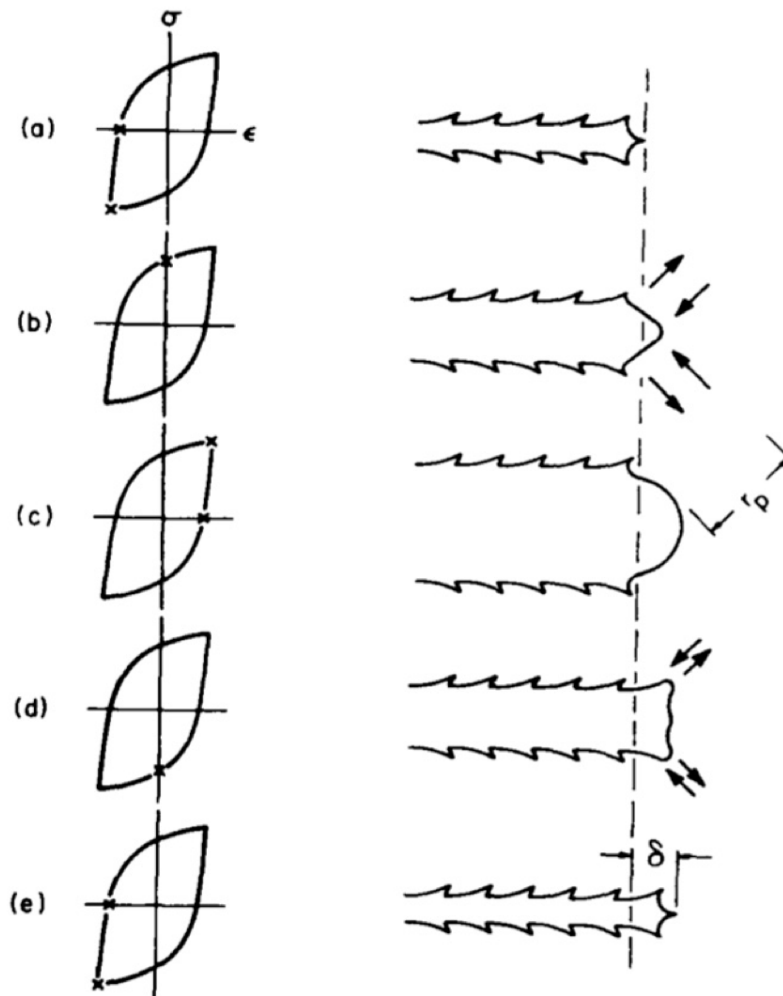
Figure 2.15: "Fatigue Crack growth by the Plastic Blunting Mechanism. Drawings at Left Indicates Points on the Cyclic Hysteresis Loop for Which Crack-Tip Geometry Obtains r_p = Plastic Zone Size Along Planes of Maximum Shear." [Wood et al., 1970].
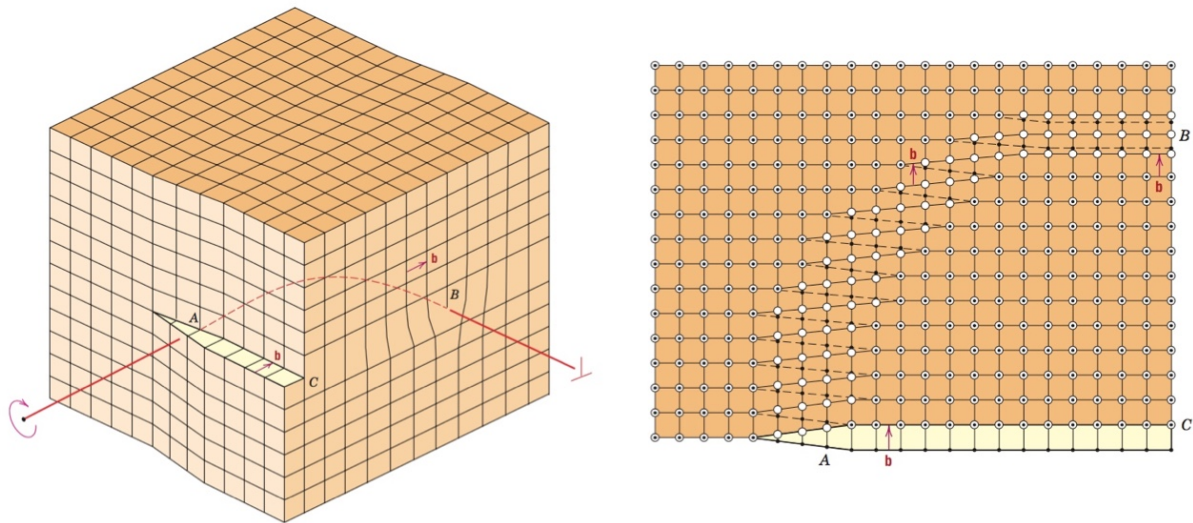
Figure 2.16: Schematic representation of a dislocation that has edge, screw and mixed character. Right picture: Top view, where open circles denote atom positions above the slip plane, and solid circles, atom positions below. At point A, the dislocation is pure screw, while at point B, it is pure edge. For regions in between where there is curvature in the dislocation line, the character is mixed edge and screw [Callister and Rethwisch, 2009].
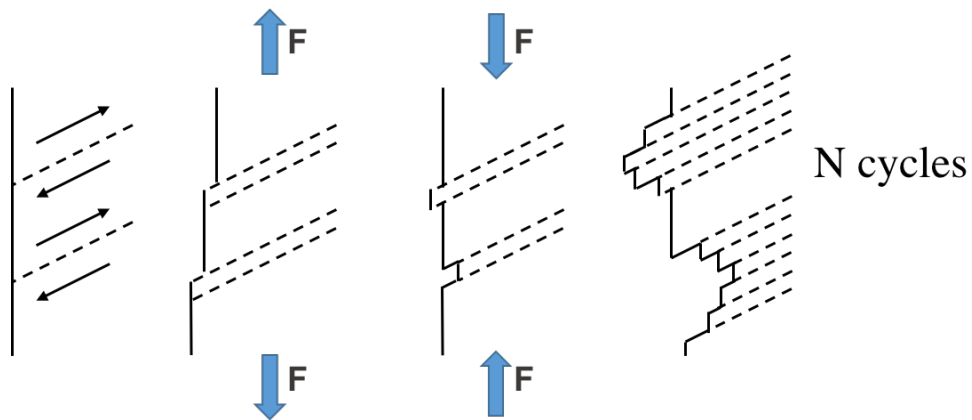
Figure 2.17: Slip bands are formed under cyclic loading.

2.8   Material Behaviour Under Cyclic Loading

Work hardening is the phenomenon where a metal becomes stronger and harder by dislocation movements and plastic deformation. Recovery is the relief of internal strain energy by rearrangement of dislocations, where they cancel each other out [Callister and Rethwisch, 2009].

For strain controlled cyclic testing a phenomenon called cyclic softening (or cyclic relaxation) can occur. This can be observed by the stress level decrease while cycling, illustrated in figure 2.18. Normally the stress level will converge and stabilize after a number of cycles. Cyclic hardening is the opposite, where the stress level increase during cycling. For a test that is cyclic softening the test will be more conservative when it is stress controlled, whereas a cyclic hardening test will be more conservative when strain controlled.

Another phenomenon is ratchetting, which can occur during cyclic testing with stress control when R-ration $\neq -1$. "[...] ratchetting behavior is concerned with secondary deformation accumulating cycle by cycle in the direction of non-zero mean stress" [Ohno and Wang, 1995]. Ratchetting can be observed by strain cycling in positive or negative direction during a biased loding condition, as in figure 2.19. There are no distinction between ratchetting and cycle dependent creep in [Dowling et al., 2013], whereas Ohno argues in [Ohno and Wang, 1995] for cycle dependent creep to be a specific type of ratchetting where the temperature is above $0.3T_m$. This will not be of any concern in this thesis, as ambient temperature is $> 0.3T_m$ for the lead sheathing.
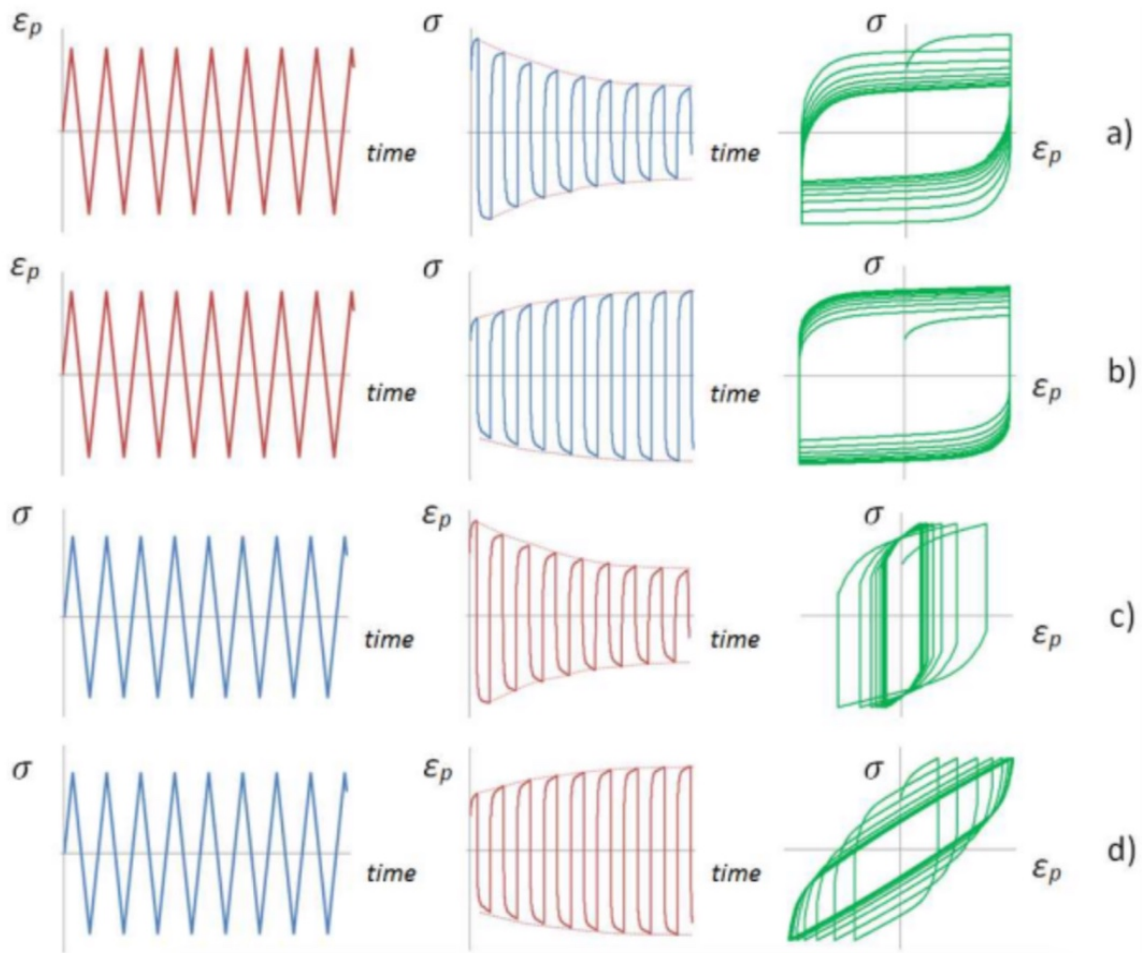
Figure 2.18: Uniaxial fatigue test material response: (a) Cyclic softening under strain controlled loading, (b) cyclic hardening under strain controlled loading, (c) cyclic softening under stress controlled loading, and (d) cyclic hardening under stress controlled loading, [Halama et al., 2012].
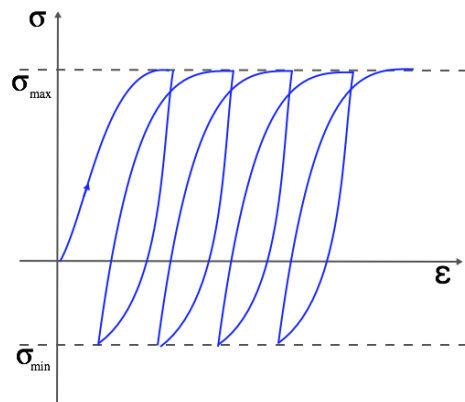
Figure 2.19: Ratchetting effect caused by a biased stress state.

2.9   Creep-Fatigue Interaction

The fatigue life of lead components is strongly dependent of frequency/strain rate. At high strain rates, the main mechanism governing is fatigue, described in section 2.7, where crack initiation starts from the surface, illustrated in figure 2.20a; whereas for low strain rates, creep causes small voids to develop at the grain boundaries in the material, figure 2.20b. Four different creep mechanisms are presented in section 2.6, and which one is acting in the material are depending on stress state and temperature.

As the strain rate is decreased from a high strain rate, creep gain a more and more predominant role, and there will be an interaction between fatigue and creep. This is a severe condition where creep voids will start to form as a consequential damage to fatigue in immediate distance to the fatigue crack, illustrated in figure 2.20c. If the strain rate is further decreased creep will take place independent of fatigue, as illustrated in figure 2.20d. Now fatigue cracks and creep voids forms simultaneously and eventually they will grow into each other, causing a premature failure.
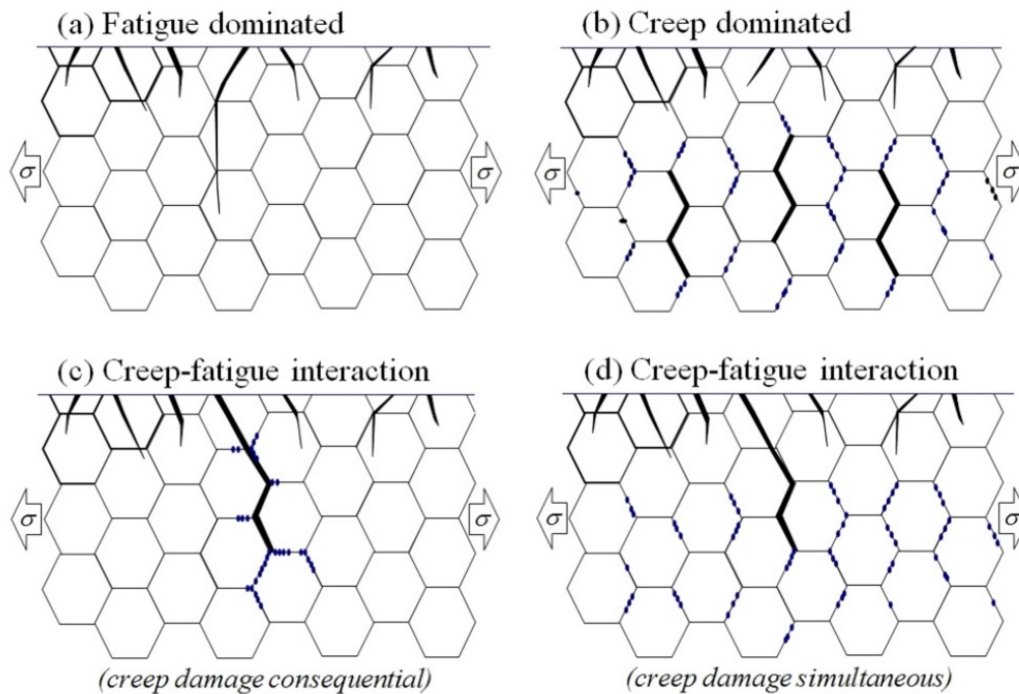
Figure 2.20: Creep-fatigue cracking mechanisms: (a) fatigue dominated, (b) creep dominated, (c) creep-fatigue interaction (due to "consequential" creep damage accumulation), and (d) creep-fatigue interaction (due to "simultaneous" creep damage accumulation) [Holdsworth, 2015].

CHAPTER 3

Methodology

3.1 Numerical Simulations

An outline of the numerical simulations that has been conducted is presented in appendix section
B.

3.1.1 Setup for the Numerical Simulation

The software used for numerical simulation by Finite Element Method (FEM) is *Abaqus 6.14*. To
reduce the computational time the models are made with a symmetry plane over the transverse and
longitudinal direction. One node is set to hold in the "Y-direction" to prevent free body move-
ment. The analysis is displacement controlled. The grips are modeled as displacements acting on
the surface of the specimen. Since the displacements are small and the strain rate is low, this is
calculated as a static general calculation. The maximum strain in the simulation is set to 0.5 %, as
the maximum strain of interest for fatigue testing. The mesh is built with C3D8R elements. The
output request is "Strain - Max Principal" and "Stress - Max Principal", which displays the maxi-
mum principal strain and maximum principal stress in every individual element. The displacement
of two points on the center line, with initial $30\,\mathrm{mm}$ displacement, are used as the reference strain.
This is comparable to using an extensometer on the TSG.

The material data used:

- The density is set to $\rho = 11.3\,\mathrm{g/cm^3}$.
- The E-module is set to $13.5\,\mathrm{GPa}$.
- The Poisson ratio is set to $\nu =$0,44.
- The plastic area is displayed in figure 3.1.
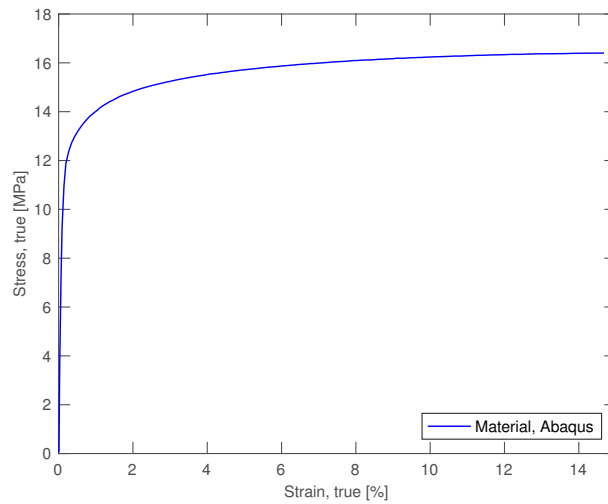
Figure 3.1: The material properties for plastic behavior implemented in the numerical simulations in *Abaqus 6.14*.

3.1.2 Specimen A to D
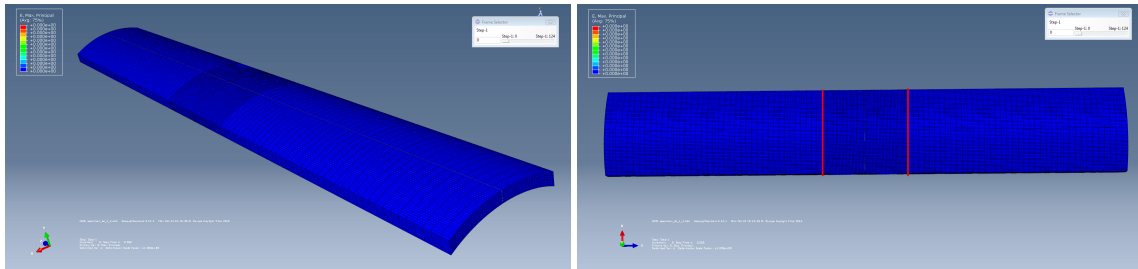
Figure 3.2: Specimen A curved, with grips indicated by red lines.
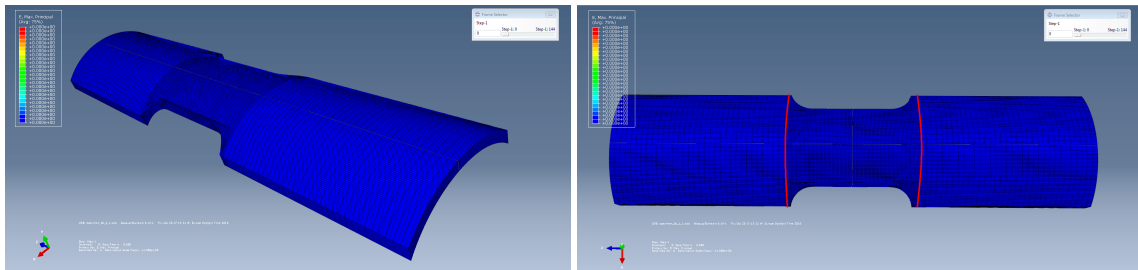
Figure 3.3: Specimen B curved, with grips indicated by red lines.
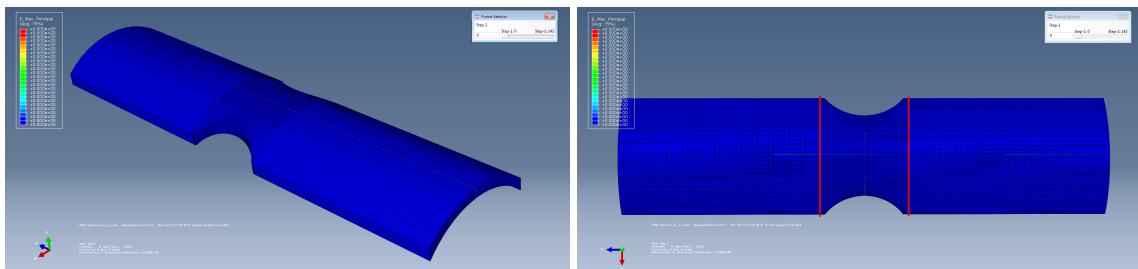
Figure 3.4: Specimen C curved, with grips indicated by red lines.
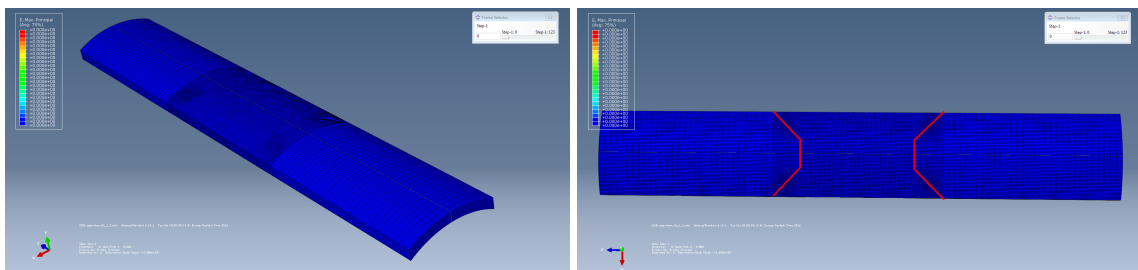
Figure 3.5: Specimen D curved, with grips indicated by red lines.

The TSGs analyzed for fatigue testing are specimen A, B, C and D presented with grips in respectively figure 3.2, 3.3, 3.4 and 3.5. All the TSGs are analyzed both curved and straightened. The *Abaqus 6.14* models are made in accordance with the machine drawings which is presented in figure A.2 in appendix section A.

Specimen A is a simple strip specimen. The distance between the grips is $30\,\mathrm{mm}$, see figure 3.2. Specimen B is improved with introducing a stress raiser. This is expected to give a higher strain in the narrowed area, as well as having less stress by the grips, see figure 2.7 and figure 3.3. To prevent buckling a shorter distance between the grips is beneficial. Specimen C has both a shorter area between the grips than specimen B and also it only has one "hinge" to rotate around, see figure 3.4. This means it can only buckle where the cross-section area is the lowest. Specimen D is an improvement of specimen A, where the shear forces from the extension of the $45°$ grips are intended to create an increased strain field in combination with the uni-axial tension, see figure 3.5.

3.2 Laboratory Testing

An outline of all the laboratory tests that has been conducted is presented in appendix section B.

3.2.1 Material and Specimens

The material used for testing was a composition of lead, tin and antimony. It was provided by customer as tubes of lead sheathing, see figure 3.6. Three different thicknesses were provided, t = $1.0\,\mathrm{mm}$, $1.8\,\mathrm{mm}$ and $3.3\,\mathrm{mm}$. Testing was carried out on specimens retrieved directly from the lead sheathing, where the straight specimens had undergone flattening.

Regular dog bone specimens were used for the laboratory tests carried out to obtain material properties. The specimens had a size relative to the thickness, see figure 3.7. The machine drawings of the specimens are presented in appendix section A figure A.1. All the three dog bone specimens was flattened.

For the laboratory testing carried out to find the most suitable TSG, all the specimens had thickness t = $3.3\,\mathrm{mm}$. Figure 3.8 displays the machined specimen A to D both curved and straight. Specimen A and D have the same geometry, but different grips. The machine drawings of the specimens can be found in appendix section A figure A.2.
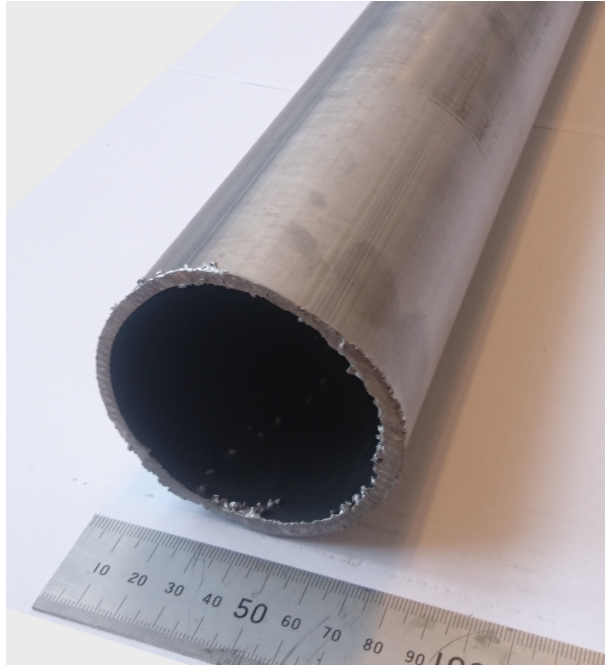
Figure 3.6: Lead sheathing with thickness $3.3\,\mathrm{mm}$ prior to machining and flattening.

Figure 3.7: Dog bone specimens with thickness $1.0\,\mathrm{mm}$, $1.8\,\mathrm{mm}$ and $3.3\,\mathrm{mm}$.
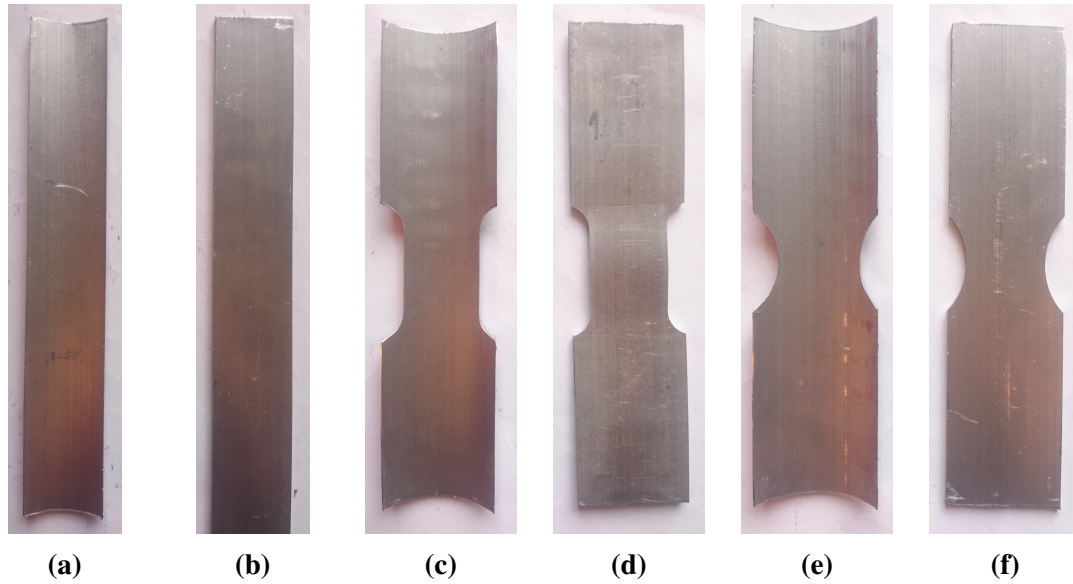
Figure 3.8: (a) Specimen A and D curved, (b) Specimen A and D straight, (c) Specimen B curved, (d) Specimen B straight, (e) Specimen C curved, and (f) Specimen C straight.

3.2.2 Test Machines

The test machine used for all laboratory experiments in this thesis, with exception of the fatigue test, was a *Zwick/Roell Z030* with a $30\,\mathrm{kN}$ load cell. Tension or compression tests can be performed with this test machine in a regular tension test configuration, displayed in figure 3.9. The test speed was given as strain rate, and was calculated by stroke relative to the parallel area of the test specimen. Example: $\dot{\epsilon}$ = 1E-4 s^{-1} is derived from a stroke speed of $0.0044\,\mathrm{mm/s}$ on a specimen with a parallel lenght area of $44\,\mathrm{mm}$. Stroke is the displacement of the crosshead on the machine measured by a linear transducer, indicated in figure 3.9. Stroke and load are the only direct output from the test machine.

The fatigue test was carried out on a *Instron 8550* with curved grips with a $45°$ angel (Specimen D).

For tests conducted with extensometer it was used a *MTS 643.31F-25* extensometer with gauge length $25\,\mathrm{mm}$. Different grips were used depending on whether the specimen were straightened or curved.

3.2.3   DIC - Setup

The camera used for DIC was a *Allied Vision PROSILICA GA 2450*, with a *Nikon AF Nikkor 50mm f/1.8 D* lens. This is quality equipment which limits the error and noise in the results. The acquisition rate on the camera was set according to the total test time and regulated for the most interesting parts of the test. The acquisition rate is limited to a maximum of $15\,\text{Hz}$ and a minimum of $0.01\,\text{Hz}$. Test with a low test time will not have an adequate amount of data points, as the desired amount of 1,000 images can not be met. Whereas tests going for a long period of time will require a large storage space.

The specimens were coated with a white spray paint, and then speckled with black. The nozzle on the spray can with black paint were customized with a larger hole to get larger speckles. Some types of paint dries, looses adhesion and slips or cracks, instead of follow the surface of the specimen. This is especially a problem for certain materials or for tests going over a longer period of time. The paint used in this laboratory did behave well together with lead at ambient temperature. LED-lights were used for additional background light. How the experimental setup with two cameras looked like is showed in figure 3.9. In appendix section D a presentation of different grips, lights and methods for creating a speckle pattern is presented.
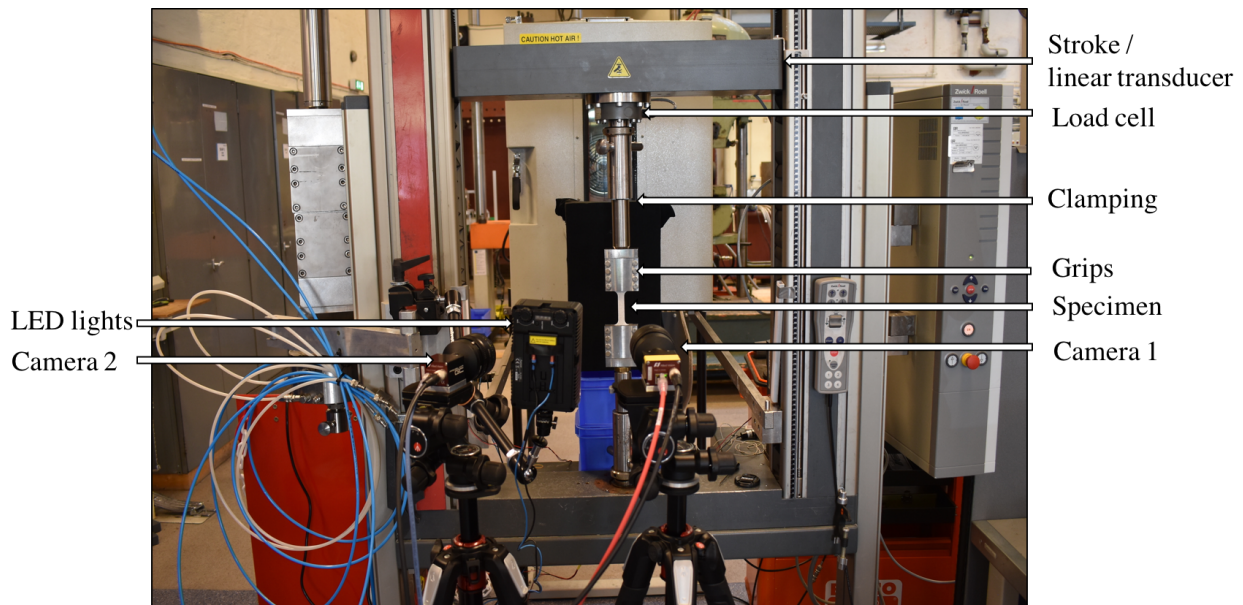
Figure 3.9: Setup with tension test configuration for 3D-DIC.

3.2.4 DIC - Software

Two different software were used for post-processing the images, respectively *VIC-2D v6*, and *eCorr v4.0*. *VIC-2D v6* is a commercial software [Simonsen and Solutions, 2016], while *eCorr v4.0* is made in-house by Egil Fagerholt, [Fagerholt, 2017]. To run a numerical computation an area for where data are to be extracted from has to be defined. This is done by creating a virtual mesh over the speckle pattern. This will allow for strain and displacement to be calculated, and the ratio pix/mm will convert it from pixels to mm. In figure 3.10 a screen shot from a 3D-DIC computation in *eCorr v4.0* is displaying a strain field on the front facing specimen on the left. The virtual mesh created by the second camera is displayed on the image to the right. A mirror is to get a visual observation of the specimen facing $90°$.
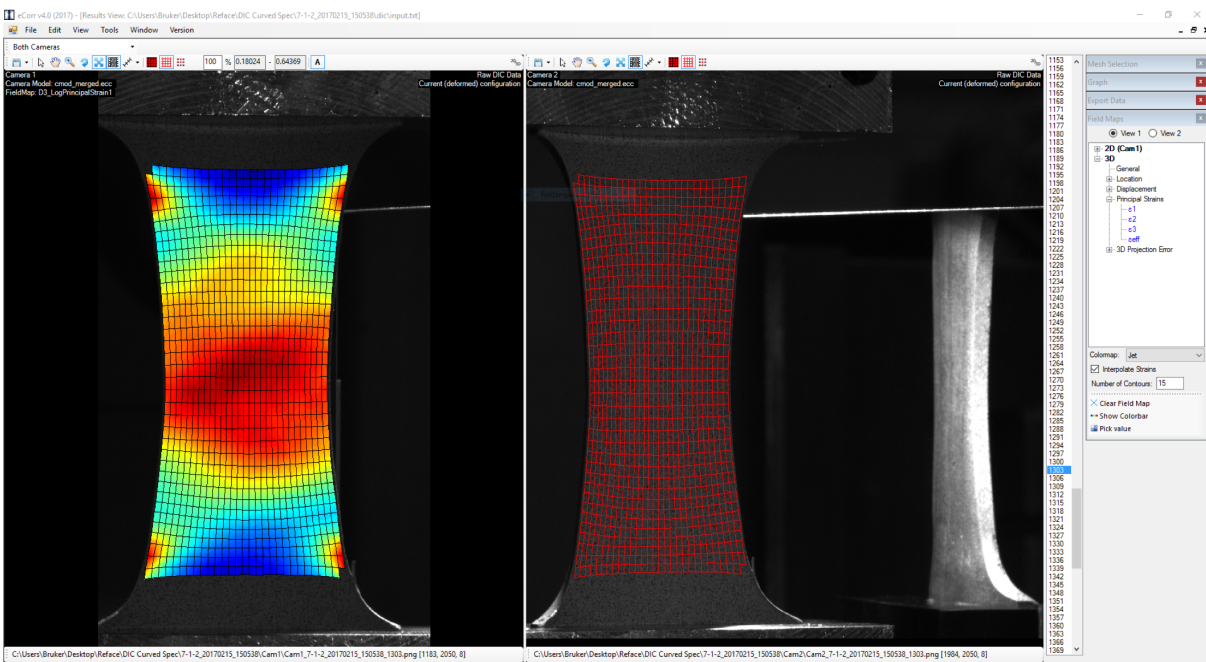
Figure 3.10: A screen shot from *eCorr v4.0* showing how 3D-DIC output looks like. The images are from a stereo camera setup, with the strain field on the left image and only the mesh on the right image. The specimen without a mesh is from a mirror used to get a $90°$ image for observation.

Data from the two software can be extracted in different ways. *VIC-2D v6* outputs data from an average of the elements within a defined area. *eCorr v4.0* outputs data either from individual elements or virtual vectors. The vectors are basically simple extensometers, and must be placed carefully as they only measure the difference in distance between the two endpoints. There are no possibility to output an average of elements in *eCorr v4.0*, so an external *MATLAB R2017a*

script was created to do this. When elements from AOI are averaged, noise will decrease and the data is less sensitive compared to selecting single elements. To average principal strains are not mathematically correct since every element has its individual direction. But in uniaxial tension testing the difference in the individual directions were found to be negligible before necking. For the post-processing with DIC both vectors and elements were outputted and compared to get the most stable results with the least noise. The comparison of engineering strain from vectors and true strain from elements are valid since the difference between the two are negligible for low strain levels where necking had not occurred, ref section 2.2.

3.2.5   Tension Tests

The tests were performed with a *Zwick/Roell Z030*, ref section 3.2.2. The specimens used had a regular dog bone shape, with thicknesses of t = $1.0\,\text{mm}$, $1.8\,\text{mm}$ and $3.3\,\text{mm}$, ref section 3.2.1. DIC were set up as described in section 3.2.3. Strain rate was held constant through the test. The strain rates tested were $\dot{\epsilon}$ = 1E-2 s^{-1}, 1E-3 s^{-1}, 1E-4 s^{-1}, 1E-5 s^{-1} and 1E-7 s^{-1}. Also a test with $\dot{\epsilon}$ = 1E-8 s^{-1} was performed on a specimen with thickness t = $3.3\,\text{mm}$.

3.2.6   E-modulus Test

The test was performed with a *Zwick/Roell Z030*, ref section 3.2.2. The specimen used had a regular dog bone shape, with thickness t = $3.3\,\text{mm}$, ref section 3.2.1. DIC were set up as described in section 3.2.3. The strain rate was $\dot{\epsilon}$ = 1E-4 s^{-1}. To reduce the deviation in the machine and get a more accurate measurement, the test were run with an unloading cycle, "tension-compression-tension", as described in [Standard, 2009].

3.2.7   Creep Test - Constant Stress

The test was performed with a *Zwick/Roell Z030*, ref section 3.2.2. The specimen used had a regular dog bone shape, with thickness t = $3.3\,\text{mm}$, ref section 3.2.1. DIC were set up as described in section 3.2.3. The strain rate for loading and unloading was $\dot{\epsilon}$ = 1E-3 s^{-1}. The load were held constant at σ = $10\,\text{MPa}$ for hold time ht = $18\,\text{h}$.

3.2.8   Relaxation Tests - Constant Strain

The tests were performed with a *Zwick/Roell Z030*, ref section 3.2.2. The specimen used had a regular dog bone shape, with thickness t = 3.3 mm, ref section 3.2.1. DIC were set up as described in section 3.2.3. A relaxation test is commonly performed by loading the specimen to a strain level and hold it there. Due to the challenge by controlling a test by strain, discussed in section 5.2.7, a hybrid between creep test and relaxation test were used. The specimen were loaded to a target value, where the position was held constant. A complete list of tests conducted is found in appendix section B.

3.2.9   Cyclic Relaxation Tests

The tests were performed with a *Zwick/Roell Z030*, ref section 3.2.2. The specimen used had a regular dog bone shape, with thickness t = 3.3 mm, ref section 3.2.1. DIC were set up as described in section 3.2.3. The strain rate for loading and unloading was $\dot{\epsilon}$ = 1E-4 s^{-1}. A relaxation test is commonly performed by loading the specimen to a strain level and hold it there. Due to the challenge by controlling a test by strain, discussed in section 5.2.7, a hybrid between creep test and relaxation test were used. The specimens were loaded to a target value where the position was set constant for a hold time, before it was loaded to the same stress level again. 10 cycles were performed each test. A complete list of tests conducted is found in appendix section B.

3.2.10   Alternating Cyclic Relaxation Tests

The tests were performed with a *Zwick/Roell Z030*, ref section 3.2.2. The specimen used had a regular dog bone shape, with thickness t = 3.3 mm, ref section 3.2.1. DIC were set up as described in section 3.2.3. The strain rate for loading and unloading was $\dot{\epsilon}$ = 1E-4 s^{-1}. A relaxation test is commonly performed by loading the specimen to a strain level and hold it there. Due to the challenge by controlling a test by strain, discussed in section 5.2.7, a hybrid between creep test and relaxation test were used. The specimens were loaded to a target value where the position was set constant for a hold time, then it was loaded to a target value in compression, where the position was set constant for a hold time, before it was loaded to the same stress level again. 10 cycles were performed each test. The same test was performed, but instead of being loaded to a stress level, it was loaded to a stroke level. A complete list of tests conducted is found in appendix section B.

3.2.11 Hysteresis Loops

The tests were performed with a *Zwick/Roell Z030*, ref section 3.2.2. The specimen used had a regular dog bone shape, with thickness t = $3.3\,\text{mm}$, ref section 3.2.1. DIC were set up as described in section 3.2.3. The strain rate for loading and unloading was $\dot{\epsilon} = \text{1E-4 s}^{-1}$. Both a stress controlled test with $\pm\sigma = 5\,\text{MPa}$ and a strain controlled test with $\pm\epsilon = 0.03\,\%$ were conducted with 20 cycles each.

3.2.12 Specimen A to D - Tension and Compression Tests

The tests were performed with a *Zwick/Roell Z030*, ref section 3.2.2. The specimens used was straight and curved specimen A, B, C and D, see figure 3.8 in section 3.2.1. DIC were set up as described in section 3.2.3. The strain rate for loading was $\dot{\epsilon} = \text{1E-4 s}^{-1}$. The tests were run to failure both in tension and compression.

3.2.13 Fatigue Test

The test was performed with an *Instron 8550*, ref section 3.2.2. The specimen used was a curved specimen D where the area between the grips were customized to $30\,\text{mm}$, see figure A.2 in section A. The fatigue test were conducted in position control, with a strain range of $\Delta\epsilon = 0.15\,\%$ and a frequency of $5\,\text{Hz}$ with a ramp up. Failure were defined as maximum load decreasing to $0.2\,\text{kN}$.

Before the fatigue test started, the specimen was preloaded in position control to the strain target value, $\Delta\epsilon = 0.15\,\%$, measured by an extensometer. The strain amplitude is half the strain range, $\epsilon_{amp} = \frac{\Delta\epsilon}{2}$, and ϵ_{mean} is in the middle. If the machine did not cycle back to the start position when unloaded, then ϵ_{mean} would be corrected with an average between initial position and the new unloaded position. Before the start of each test marks due to the extensometer were removed by manual grinding for all the specimens. The grinding did not affect the geometry of the specimen.

Results

## 4.1 Numerical Simulations

4.1.1 Specimen A to D
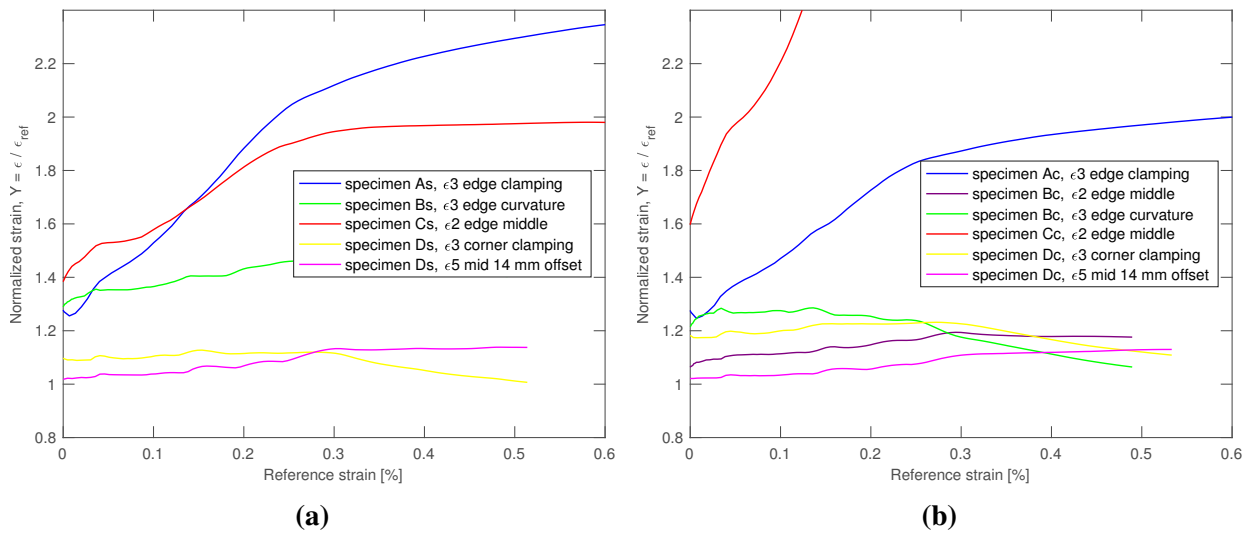
Figure 4.1: Comparison of numerical simulations of specimen A to D: (a) straight, and (b) curved

The plots in figure 4.1a and 4.1b shows a comparison of the results from the numerical simulation of specimen A to D in tension, respectively straight and curved. Only the critical strain area, the hot spot, is considered for each specimen. The normalized strain on the Y-axis is the ratio between the strain in the localization and the reference strain. The X-axis shows the reference strain. For specimen B curved the most critical area changes from the edge curvature to the edge middle at the reference strain 0.3%. For specimen D the normalized strain is highest by the clamping, point (3), while mid $14\,\mathrm{mm}$, point (5), is second highest in the specimen. For the curved specimen D the most critical area changes from the clamping, point (3), to mid $14\,\mathrm{mm}$, point (5), at reference strain above 0.3%. For specimen C curved, the normalized strain goes above 4. All of the numerical simulations are added in the appendix section C.

4.2 Laboratory Testing

4.2.1 Tension Tests
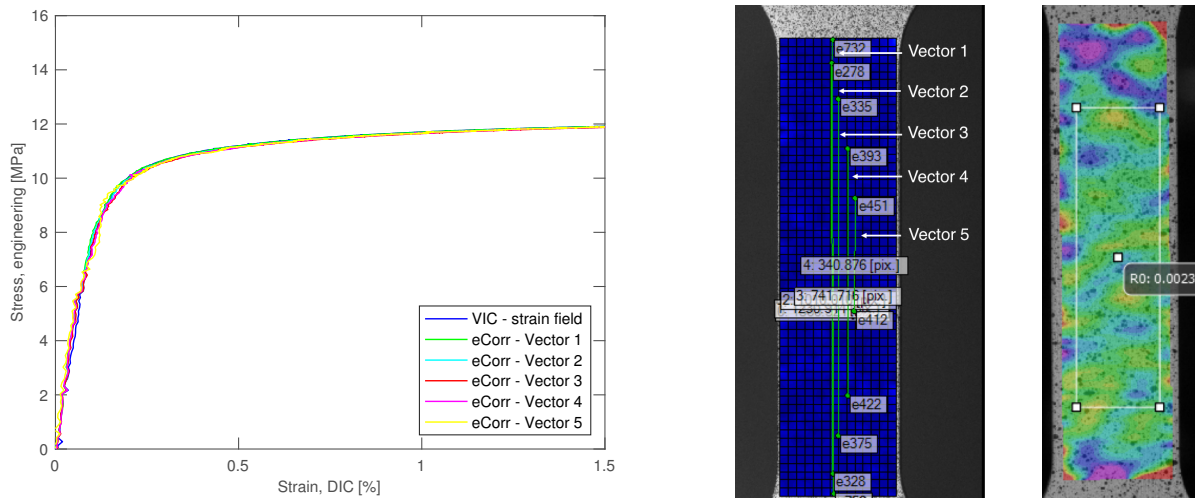
Figure 4.2: Tension test: Comparison of results from *VIC-2D v6* and *eCorr v4.0*, for tension test: t = $3.3\,\mathrm{mm}$, $\dot{\epsilon}$ = 1E-5 s^{-1}
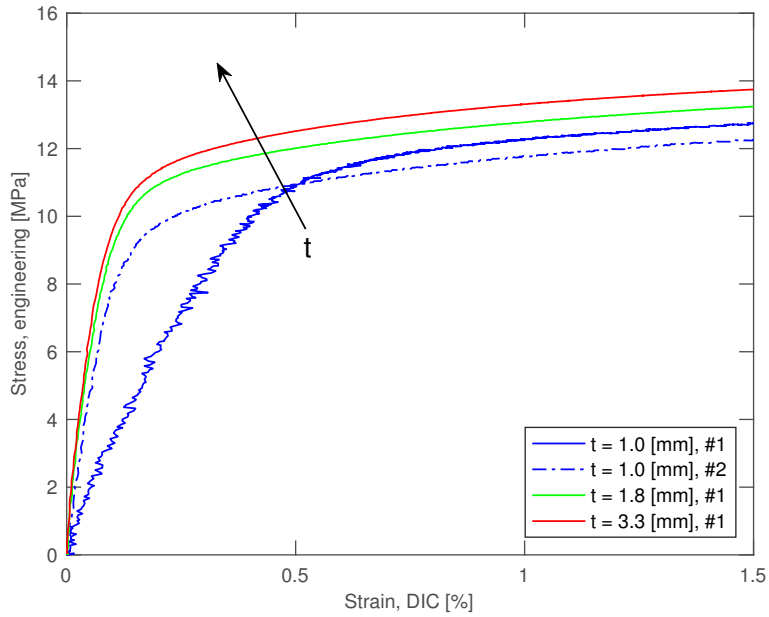
Figure 4.3: Tension test: $\dot{\epsilon}$ = 1E-4 s^{-1}, arrow indicates increasing thickness, where # specify the specimen number in each series.
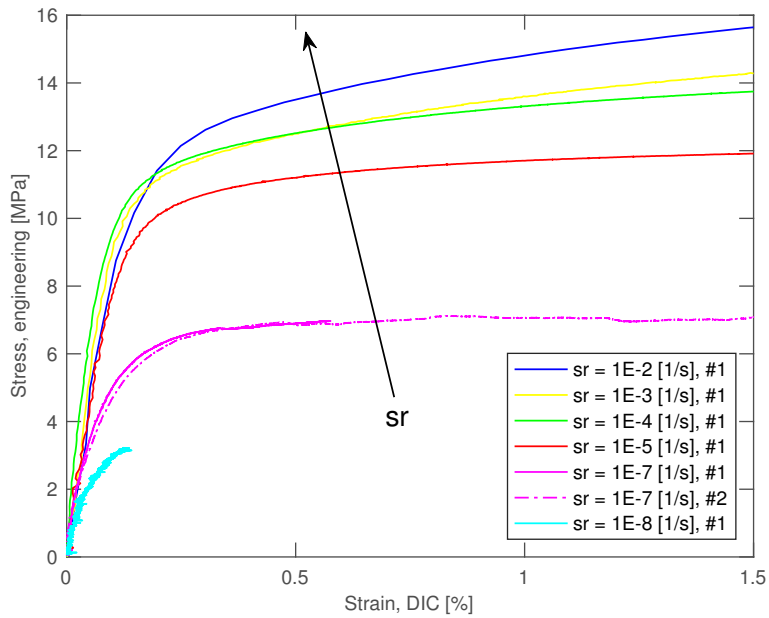
Figure 4.4: Tension test: t = 3.3 mm, arrow indicates increasing strain rate, where # specify the specimen number in each series.

Figure 4.5: Specimen to the left: t = 1.0 mm, $\dot{\epsilon}$ = 1E-2 s^{-1}. Specimen to the right: t = 1.0 mm, $\dot{\epsilon}$ = 1E-7 s^{-1}. Both at ϵ = 1.5 %. No necking has occurred.

The tension tests were conducted on dog bone specimens with thickness 1.0 mm, 1.8 mm and 3.3 mm, and strain rates from 1E-2 s^{-1} to 1E-8 s$^{-1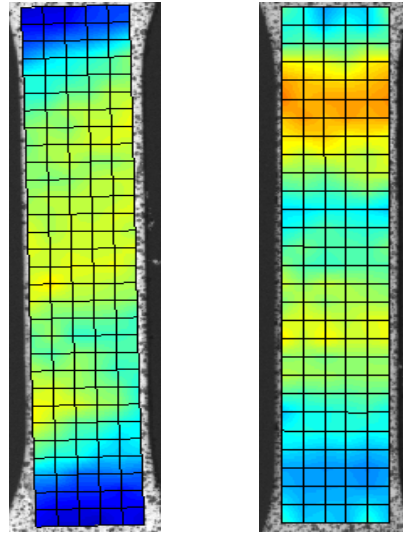}$. The total test time varied from 7 s to 70 h. The tension testing was compared in two different ways. One where the strain rate was constant with varying thickness, figure 4.3, and one where the thickness was constant with varying strain rate figure 4.4. These two plots represents the trend in the results from all thicknesses and strain rates. For the tension tests no necking has occurred in any of the specimens during testing, ref figure 4.5.
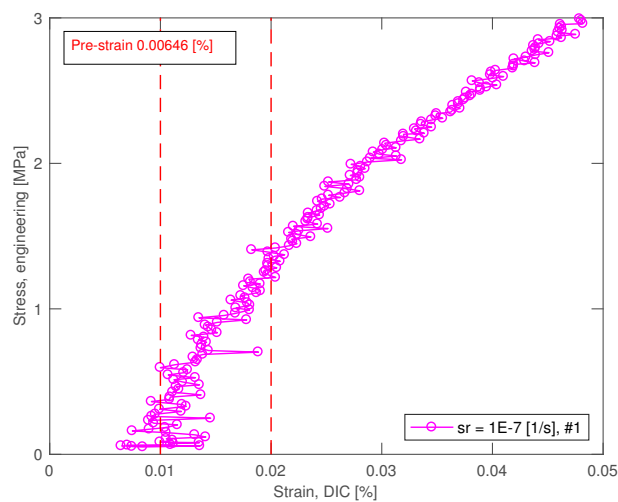
Figure 4.6: Tension test: t = 3.3 mm, $\dot{\epsilon}$ = 1E-7 s^{-1}, #1, where # specify the specimen number in each series.

A close up of the test is plotted in figure 4.6. The first recorded strain level, named "pre-strain", is indicated in the plot. This is in the range of $0.0024\,\%$ and $0.0084\,\%$ for all the tension tests. The two vertical red lines in the figure indicates the expected strain amplitude in the lead sheathing during thermo-mechanical cycling.
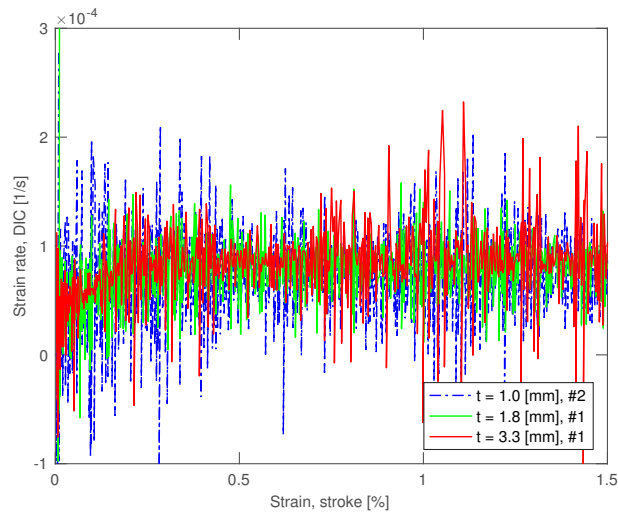
Figure 4.7: Tension test: Comparison of strain rates calculated from DIC for $\dot{\epsilon} =$ 1E-4 s^{-1}, where # specify the specimen number in each series.

In the plot of actual strain rate calculated from DIC in figure 4.7, the strain rate is just below 1E-4 [1/s] for all the test. 1E-4 [1/s] was the strain rate set by the machine. The actual strain rate is coinciding for the different thicknesses.

A full overview of all the tension tests is presented in appendix section E.2.

4.2.2 E-modulus Test
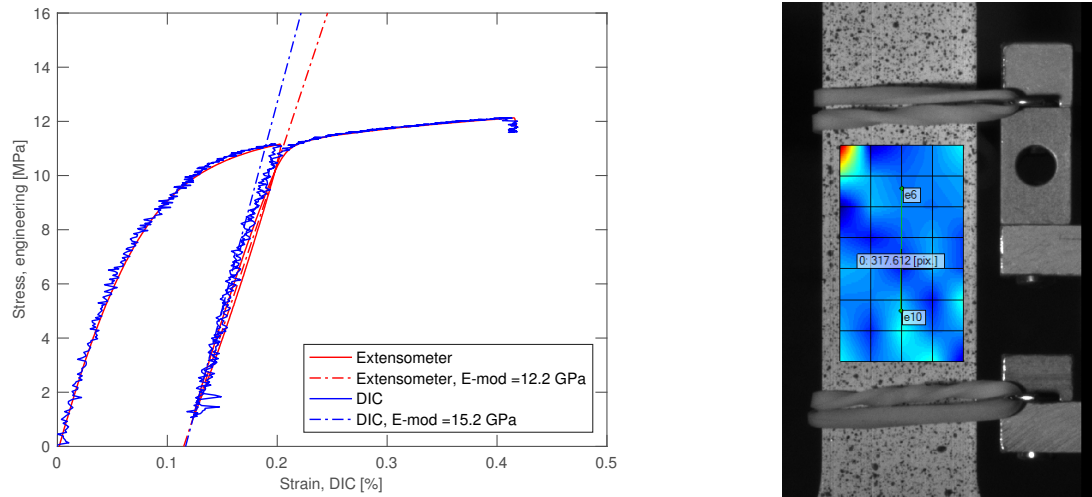
Figure 4.8: E-modulus was measured by both DIC and extensometer. From regression E-modulus is $12.2\,\mathrm{GPa}$ from extensometer and $15.2\,\mathrm{GPa}$ from DIC. To the right is a picture of the specimen with the extensometer attached and the mesh used for DIC post-processing.

Both DIC and extensometer has been used to measure the E-modulus in figure 4.8. The two measurements follow each other closely, but the DIC makes a slightly steeper E-modulus with $15.2\,\mathrm{GPa}$. The extensometer values were taken from the turning point and the intersection between up and downloading.

4.2.3 Creep Test - Constant Stress
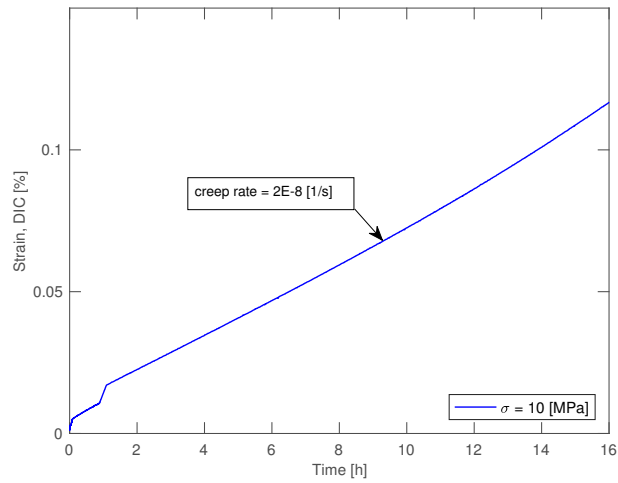
Figure 4.9: Creep test: Strain vs time, creep rate ϵ_{cr} = 2E-8 s^{-1} for σ = 10 MPa.
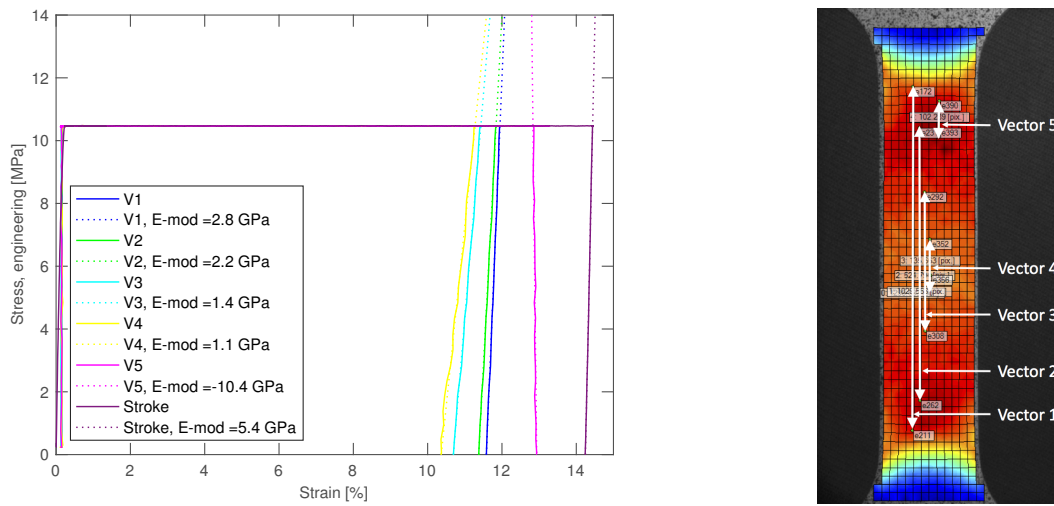
Figure 4.10: Creep test: Stress vs strain. Vector 3 was used as strain from DIC and to obtain the E-modulus from unloading.

The creep rate from the creep test with constant stress of $\sigma = 10\,\text{MPa}$ were found to be ϵ_{cr} = 2E-8 [1/s] for stress, see figure 4.9. The creep rate was stable for $16\,\text{h}$ before the test was ended.

4.2.4 Relaxation Tests - Constant Strain

(a)   **(b)**
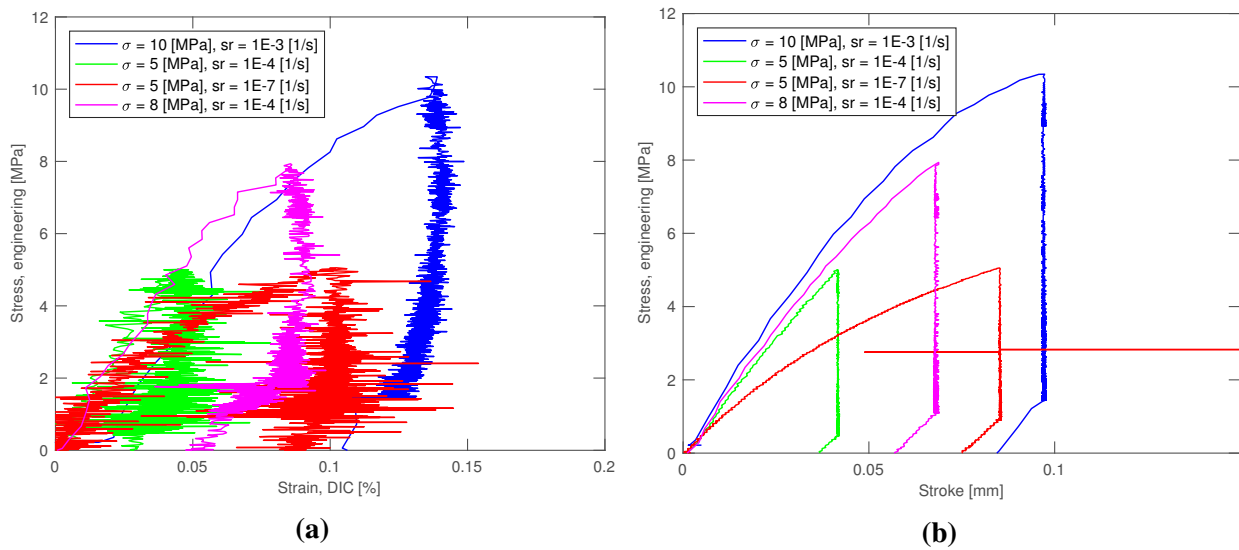
Figure 4.11: (a) Relaxation tests: Stress vs strain, (b) Relaxation tests: Stress vs stroke.
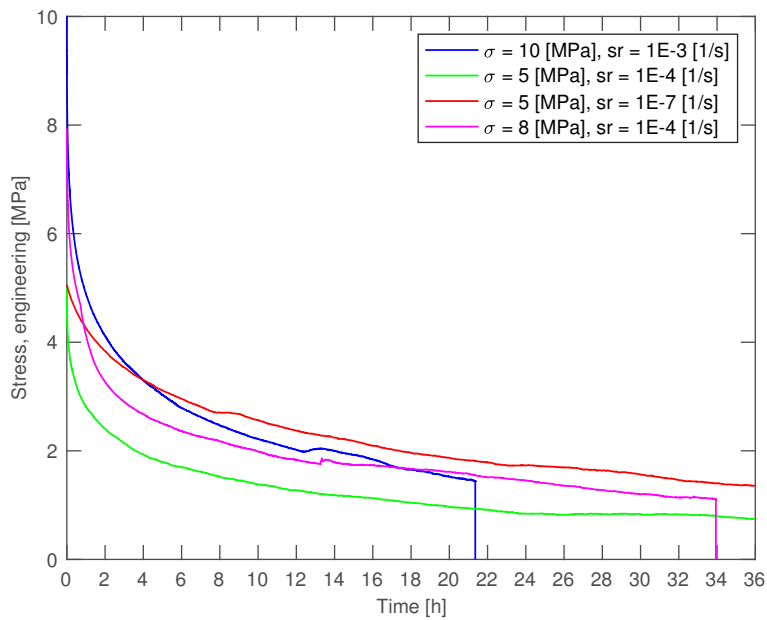
Figure 4.12: Relaxation tests: Stress vs time, without preloading.

The results from the relaxation test are plotted as stress-strain in figure 4.11. $5\,\mathrm{MPa}$, sr = 1E-4 stops at strain level = $0.05\,\%$, while $5\,\mathrm{MPa}$, sr = 1E-7 stops at strain level = $0.1\,\%$.

The stress relaxation without preloading is plotted in figure 4.12. The preloading took less than a minute for sr = 1E-3 and sr = 1E-4, while it took $5\,\mathrm{h}$ for the sr = 1e-7.

A full overview of the results can be seen in appendix section E.4.

4.2.5   Cyclic and Alternating Cyclic Relaxation Tests
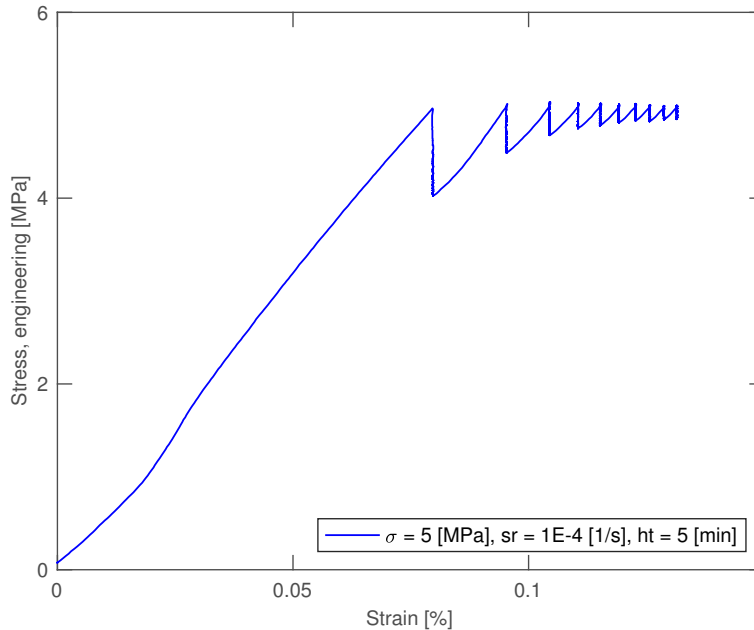
Figure 4.13: Cyclic relaxation test: Stress vs stroke. $\sigma = 5\,\mathrm{MPa}$, $\dot{\epsilon} = $ 1E-4 s^{-1}, ht = $5\,\mathrm{min}$.

Cyclic relaxation test with loading to $5\,\mathrm{MPa}$, relaxation for $5\,\mathrm{min}$ and 10 cycles is presented in figure 4.13, where the stress-stroke is plotted. The total strain level after 10 cycles measured by the stroke is 0.13 %.
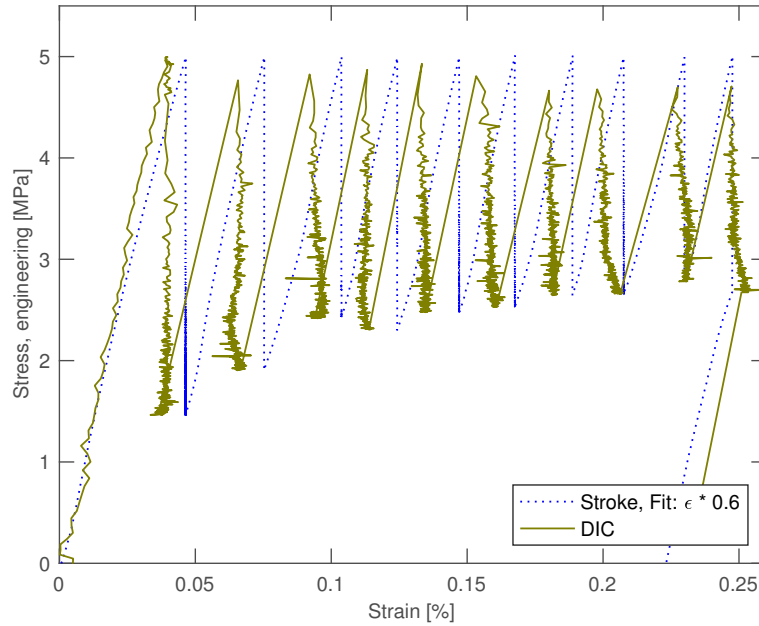
Figure 4.14: Cyclic relaxation test: Stress vs time. $\sigma = 5\,\mathrm{MPa}$, $\dot{\epsilon} = $ 1E-4 s^{-1}, ht = 12 h.

Cyclic relaxation test with loading to $5\,\mathrm{MPa}$ and relaxation for $12\,\mathrm{h}$ and 10 cycles is presented in figure 4.14. The stroke is scaled down with 0.6 due to geometry factor in the dog bone specimen. 0.6 is found by trial and error, and is used to compare the stroke the strain from DIC. The total strain level after 10 cycles are 0.25 %.
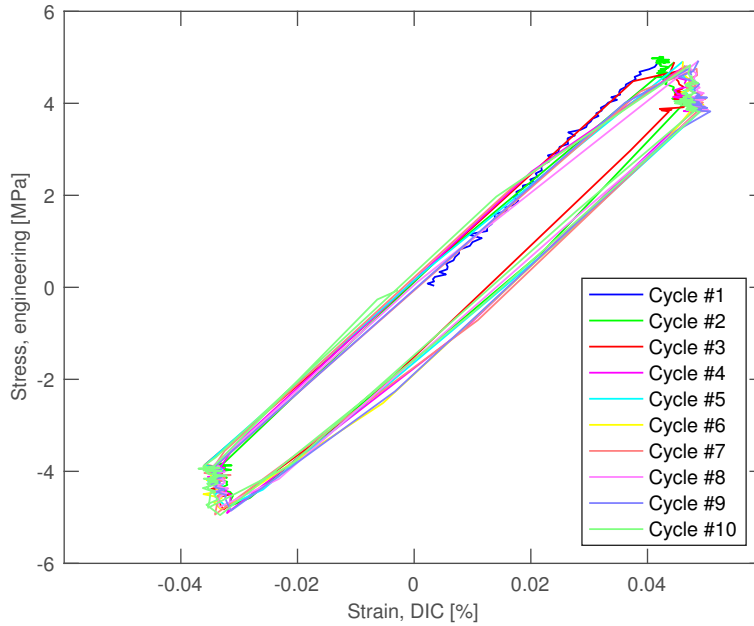
Figure 4.15: Alternating cyclic relaxation test: Stress vs strain. $\pm\sigma = 5\,\text{MPa}$, $\dot{\epsilon} =$ 1E-4 s^{-1}, ht = 5 min.

A hysteresis cycle from the alternating cyclic relaxation test with loading to $5\,\text{MPa}$ in tension, $-5\,\text{MPa}$ in compression and relaxation for $5\,\text{min}$ with 10 cycles is plotted in figure 4.15. The strain level is 0.05 % in tension and -0.035 % in compression. The relaxation is about $1\,\text{MPa}$ each cycle both in tension and in compression.
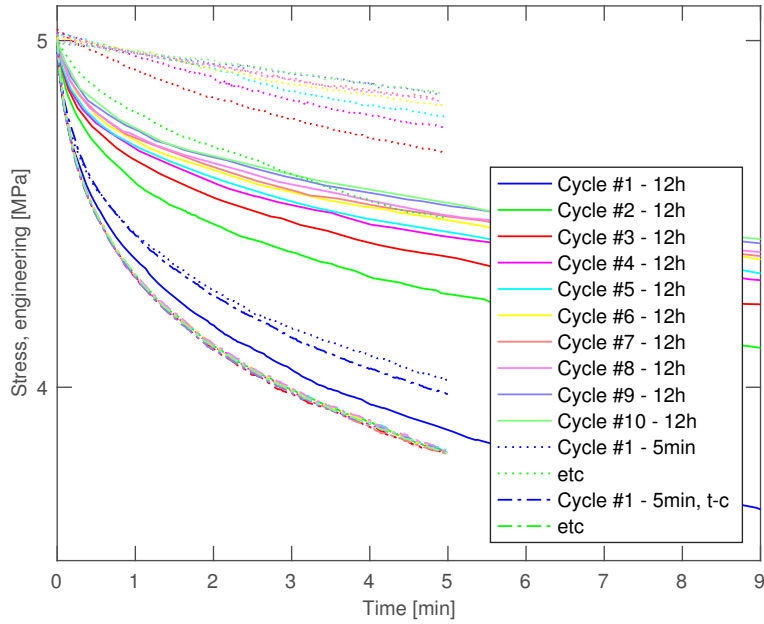
Figure 4.16: Comparison of $\sigma = 5\,\mathrm{MPa}$, ht = $5\,\mathrm{min}$; $\sigma = 5\,\mathrm{MPa}$, ht = $12\,\mathrm{h}$; and $\pm\sigma$ = $5\,\mathrm{MPa}$, ht = $5\,\mathrm{min}$. Zeroed for each cycle.

A comparison of relaxation in cyclic $5\,\mathrm{MPa}$ $5\,\mathrm{min}$, $12\,\mathrm{h}$ and the alternating cyclic relaxation test $5\,\mathrm{min}$ are compared in figure 4.16. The tests without alternations has less and less relaxation each cycle. For the one with alternation the first cycle has less relaxation than the second cycle. From the second cycle all cycles perfectly coincide.
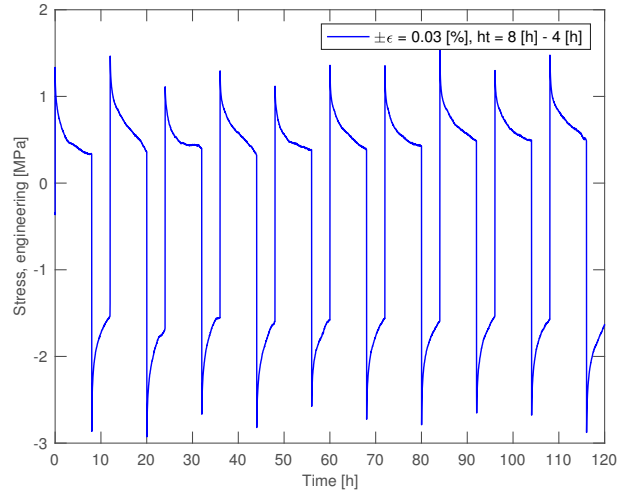
Figure 4.17: Alternating cyclic relaxation test: Stress vs time. $\pm\epsilon_{stroke} = 0.03\,\%$, $\dot{\epsilon}$ = 1E-4 s^{-1}, ht = 8 h - 4 h.
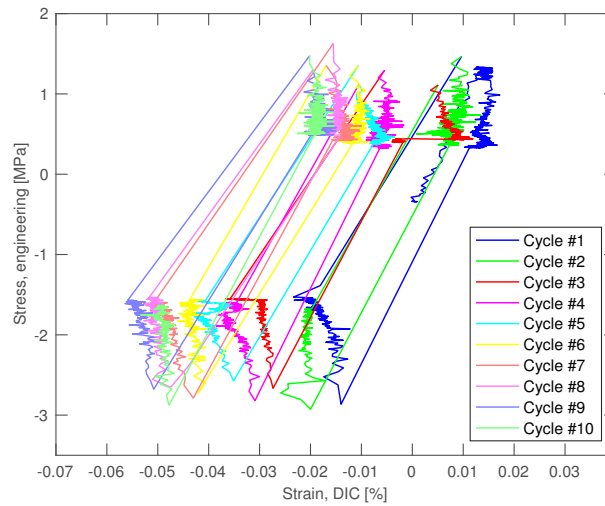
Figure 4.18: Alternating cyclic relaxation test: Stress vs strain. $\pm\epsilon_{stroke} = 0.03\,\%$, $\dot{\epsilon}$ = 1E-4 s^{-1}, ht = 8 h - 4 h.

The stroke controlled alternating cyclic relaxation test is plotted in figure 4.17. There is a biased stress condition after loading in the specimen with $1.5\,\mathrm{MPa}$ in tension and $-3\,\mathrm{MPa}$ in compression.

Each cycle is plotted individually in figure 4.18. A ratchetting effect where the strain moves into negative strain can be observed. Each cycle has an approximately strain range $0.03\,\%$, where the stroke was set to have a strain range of $0.06\,\%$.

4.2.6 Hysteresis Loops
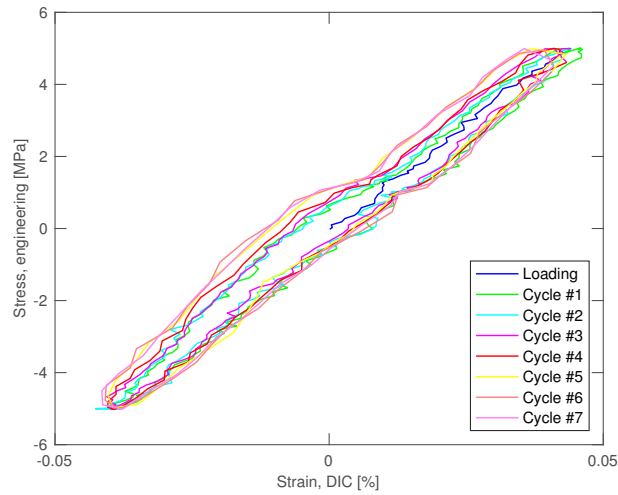
Figure 4.19: Hysteresis loop: Stress vs strain. $\pm\sigma = 5\,\mathrm{MPa}$, $\dot{\epsilon} = $ 1E-4 s^{-1}.
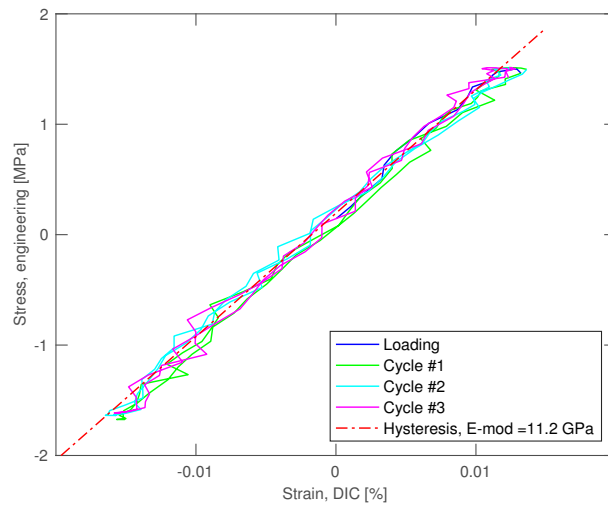
Figure 4.20: Hysteresis loop: Stress vs strain. $\pm\sigma = 5\,\mathrm{MPa}$, $\dot{\epsilon} = $ 1E-4 s^{-1}. Regression of slope is indicated in plot.

Two hysteresis tests were run, one with stress control to $\pm\sigma = 5\,\mathrm{MPa}$ and one with stroke control $\pm\epsilon_{stroke} = 0.03\,\%$. This is the same setup as the alternating cyclic relaxation tests without relaxation. The slope is calculated in the strain controlled test for comparison with the E-modulus test.

4.2.7 Specimen A to D - Tension and Compression Tests
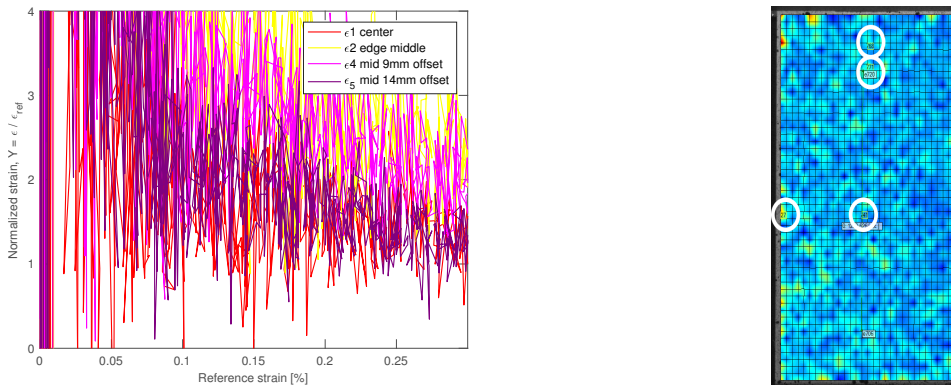
Figure 4.21: Specimen D straight, $\epsilon = 0.5\,\%$ in tension, $\dot{\epsilon} = $ 1E-4 s^{-1}, 35pix, ϵ/ϵ_{ref}
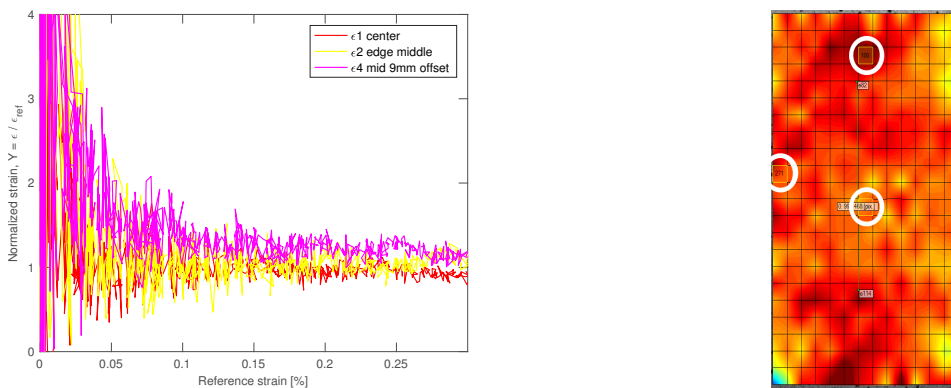
Figure 4.22: Specimen D straight, $\epsilon = 0.5\,\%$ in tension, $\dot{\epsilon} = $ 1E-4 s^{-1}, 80pix, ϵ/ϵ_{ref}
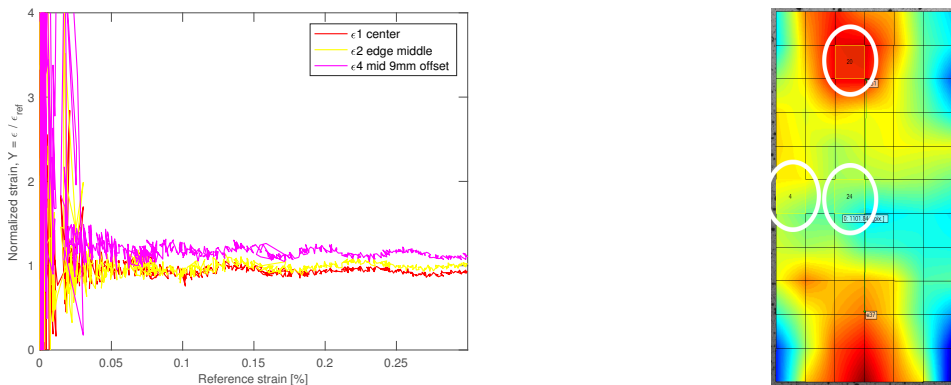
Figure 4.23: Specimen D straight, $\epsilon = 0.5\,\%$ in tension, $\dot{\epsilon} = $ 1E-4 s^{-1}, 160pix, ϵ/ϵ_{ref}.
Point 4 and 5 are merged into one point.
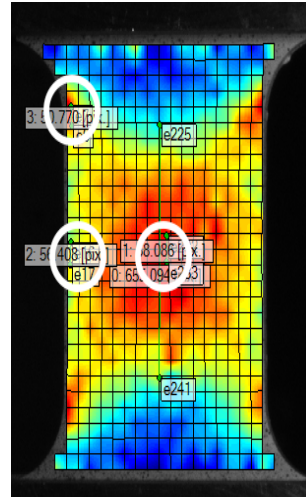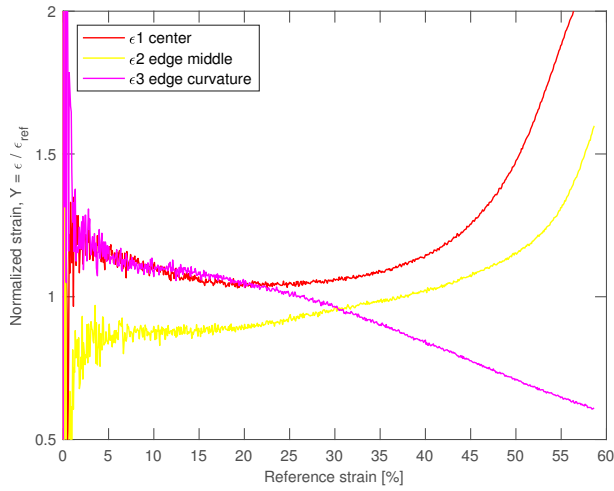
Figure 4.24: Specimen B straight, $\epsilon = 60\,\%$ in tension, $\dot{\epsilon} = $ 1E-4 s^{-1}, fine mesh, ϵ/ϵ_{ref}.
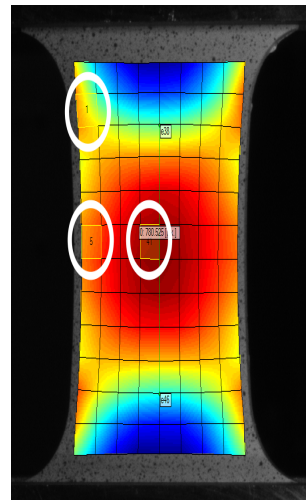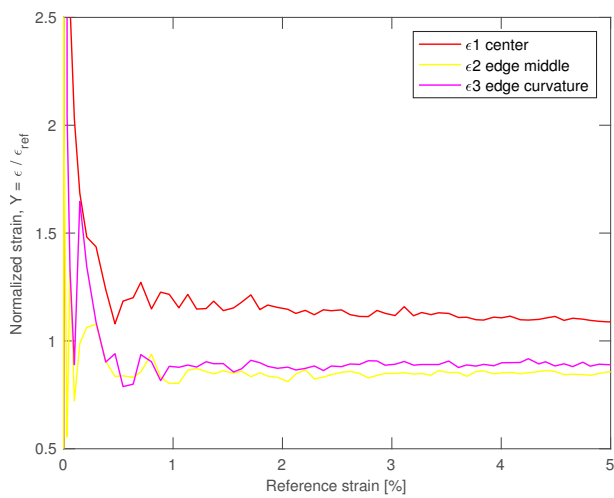
Figure 4.25: Specimen B straight, $\epsilon = 60\,\%$ in tension, $\dot{\epsilon} = $ 1E-4 s^{-1}, coarse mesh, ϵ/ϵ_{ref}.

Several tests were conducted on specimen A to D, a full overview are presented in appendix section E.1. All the tests were run to failure, except one where specimen D curved was run to strain level $\epsilon = 0.5\,\%$.

Detection of Slipping in the Grips
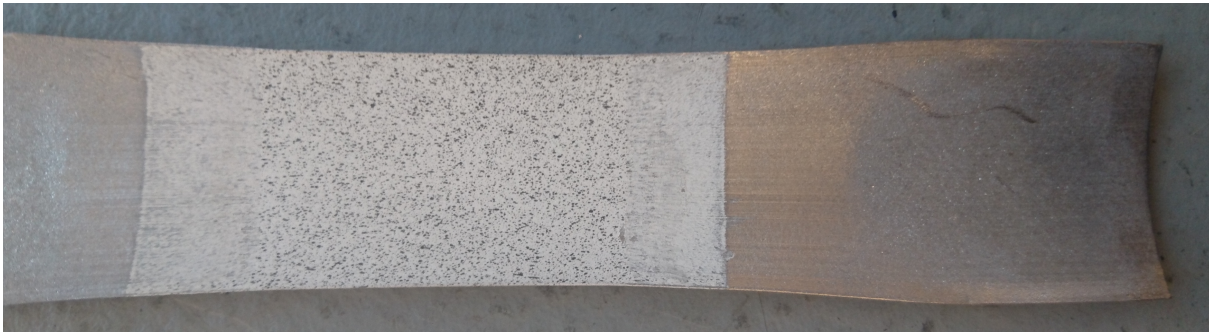
Figure 4.26: A specimen which have slipped during testing, has been taken out of the grips. The whole gripping area is scratched from slipping.
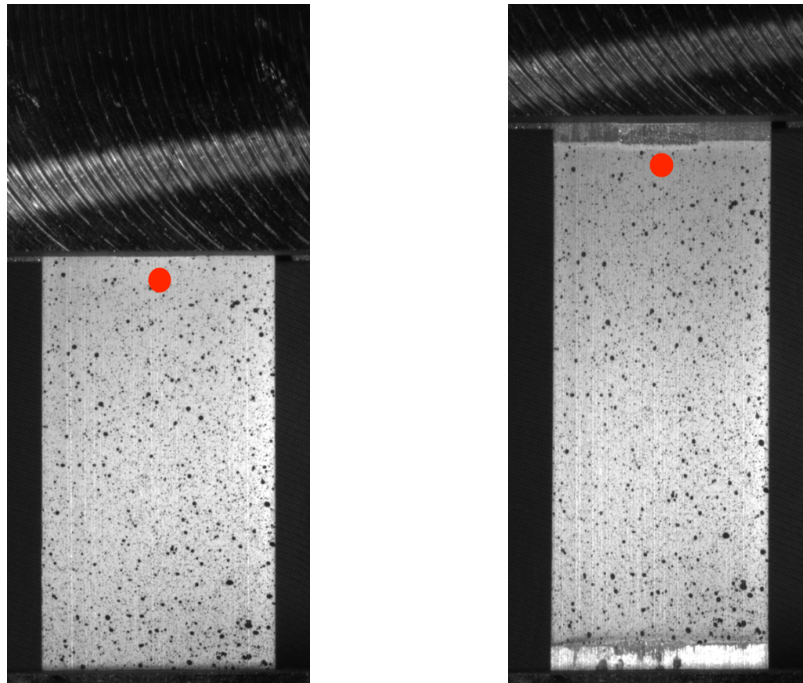
Figure 4.27: The specimen to the left is from before the test starts. The specimen to the right is after the test has finished, with a red dot indicating the position of the node used to output displacement from DIC. Slipping, seen as un-coated metal, has occurred both in top and bottom of the specimen.
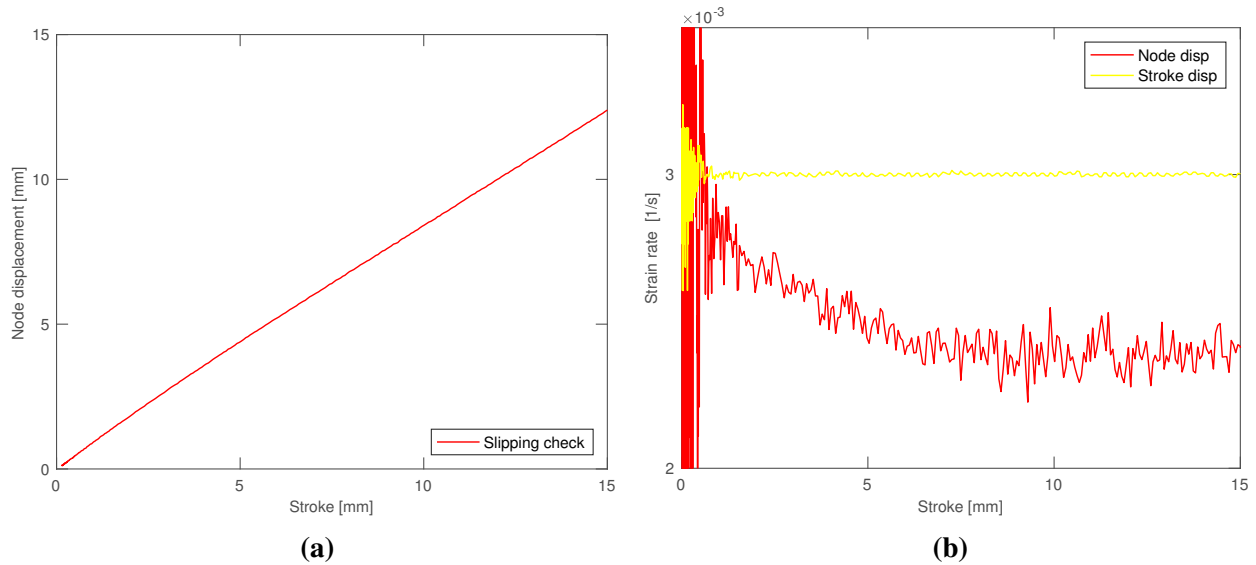
Figure 4.28: (a) Node displacement vs stroke in the machine. The node is indicated in figure 4.27, (b) Strain rate in the machine and strain rate in the node plotted against stroke in the machine.

The photos in figure 4.26 and 4.27 displays specimen A after a tension test has been performed. The specimen has been pulled out of the grips, with decreased thickness in the clamping area. Scratches in the gripping area indicates slipping while the test has been conducted.

Plots with attempts to detect slipping are presented in figure 4.28. The node displacement has a linear behavior compared to the stroke. The strain rate in the node decreases with linear behavior from the beginning of the test.

4.2.8 Fatigue test
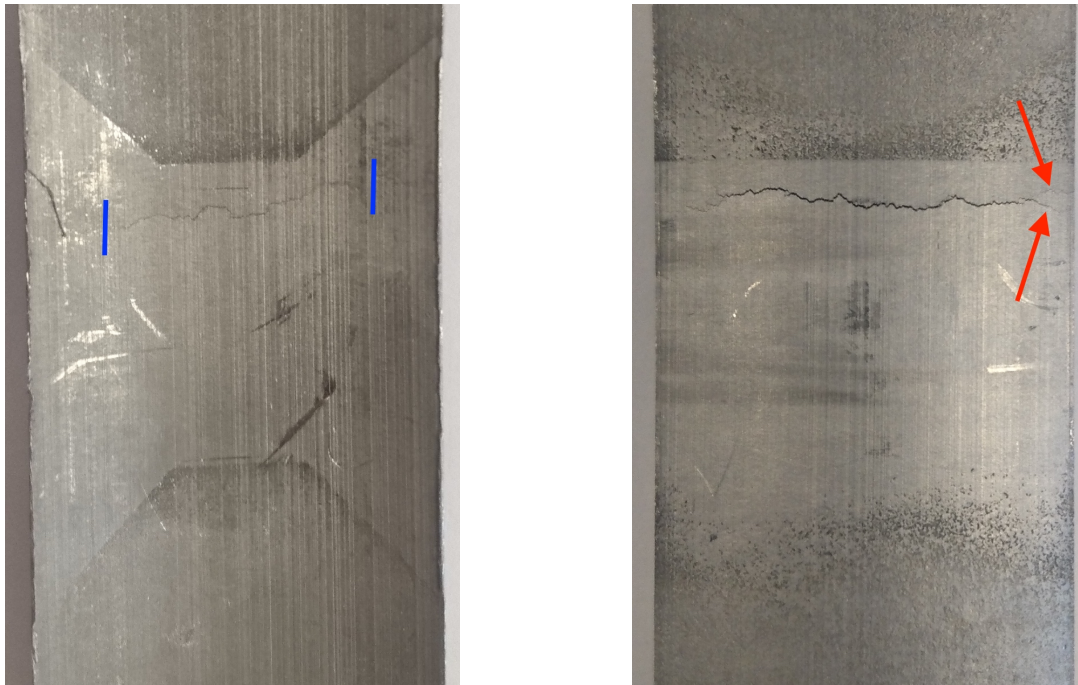
Figure 4.29: Left picture, inner radii, right picture outer of specimen D after failure. Frequency: $5\,\mathrm{Hz}$, strain range: $0.15\,\%$. Blue lines indicating ends of crack. Red arrows indicating small cracks at the edge.

The main crack is larger on the outer than the inner curvature, where the blue lines indicates the crack edges on inner curvature, see figure 4.29. The red arrows in the picture to the right indicates some small cracks going all the way to the edge. Failure happened after $N_f = 850,000$ cycles, where the load bearing capacity left were $0.2\,\mathrm{kN}$.

Discussion

5.1 Numerical Simulation

5.1.1 Specimen A to D

The numerical simulations done in Abaqus are carried out to find the most suited TSG for fatigue testing. The candidate specimens A, B C and D were investigated. The area of the specimen subjected to the highest strain is expected to be where the crack initiation takes place, ref section 2.3. The most suitable TSG would be the one with the highest small scale to real component transferability, i.e.: ideally the one which would experience crack initiation from the center rather than on the edges, since there are no edges in the lead sheathing in the SPC. From previous small scale fatigue testing performed by Alvaro in [Alvaro, 2016], crack initiation started from an edge of the TSG. This indicates that the TSG used was a limitation leading to conservative fatigue data. Due to buckling it is expected that the reference strain has to be below $\epsilon_{ref} = 0.3\,\%$. To reduce the risk for buckling it is better to have a shorter distance between the grips and to use curved specimens. The curved specimens have not been subjected to straightening, which could have an effect on the material properties, further discussed in section 5.2.3. The advantage of straightened specimens is that the tests become more universal.

To allow for a comparison between the different TSGs intended to use for fatigue testing, a common

reference had to be used since the distance between the grips and the parallel area vary for each specimen. The displacement of two points on the center line, with initial $30\,\text{mm}$ displacement were used as the reference strain, functioning as an extensometer. The ratio between the localization in AOI and the reference strain equals the normalized strain. A validation of the reference strain is done by having the normalized strain, $\epsilon_{long-mid}/\epsilon_{ref} = 1$.

Alvaro found in [Alvaro, 2016] that specimen A is more conservative than specimen B, and crack initiation happened at the onset of the parallel section both for strain range $0.15\,\%$ and $0.28\,\%$ in specimen B. This is confirmed by the predictions from the numerical simulations.

Specimen C had a very high normalized strain. Since this specimen has no parallel area, the area and volume will differ from the others within AOI. A one to one comparison with an extensometer as reference is therefore questionable and it is suggested to investigate the possibilities for using volume or a scaling factor as reference. Specimen C would be beneficial when it comes to buckling issues due to only one hinge in the geometry.

A strain hot spot were located in the center of Specimen D. The normalized strain was highest by the clamping, but this is expected to be due to numerical difficulties in the Abaqus solver. Specimen D has the lowest normalized strain, indicated that this is the most suitable TSG.

With the material properties used for these numerical simulations compression tests showed corresponding behavior of the tension tests. Therefore compression tests was not considered to be of interest for this thesis prior to obtaining a calibrated material model.

5.2   Laboratory Testing

5.2.1   Test Configuration

As explained in theory section 2.1, the stress field developing in the pipe wall under bending is mainly of tensile nature. For this reason a small scale tension test is closer than a reverse bending type of test for the lead sheathing fatigue life estimation. Therefore all the tests were conducted with a tension test configuration.

Since the lead sheathing is not providing any strength to the SPCs, a strain controlled test is more

realistic than a load controlled test. Three different methods were used to measure strain in this thesis: Extensometer, DIC and the stroke. The stroke was used by the test machine to calculate the strain. This was found to not represent the strain in the specimen very well. The strain controlled cyclic tests were examples of this. Unfortunately DIC can not be used to control the test machine, only to post-process and find the strain field afterwards. To use an laser extensometer could be a possibility, but such equipment is not available in the laboratory. From previous testing it was found that if the strain was controlled by an extensometer, the extensometer could start to slip during cycling. When the tests machine tried to compensate for this it would lead to resonance. Also the extensometer leads to crack initiation. Therefore the suggested way to control a test with the test equipment available is by load control.

The light setting is found to be unsatisfactory for tests going over a longer period of time. A better test setup should be found before running more tests.

5.2.2 Error in Test Machine

The *Zwick/Roell Z030* has a tolerance of $0.0026 \, \text{mm}$, which could possibly lead to an error of $20 \, \%$. For two of the tests the strain as low as $\epsilon = 0.03 \, \%$, which equals a stroke of $0.0132 \, \text{mm}$, on a specimen with parallel area of $44 \, \text{mm}$. The maximum force used for the tension test with thickness t = $1.0 \, \text{mm}$ and $\dot{\epsilon}$ = 1E-7 s^{-1} was $23 \, \text{N}$ and the maximum force independent of test was below $800 \, \text{N}$. The machine has the possibility to run tests up to $1755 \, \text{mm}$ and $30 \, \text{kN}$, and are therefore not the most suited machine for the testing that has been conducted. But it is assumed that the deviation in the measurements is less than the potential error. What is expected to introduce a greater uncertainty is the clamping with threads, screws in the grips and other connections causing deviation in the stroke measurement.

5.2.3 Tension Tests

To eliminate the potential error from using two different software for DIC post-processing, a comparison of results from *VIC-2D v6* and *eCorr v4.0* were made and presented in figure 4.2. The difference between the two software are minimal, indicating that the usage of different software have not influenced the results. For every DIC analysis conducted the output has been evaluated. Most of the tests had both vectors and elements outputted, and the one providing the most stable results with the least noise has been used as strain from DIC. Pictures of the two extremes $\dot{\epsilon}$ = 1E-2

s^{-1} and $\dot{\epsilon} = 1\text{E-7 s}^{-1}$ are presented in figure 4.5. There are tendencies of localization forming in the specimen to the right with, $\dot{\epsilon} = 1\text{E-7 s}^{-1}$, but the strain field is still uniformly distributed and will provided valid data for comparison.

From the plot with constant strain rate in figure 4.3, it can be seen that all the tests are work hardening. Another observation is that there is a thickness effect where the stress level increases with a larger thickness, indicated in the plot by an arrow. How the stress distribution vary between different thicknesses could be influential. Prior to testing the specimens had been machined out of pipes that had been flattened. The pipes had the same radii, so the impact on the thinnest pipe would be greater than the thickest. Flattening could have the same effect on the material as rolling, where grain size and orientation is changed during the process, which again will affect the material properties. Due to recrystallization the affect of flattening could have been restored. It is also a possibility for refinement of the grains in the thinner specimen which had undergone the greatest impact. From production the extrusion speed is greater for larger thicknesses, this could influence the material, and should be investigated trough microscopy. The author has not succeeded in pin pointing the main cause to thickness effect.

All the slopes are equal in the elastic region, except the t = 1.0 mm #1. This specimen had been clamped several times. From the plot it can be seen that the straining prior to the test severely impacted the results on the test. To handle a lead specimen with a thickness of t = 1.0 mm requires the greatest care, as it can be deformed by pinching. If the clamping was not carefully aligned a torsion would be introduced in the specimen, which would strongly influence the results.

From the plot with constant thickness in figure 4.4, it can be seen that lead is strongly dependent on strain rate. The stress decreases with decreasing strain rate. For the lower strain rates dislocations have time to cancel each other out by recovery. Recrystallization is also predicted to influence the material. With a low strain rate the material will have time to creep during testing, and therefore the maximum stress is much lower. For the $\dot{\epsilon} = 1\text{E-7 s}^{-1}$ the stress reaches a plateau in the plastic area at $\sigma = 7\,\text{MPa}$. It was investigated if this was a creep limit by running a test with sr = 1E-8, where it then should coincide. This did not happen, so further testing to find the creep rate was conducted, with results presented in section 4.2.3. For $\dot{\epsilon} = 1\text{E-7 s}^{-1}$ two parallels were carried out due to a stop in the data logging. The curves coincides, which verifies that the results are stable. For a high strain rate the yielding starts at $\epsilon = 0.1\,\%$ and for a low strain rate at $\epsilon = 0.05\,\%$.

The machine was programmed to pull the specimen to strain level $\epsilon = 3\,\%$, but AOI was found to be strained to $\epsilon = 2\,\%$ when analyzed in DIC. The actual strain rate was therefore lower than expected. To reveal if the actual strain rate from AOI differed for the different thicknesses it was plotted in figure 4.7. For strain rate $\dot{\epsilon} = $ 1E-4 s^{-1} it can be seen that the actual strain rate is lower than what the position control provides, but it is equal for all thicknesses. This indicates that the actual strain rate is not what causes the thickness effect with the different stress levels for the three thicknesses.

When running the test it starts by clamping the specimen. The stress level after clamping is $\sigma = 0.05\,\mathrm{MPa}$. Then the DIC starts recording a couple of seconds before the tests starts to load. From the recording starts to the machine starts there are no variation in stress or stroke.

If the clamping caused a pre-strain at $\epsilon = 0.006\,46\,\%$, as indicated in figure 4.6, this would be a significant part of a thermo-mechanical cycle. The stress required to reach the pre-straining is significantly higher than $\sigma = 0.05\,\mathrm{MPa}$. This stress is not high enough, nor is it enough time, for creep to take place in the specimen from the recording starts to the loading. The pre-strain observed must therefore be due to noise from the reference image in the DIC. All the curves from the tension test have therefore been moved to the origin.

5.2.4   E-modulus

To validate a test it either has to be calibrated with something that is known, or different measuring techniques has to be used. Therefore the E-modulus test in figure 4.8 was conducted with both measurements from DIC and extensometer. The results should have given the same result, since it is from the same test. The exact E-modulus is not found, but is in the area of $12\,\mathrm{GPa}$ to $15\,\mathrm{GPa}$ for this alloy. Attempts to obtain E-modulus from creep test and a hysteresis loop are compared in with the E-modulus test in figure 5.1. In literature such as [Callister and Rethwisch, 2009] and [Hofmann, 1970], lead has the E-modulus in the same range, but how the data has been obtain is seldom stated. From different testing in the laboratory it is found that lead is very sensitive to how the test is run. Therefore the accuracy of the E-modulus suggested in literature is questionable, and a further investigation should be done to obtain a more precise detection of E-modulus for this alloy. The creep test had localization in the specimen, so that was not a valid way to obtain the E-modulus. The hysteresis loop was plotted to confirm it cycled in the elastic region.
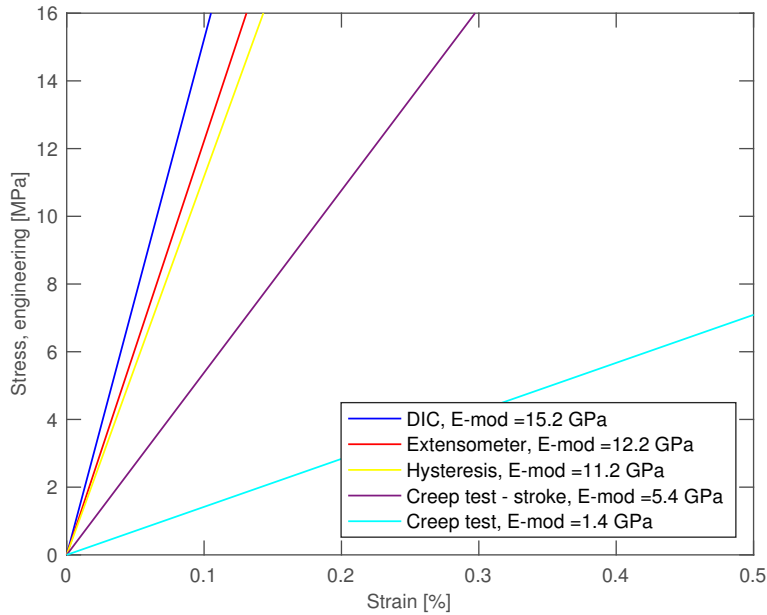
Figure 5.1: Comparison E-modulus obtained from E-modulus testing and creep test.

5.2.5 Creep Test - Constant Stress

According to [Hofmann, 1970] the secondary creep area will first be reached after several days, which implies that the creep test conducted still operates in the primary area. If that is the case, then the creep rate found will be higher than the actual creep rate in the steady state area, giving a conservative result. A creep test should be run for 10 days to confirm this, but then at a lower stress.

From the tension test in section 5.2.3 with t = 3.3, $\dot{\epsilon}$ = 1E-7 s^{-1} it reaches a plateau at $\sigma = 7\,\text{MPa}$, which implies the creep rate equals the strain rate. This is significantly higher than the creep rate found from the creep test. Further testing must be carried out to confirm the creep rate.

An attempt was made to obtain an E-modulus from unloading after the creep test. Data from different vectors were plotted in figure 4.10. Vector 1 and 2 shows a steeper curve than vector 3 and 4. A steeper curve indicates that the area has been more affected by plasticity, and will therefore not contract as much during unloading. Vector 5 shows the effects of strain localization in that area of the specimen, where no contraction takes place during unloading. Vector 3 were used for E-modulus comparison with $1.4\,\text{GPa}$, but is not valid due to a non-homogeneous specimen.

5.2.6 Relaxation Tests - Constant Strain

During the work with this thesis it was found beneficial to use a hybrid test configuration for creep and relaxation testing, to isolate the influence from different parameters. The hybrid setup is closer to the real load condition in the SPC where the lead sheathing is not providing strength (constant stress), but a displacement (constant strain). Therefore the creep testing was discontinued and the hybrid test was introduced. In the hybrid relaxation test, the specimen was loaded to a target value, and then the strain was held constant. This was found beneficial as the strain was difficult to control with the equipment available in the laboratory.

The strain obtained from DIC has a lot of noise, but are validated by following the same trend as the stroke in the stress-stroke plot in figure 4.11.

An attempt was made to obtain the E-modulus from unloading, but not enough data points could be provided. Due to non-homogeneous behavior in the specimen the results would not be valid.

The tests with a high strain rate is expected to be in the instantaneous creep area during loading, while the lower strain rates are in a transition between transient and secondary creep, ref section 2.6. The low strain rates are therefore more affected by creep damage when reaching constant strain. This resulted in a steeper relaxation slope for the tests with a high strain rate, compared to the tests with a low strain rate. Since the machine was set to reach a target load before constant strain, the strain rate strongly affected the strain level reached.

Due to the high dependency on strain rate it is suggested to compare tests with equal strain rate, rather than equal loading stress. It can be seen that the two lines $\sigma = 5\,\mathrm{MPa}$, $\dot{\epsilon} = 1\mathrm{E}\text{-}4\,\mathrm{s}^{-1}$ and $\sigma = 8\,\mathrm{MPa}$, $\dot{\epsilon} = 1\mathrm{E}\text{-}4\,\mathrm{s}^{-1}$ has a similar slope, in figure 4.12, with $1\,\mathrm{MPa}$ in difference. An attempt to find a trend was made in appendix section E.4 figure E.40.

In these tests the different slopes shows strong dependency on loading history, where the stress decreases faster for the tests which have been subjected to less creep (high strain rate). It was expected that the curves would come to the same stress level in the end of the test. Hopkin and Thwaites presented in [Hofmann, 1970] that a creep test with different pre-strain will stabilize after 30 to 40 days. For the relaxation test to reach the same stress level could take weeks. For polymers it is normal to make the different test historyless, but this turned out to be challenging with lead

where the history makes a significant impact on the test.

5.2.7   Cyclic and Alternating Cyclic Relaxation Tests

Unfortunately it was not possible to obtain strain from DIC from the cyclic relaxation test, $\sigma = 5\,\mathrm{MPa}$, ht = 5 min, due to error in the data logging. Instead the stress-stroke was plotted in figure 4.13. During the relaxation no movement can be detected in the stroke, nor can it for the other tests, indicating that the test machine does not influence the relaxation measurement by strain.

A decrease in relaxation is observed in figure 4.13. Relaxation appears to be most prominent for the early loading, reducing stresses in the material by $1\,\mathrm{MPa}$. Following 5-6 cycles, the relaxation component is reduced by a factor of 5. If the dominant creep mechanism in the sample is dislocation glide, the reduction in recovery might be explained by a strain hardening of the material, reducing dislocation mobility and thereby relaxation. Dislocation climb will, if present, allow for dislocation movement even in heavily work hardened material, allowing for some relaxation. Dislocation climb is a more probable mechanism in the steady state area of the graph, indicated by reduced relaxation.

Figure 4.14 shows relaxation in a material allowed to rest for 12 hours between each loading. Only minor changes in relaxation is seen throughout this test, contrary to the results in figure 4.13. The reason for this could be that the additional time between each loading allows for recovery and recrystallization, removing any effect of work hardening between each cycle. In this period diffusion controlled creep mechanisms could contribute to the total relaxation of the sample.

The hysteresis curve of the alternating cyclic relaxation test represented in figure 4.15 implies similar results as in figure 4.14. This result is unexpected, as this would imply that the material experiences significantly more creep after being subjected to a combination of compression and tension than pure tension tests. If the reduction in relaxation seen in figure figure 4.13 is in fact due to work hardening of the material, the same would be expected in figure 4.15 given the extensive deformation caused by cyclic compression - tension. The steady state of relaxation observed in figure 4.15 challenges the understanding of creep in figure 4.13, without offering further explanations. The author has not succeeded in finding an adequate explanation to the combination of figures 4.13 - 4.15.

Due to few logging points in the DIC logging, some relaxation has already taken place for the

first data point after a cycle in figure 4.14. The scaled down stroke provides the correct stress level, but the the DIC and the stroke does not follow each other properly. This indicates that the strain should not be obtained from the stroke, and a geometry factor can not be used to predict the strain from the stroke.

The first cycle in figure 4.16 should be identical for all the tests, since it has the same pre-stress and strain rate. Even though the tests are not coinciding the first cycle, they are thought to be close enough for a valid comparison.

Since the relaxation tests are a hybrid between a relaxation test and a creep test, the strain range for each cycle will not be constant for the tests without alternation. For the alternating cyclic relaxation test, the strain range each alteration is constant. A correlation can be seen between the strain range from the previous cycle and the amount of relaxation. Even though the strain range is different, the driving force after each loading is equal allowing for a comparison between the three tests.

According to customer a test configuration with a biased relaxation time is close to the real condition in a SPC. The test to simulate this is presented in figure 4.17 with ht = $8\,\mathrm{h}$ in tension and ht = $4\,\mathrm{h}$ in compression with alternating strain level $\pm\epsilon = 0.03\,\%$.

With a logging acquisition at $0.01\,\mathrm{Hz}$ a pictures is taken every $100\,\mathrm{sec}$ in the DIC. That allows for some relaxation before the first logging after a loading, in figure 4.17. How long it takes for the first logging after loading varies, therefore the maximum stress in tension and the minimum stress in compression can not be compared.

For every tension cycle the relaxation in about $1\,\mathrm{MPa}$, while in compression about $1.5\,\mathrm{MPa}$. The difference in relaxation is expected to be due to the biased stress condition causing a higher driving force in compression.

From cycle 3 to cycle 4 there is a drop in the strain. This is caused by the light conditions changing, which affects the DIC analysis. Therefore the strain level is not trust worthy in this test, but the tendency with ratchetting is believed to be valid, due to the biased stress.

To validate the test it should be re-run with better light conditions to improve the DIC results.

To find what influence a biased relaxation time has, it should be tested in a separate test without biased stress state. To verify that the ratchetting effect was due to a biased stress state, and not noise in the DIC or biased relaxation time, a test without biased relaxation time should be performed. This will reduce the complexity of the test results, and reveal how the material behaves under a biased stress state without the influence of other unknown parameters.

Due to very low strain levels, the deviation in the clamping and grips could influence the measurements significantly when the test cycles from tension to compression. The stroke measurement did not account for this, so the actual strain was diverging from the stroke, as seen in figure 4.18. A stroke controlled test could not be used as a strain controlled test. It is better to have a test controlled with loading, when the stroke is not representing the strain.

5.2.8   Hysteresis Loops

The stress control is plotted in figure 4.19 and strain control in figure 4.20. The stress controlled test stabilizes after 5 cycles, and seems to have an elastic behavior the whole test. No cyclic softening or hardening is observed. This could also be due to noise in the data.

A jump in strain can be observed at $\sigma = 1\,\mathrm{MPa}$. This is probably due to an error, and should be checked by running a new test. The stress controlled hysteresis loop and the alternating cyclic relaxation test with stress $\pm\sigma = 5\,\mathrm{MPa}$ in figure 4.15, show similar behavior, and goes to the same strain level each cycle. Relaxation does not seem to affect the stress strain cycle significantly.

The strain controlled hysteresis loop is going up and down the same path, and is in the elastic area. Even though it is stroke controlled, the strain goes to the reversed value in compression. There is no sign of deviation in the clamping. Since R = -1, the biased stress condition in the stroke controlled alternation cyclic relaxation test in figure 4.18 is likely due to relaxation.

5.2.9   Specimen A to D

Due to difficulties with the grips, specimen A straight and curved and specimen D curved had no valid tests. Compression tests were conducted, but the results has not been presented here since the noise from the post-procession with DIC was more critical than the tension tests. The compression tests did not experience the same problem with slipping in the grips though.

Numerical simulations of specimen A to D was intended to be compared with laboratory testing. This turned out to be challenging due to noise in the DIC analysis prior to the strain level $\epsilon = 3\%$, and the numerical simulations only went to the strain level $\epsilon = 0.5\%$. The results from DIC were only valid for a qualitative, not quantitative, comparison. To get more images from strain of interest in the DIC analysis one test was run to strain level $\epsilon = 0.5\%$.

The size of the elements used for post-processing in the DIC analysis are of great importance, where there will be a compromise between noise in the data and the degree of localization. This is demonstrated in figure 4.21, 4.22 and 4.23. The noise decreases as the element size in the DIC analysis increases. The strain hot spot can not be detected when the elements get to big. This is clearly displayed in figure 4.24 and 4.25, where the edge curvature, point (3), loses the hot spot when the element size increase.

The strain rate in the laboratory testing was calculated based on the reference strain. Since the reference area are the same, but the distance between the grips is different, the strain rate will be different for specimen A, B, C and D. The strain rate is found to be an important variable for lead, but is not expected to make a difference for comparison of strain field, since it is the ratio between the reference area and localization that is of interest.

A test will not be valid after slipping in the grips has occurred, therefore attempts to detect it was made. After a test is finished, a visual inspection would reveal if the specimen was slipping, as in figure 4.26 and 4.27. The displacement in the node from DIC analysis was plotted against stroke in the machine in figure 4.28a. A deviation from linear behavior, which was not observed, would indicate slipping. In figure 4.28 the strain rate in the node was compared with the strain rate in the stroke. Since the strain rate decreases from the beginning of the test it is found that slipping from the grip happens smoothly. Even though it has been used sandblasted grips, sandpaper and screws for the test, a specimen without narrowing should not be used for testing at large strain levels.

5.2.10   Fatigue Test

The fatigue test was conducted with a shortened specimen D to verify the finding from numerical simulations. From the fatigue test conducted in the laboratory, the crack was located close to the clamping, ref figure 4.29. This makes it difficult to predict if the clamping or the shear forces caused the strain hot spot. The small cracks going to the edge are not trough thickness. Therefore

it is not expected to be where the crack is initiated.

Failure happened after N_f = 850,000 cycles. This is an improvement from previous tests done by Alvaro in [Alvaro, 2016]. Specimen D is very promising as a TSG to use for further fatigue testing.

Unfortunately a outer grip with $45°$ could not be provided for this test. This is not expected to have a significant influence on the results, as the pressure of the inner clamping will be governing.

The strain target value could have been loaded to ϵ_{amp} instead of ϵ_{mean}, but this would be further from the real condition in the SPC where the minimum value is limited by the core of the cable.

From previous testing conducted by Alvaro in [Alvaro, 2016] it is found that there is a large strain in the lead sheathing when the fatigue testing starts. Due to the high plasticity in the material there will be plastic deformation in both directions of the fatigue test, causing compression when cycling back to the initial position. After a few cycles the load stabilizes, and the R-ratio $\approx$ -1, even though this test is strain controlled.

5.2.11   Main Findings

Time is found to be one of the main governing parameters for lead, since it controls strain rate, creep, relaxation, recovery and recrystallization. Strain level is another important parameter which is affecting the number of dislocations, and is together with strain rate closely related to stress level.

The main findings from the laboratory testing of the lead sheathing are illustrated in figure 5.2. This plot shows the number of cycles to failure plotted against strain rate, where the expected qualitative behavior of the lead sheathing is indicated. The quantitative measurements added in the plot will vary for different lead alloys.
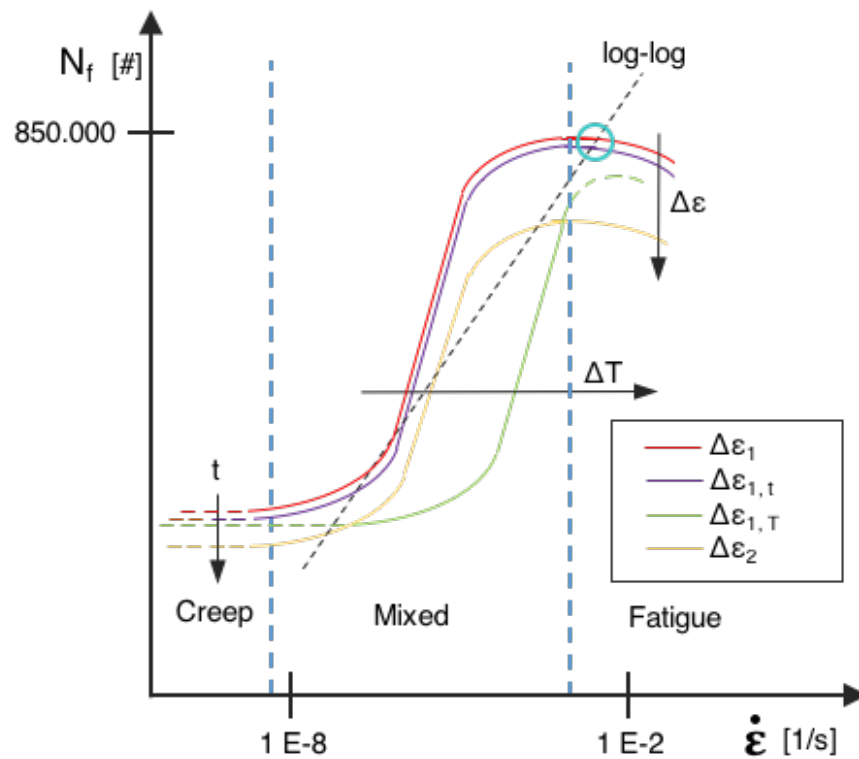
Figure 5.2: Main findings presented in a number of cycles to failure vs strain rate plot. Blue lines indicates area where creep and fatigue is the governing failure mechanism.

There are four lines in the plot: The red line indicates the reference, the purple line indicates tests conducted with a thicker specimen, the green line indicates tests that were conducted at an elevated temperature and the yellow line indicates tests that were conducted with a higher strain range. The Y-axis indicates the number of cycles to failure. The strain rate on the X-axis is divided into three stages by two vertical blue lines. They indicate the transition from the lowest strain rate where creep is the governing failure mechanism, the mixed zone where there is creep-fatigue interaction, and the fatigue governed area with the highest strain rate, at ambient temperature. The material does not have time to creep at high strain rates. The number of cycles to failure goes down from $\dot{\epsilon} = 7.5\text{E-}3$ s^{-1} to $\dot{\epsilon} = 1.5\text{E-}2$ s^{-1} based on the findings done by Alvaro found in [Alvaro, 2016]. A tension test was run at strain rate $\dot{\epsilon} = 1\text{E-}8$ s^{-1}, but this was not coinciding with the stress level of $\dot{\epsilon} = 1\text{E-}7$ s^{-1} so the creep governed area is expected to be a bit lower than $\dot{\epsilon} = 1\text{E-}8$ s^{-1}. The highest strain rate used for a tension test was $\dot{\epsilon} = 1\text{E-}2$ s^{-1}, and this was close to the stress level of $\dot{\epsilon} = 1\text{E-}3$ s^{-1}, so the transition from mixed mechanism to fatigue dominated degradation is expected to be found there. Based on this observation the SPC will always be operating in mixed mechanism both

during installation and daily cycles.

The purple line represents the thickness effect seen in tension testing section 5.2.3. With increasing thickness, the number of cycles to failure is expected to decrease. From tension testing it is found that a thicker specimen is subjected to a higher stress at the same strain both at low and high strain rates. In the creep governed area the creep defects will be more severe causing fewer cycles to failure. In the fatigue governed area a higher stress will cause more severe crack initiation. A thinner specimen is expected to have more cycles to crack initiation, but the number of cycles to failure after the crack is initiated will be low due to rapid growth trough the ligament.

The yellow line represents tests with higher strain range than the red reference line. The higher range strain causes greater dislocations each cycle, leading to failure sooner, as described in section 2.7. From the relaxation test in section 4.2.4, it was found that tests with equal strain rate had a similar slope during relaxation. Therefore the yellow line and the red reference line has the same slope, only phase displaced.

The green line represents tests conducted at a higher temperature than the red reference line. Since creep is temperature dependent, it will become more critical if the temperature is elevated. Creep and relaxation are two different mechanisms accommodating each other. A higher creep is indicated in the figure by the green line being phase displaced from the red line. The blue vertical lines would also have to be moved to show the new transition from creep to mixed to fatigue governed area. For lowered temperatures it is expected to go the other way. The customer has not provided information of what the temperature will be in the SPC during operation in the seabed, but this should be taken into account for further testing when temperature will be an investigated parameter.

The SPC is operating in the mixed area. This means that the number of cycles to failure will be too high for a fatigue test performed with a strain rate where creep does not affect the test. From fatigue testing it is normal to find a log-log trend from the test data, which can be extrapolated. But to extrapolate data over strain rates can introduce great errors, due to different creep mechanisms acting at different strain levels. A more accurate method to use is to run tests at elevated temperatures to have a common creep mechanism between the real situation and the test. A time–temperature parameter will then have to be used.

The fatigue test failed after N_f = 850,000 cycles with the strain range $\Delta\epsilon = 0.15\,\%$ and the frequency $5\,\mathrm{Hz}$. This equals a strain rate of $\dot{\epsilon}$ = 7.5E-3 s^{-1}, which is marked by an "O" in the plot. Results from [Alvaro, 2016] are confidential, and can not be added in the plot.

5.2.12   Safety Factor

"The mechanical properties of lead and its alloys, particularly the more dilute alloys, are extremely sensitive to variations in composition, grain size, metallurgical history and temperature and rate of testing. They are therefore rarely reproducible with any degree of accuracy, except on the same sample under identical test conditions and, even then, a delay of a few hours between tests may affect the results obtained" [Gale and T. C. Totemeier, 2004]. When calculation the fatigue life for a component where lead is used, there will be uncertainties in the data obtained. Also Gale and Totemeier experienced during their work that lead is vulnerable to the circumstances, and easily affected by the environment. The authors recommendation is that a safety factor for life time estimations of a component should be set accordingly.

Conclusion

- For small scale fatigue testing and fatigue lifetime estimation of the lead sheathing in a SPC, a tension test configuration is suggested, instead of a three point bending test, since the stress field over the cross-section area is more realistic. In general a specimen in curved configuration is recommended for two reasons: it offer an higher resistance against buckling, and it excludes any possible material variation induced by a flattening procedure. On the other hand, a straight specimen would be more universal. Specimen D seems to be a very promising TSG based on the results from the numerical simulations and the fatigue test conducted. The specimen has a short distance between the grips, and interaction between tension and shear forces causing a hot spot in the center of the specimen.

- Three different lead sheathing thicknesses have been investigated, and a thickness effect was found on the material stress-strain response. This can be due to several reasons: different pre-strain levels induced by the flattening procedure; different microstructures inherited by the different manufacturing parameters; different stress distribution in the specimens or; the actual strain rate for the three thicknesses differ.

- Since lead is a soft and ductile material it is suggested to use strain to control tests. In this thesis strain measurements have been performed through extensometers, DIC technique and calculations based on the stroke from the test machine. Stroke has proven to be a very inaccurate strain measurement. Also extensometers are very challenging to use with lead.

Since DIC can not be used as a test machine controller, load control was found to be the best way to control a test, as the strain field still can be obtained by using DIC for post-processing. To obtain satisfying results for strain measurements by DIC from tests going over a long period of time, better lights must be provided.

- Time is found to be a very important parameter for lead, as strain rate, creep, relaxation and recrystallization depends on it. During operation the SPC will be subjected to both creep and fatigue. This condition is more severe than only fatigue. Creep will only take place at lower strain rates and a fatigue test will therefore not represent the real situation. To adjust for this, the test can be performed with elevated temperatures. This will allow for the test to be subjected to the same creep mechanisms, as during operation, at higher strain rates. A time-temperature parameter can then be used to find the number of cycles to failure at operation temperatures.

CHAPTER 7

Further Work

- On a continuum scale, the material behavior in lead is more comparable with a polymer than a metal, due to the ductile character with low yield strength and high plasticity. Based on the laboratory results a calibrated material model should be made for further numerical simulations.

- A better understanding of the creep mechanisms in alternating relaxation cycles is needed. The material response during compression is therefore crucial to observe, for a comparison with tension tests. Compression testing will also obtain required strain rate and thickness dependency data for compression for the material model calibration.

- Microstructural investigation is of great importance, as the only mean to unveil the interplay between the different mechanisms in the creep-fatigue interaction. Furthermore the effect of recrystallization and grain size should be studied, to find how flattening and production methods influence the material.

- A study to reveal how the failure mechanisms in lead is affected by temperature should be conducted. This will allow for a time-temperature parameter to be found, to better predict the number of cycles to failure in the lead sheathing during operation, compared to the fatigue testing at elevated strain rates.

Bibliography

[AST, 2012] (2012). Astm e606/e606m-12 standard test method for strain-controlled fatigue testing.

[Alvaro, 2016] Alvaro, A. (2016). Test report: Effect of particles on fatigue life of lead protective sheathing. Technical report, SINTEF.

[Anderson and Anderson, 2005] Anderson, T. and Anderson, T. (2005). *Fracture Mechanics: Fundamentals and Applications, Third Edition*. Taylor & Francis.

[Anelli et al., 1988] Anelli, P., Donazzi, F., and Lawson, W. G. (1988). The fatigue life of lead alloy e as a sheathing material for submarine power cables. *IEEE Transactions on Power Delivery*, 3((1)):69 – 75.

[Blaskett and Boxall, 1990] Blaskett, D. R. and Boxall, D. (1990). *Lead and its Alloys*. Ellis Horwood Limited.

[Brinson and Brinson, 2015] Brinson, H. F. and Brinson, L. C. (2015). *Polymer Engineering Science and Viscoelasticity*. Springer, second edition.

[Callister and Rethwisch, 2009] Callister, W. and Rethwisch, D. (2009). *Materials Science and Engineering: An Introduction, 8th Edition*. John Wiley & Sons, Inc. ISBN: 9780470941669.

[Corporation, 2015] Corporation, P. D. C. T. (2015). Phelps dodge conductor type xlpe insulated lead sheathed cable. `http://www.pdcable.com/Lead_Sheathed/ls-lv-mc.htm`. Accessed: 2016-12-01.

[Dieter, 1988] Dieter, G. E. (1988). *Mechanical Metallurgy*. McGraw-Hill Book Co.

[Dowling et al., 2013] Dowling, N., Prasad, K., and Narayanasamy, R. (2013). *Mechanical Behavior of Materials: Engineering Methods for Deformation, Fracture, and Fatigue*. Always learning. Pearson.

[Drury et al., 1989] Drury, M. R., Humphreys, F. J., and White, S. H. (1989). Effect of dynamic recrystallization on the importance of grain-boundary sliding during creep. *Journal of Materials Science*, 24(1):154–162.

[Fagerholt, 2011] Fagerholt, E. (2011). Phd - field measurements in mechanical testing using close-range photogrammetry and digital image analysis. *Synopsis*.

[Fagerholt, 2017] Fagerholt, E. (2017). ecorr v4.0 documentation. `http://folk.ntnu.no/egilf/ecorr/doc/index.html`. Accessed: 2017-03-17.

[Felippa, 2016] Felippa, C. (2016). *Nonlinear Finite Element Methods*. University of Colorado at Boulder.

[Gale and T. C. Totemeier, 2004] Gale, W. F. and T. C. Totemeier (2004). *Smithells Metals Reference Book*. Elsevier, 8th edition edition.

[Halama et al., 2012] Halama, R., Sedlák, J., and Šofer, M. (2012). Phenomenological modelling of cyclic plasticity, numerical modelling. `https://www.intechopen.com/books/numerical-modelling/phenomenological-modelling-of-cyclic-plasticity`. Accessed: 2017-04-26.

[Hofmann, 1970] Hofmann, W. (1970). *Lead and Lead Alloys*. Springer-Verlag, second revised german edition edition.

[Holdsworth, 2015] Holdsworth, S. (2015). Creep-fatigue failure diagnosis. *Materials*, 8(11):7757–7769.

[Hotta et al., 2007] Hotta, S., Matsumoto, K., Murakami, T., Narushima, T., and Ouchi, C. (2007). Dynamic and static restoration behaviors of pure lead and tin in the ambient temperature range. *Materials Transactions*, 48:2665–2673.

[Nexans, 2015] Nexans (2015). Project description: Next-generation damage based fatigue design of cable sheathing (reface).

[Ohno and Wang, 1995] Ohno, N. and Wang, J. (1995). On modelling of kinematic hardening for ratcheting behaviour. *Nuclear Engineering and Design*, 153(2):205 – 212.

[Pan et al., 2009] Pan, B., Qian, K., Xie, H., and Asundi, A. (2009). Two-dimensional digital image correlation for in-plane displacement and strain measurement: a review. *Measurement science and technology*, 20(6):062001.

[Simonsen and Solutions, 2016] Simonsen, M. and Solutions, C. (2016). Vic-2d v6 reference manual. `http://correlatedsolutions.com/support/index.php?/Knowledgebase/Article/View/56/14/vic-2d-6-manual`. Accessed: 2017-10-02.

[Standard, 2009] Standard, E. (2009). Metallic materials - tensile testing - part 1: Method of test at room temperature (iso 6892-1:2009). Technical report, European Standard.

[Sutton et al., 2009] Sutton, M. A., Orteu, J.-J., and Schreier, H. W. (2009). *Image Correlation for Shape, Motion and Deformation Measurements*. Springer.

[Wood et al., 1970] Wood, H. A., Bader, R. M., Trapp, W. J., Hoener, R. F., and Donat, R. C. (1970). Proceedings of the air force conference on fatigue and fracture of aircraft structures and materials held at miami beach, florida on 15-18 december 1969.

[Worzyk, 2009] Worzyk, T. (2009). *Submarine Power Cables*. Number 1. Springer-Verlag Berlin Heidelberg.

APPENDIX A

Machine Drawings

This page is intentionally left blank.

A.1   Dog Bone Specimens
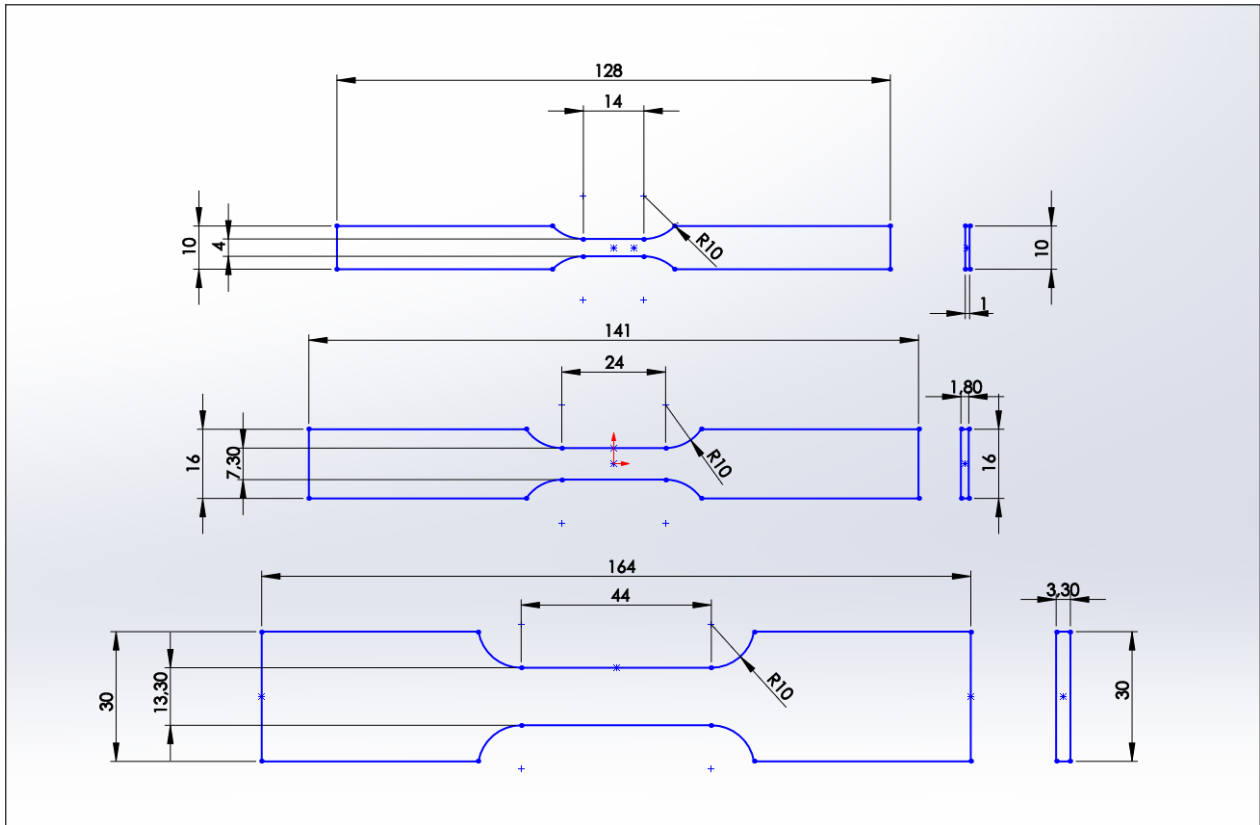
Figure A.1: Machine drawings of dog bone specimens used for tension testing, machined from lead sheaths with thickness $1.0\,\mathrm{mm}$, $1.8\,\mathrm{mm}$ and $3.3\,\mathrm{mm}$.

A.2 Specimen A to D
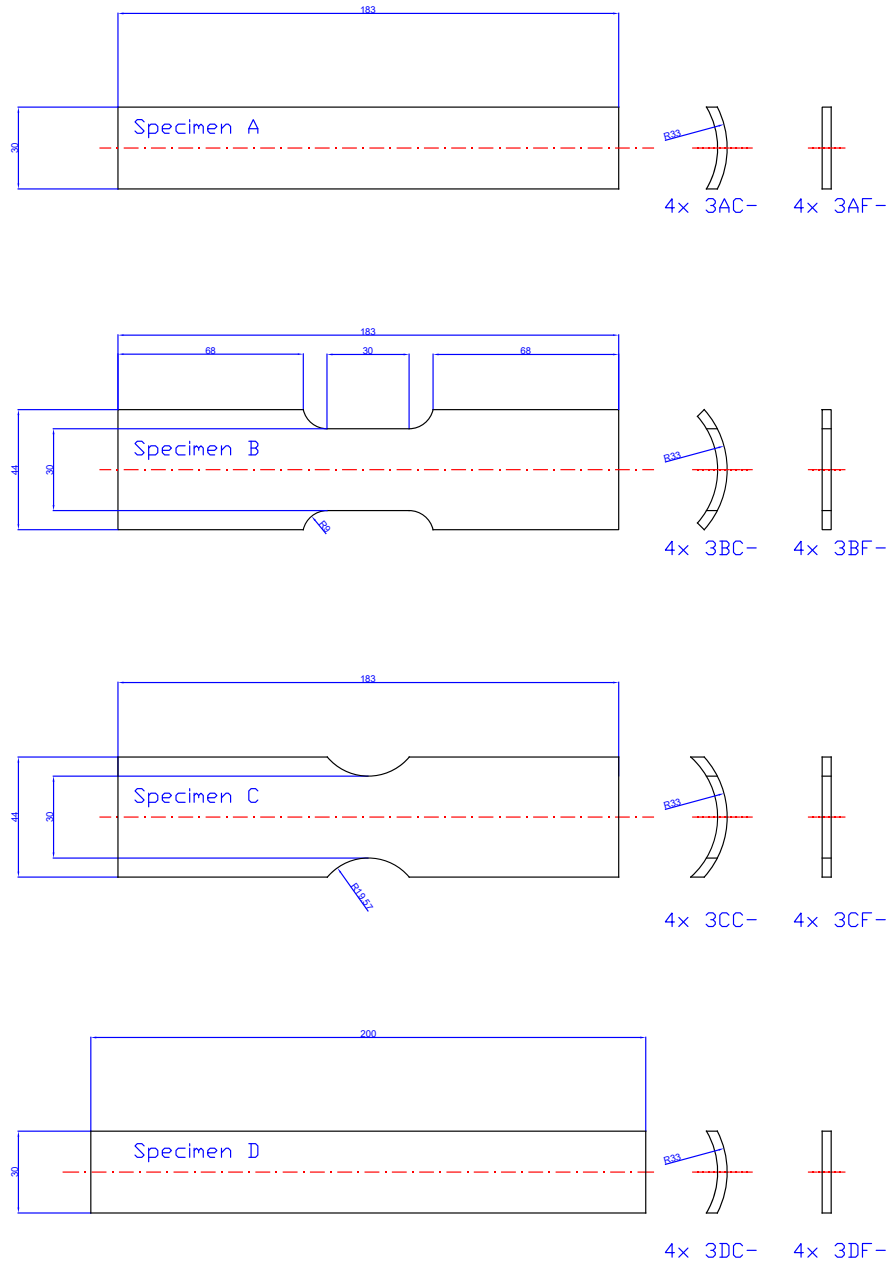
Figure A.2: Machine drawings of specimen A, B, C and D both curved and straight, machined from lead sheaths with thickness $3.3\,\mathrm{mm}$.

Numerical Simulations and Laboratory Tests Conducted

.

This page is intentionally left blank.

Numerical Simulations		
Tension:	Specimen A curved	
	Specimen A straight	
	Specimen B curved	
	Specimen B straight	
	Specimen C curved	
	Specimen C straight	
	Specimen D curved	
	Specimen D straight	
Compression:	Specimen A curved	Missing calibrated material model
	Specimen A straight	Missing calibrated material model
	Specimen B curved	Missing calibrated material model
	Specimen B straight	Missing calibrated material model
	Specimen C curved	Missing calibrated material model
	Specimen C straight	Missing calibrated material model
	Specimen D curved	Missing calibrated material model
	Specimen D straight	Missing calibrated material model

Laboratory Testing	

Tension Test	
Dog Bone Specimen	
Thickness:	Strain Rate:
1,0	1E-02
1,0	1E-03
1,0	1E-04
1,0	1E-05
1,0	1E-07
1,8	1E-02
1,8	1E-03
1,8	1E-04
1,8	1E-05
1,8	1E-07
3,3	1E-02
3,3	1E-03
3,3	1E-04
3,3	1E-05
3,3	1E-07
3,3	1E-08

E-modulus Test	
Dog Bone Specimen	
Thickness: 3,3	
Strain Rate [1/s]:	
1,00E-04	

Creep Test	
Dog Bone Specimen	
Thickness: 3,3	
Stress [MPa]:	Pre-Strain Rate:
10	1E-03

Relaxation Test	
Dog Bone Specimen	
Thickness: 3,3	
Pre-stress [MPa]:	Pre-Strain Rate [1/s]:
10	1E-03
5	1E-04
5	1E-07
8	1E-04

Cyclic Relaxation Test		
Dog Bone Specimen		
Thickness: 3,3		
Cycles: 10		
Pre-stress [MPa]:	Strain Rate [1/s]:	Hold Time:
5	1E-04	5 [min]
5	1E-04	12 [h]

Alternating Cyclic Relaxation Test		
Dog Bone Specimen		
Thickness: 3,3		
Cycles: 10		
Tension [MPa]:	Hold Time [min]:	Strain Rate [1/s]:
5 to -5	5 and 5	1E-04
Strain [%]:	Hold Time [h]:	Strain Rate [1/s]:
0,03 to -0.03	8 and 4	1E-04

Hysteresis Loop		
Dog Bone Specimen		
Thickness: 3,3		
Cycles: 20		
Tension [MPa]:	Compression [MPa]:	Strain Rate [1/s]:
5	-5	1E-04
Strain [%]:	Strain [%]:	Strain Rate [1/s]:
0,03	-0,03	1E-04

Specimen A to D		
Thickness: 3,3		
Strain Rate [1/s]: 1E-04		
Tension:	Specimen A curved	Failed
	Specimen A straight	Failed
	Specimen B curved	
	Specimen B straight	
	Specimen C curved	
	Specimen C straight	
	Specimen D curved	Missing grips
	Specimen D straight	
Compression:	Specimen A curved	
	Specimen A straight	
	Specimen B curved	
	Specimen B straight	
	Specimen C curved	
	Specimen C straight	
	Specimen D curved	Missing grips
	Specimen D straight	

Fatigue Test	
Thickness: 3,3	
Specimen D curved	
Frequency [1/s]:	Strain Range [%]:
5	0,15

APPENDIX C

Results from Numerical Simulations

Both a figure of the strain and the stress field is showed in this section for a qualitatively comparison. The areas where data is outputted from is indicated with red circles and lines, while the grips are indicated by pink lines.

- $\epsilon_{long-mid}$ = average of max principal strain in the longitudinal mid plane.
- $\epsilon_{trans-mid}$ = average of max principal strain in the transverse mid plane.

C.1 Specimen A

Specimen A has the highest strain peak at the edge by the clamping, point (3), see figure C.1. This would be where cracking is expected to happen during testing, even though FEM analysis are not trust worthy at sharp edges. $\epsilon_{long-mid} = 1$, which validates the reference strain. Both the curved and the straight show the same tendency.
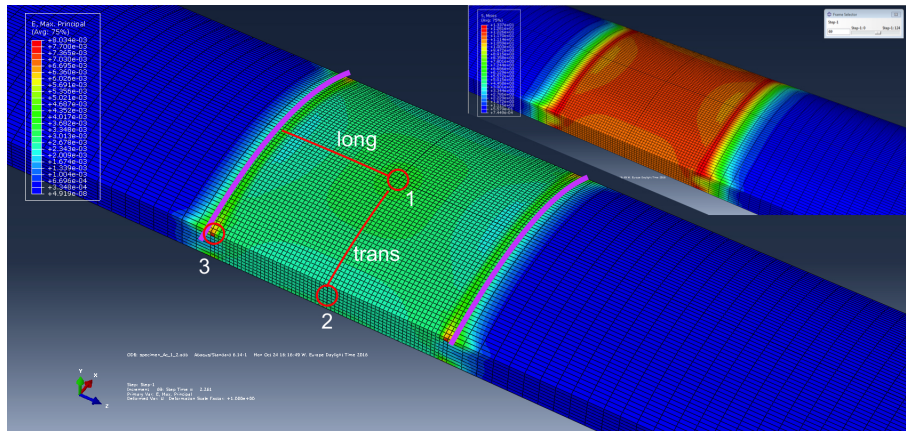
Figure C.1: FEM model of specimen A stress curved with data extraction points and clamping indicated in figure: (1) center, (2) edge middle, (3) edge clamping, avg longitudinal, avg transverse. Stress field is displayed in top right corner.
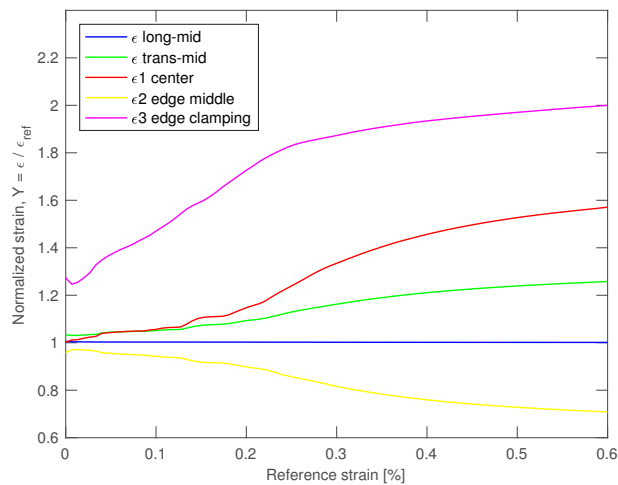
Figure C.2: Specimen A curved, normalized strain in the TSG.
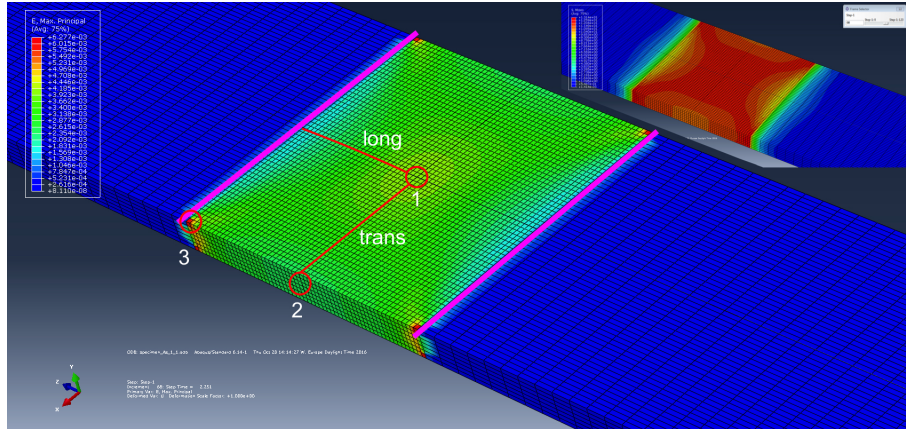
Figure C.3: FEM model of specimen A straight, data extraction points and clamping indicated in figure: (1) center, (2) edge middle, (3) edge clamping edge clamping, avg longitudinal, avg transverse. Stress field is displayed in top right corner.
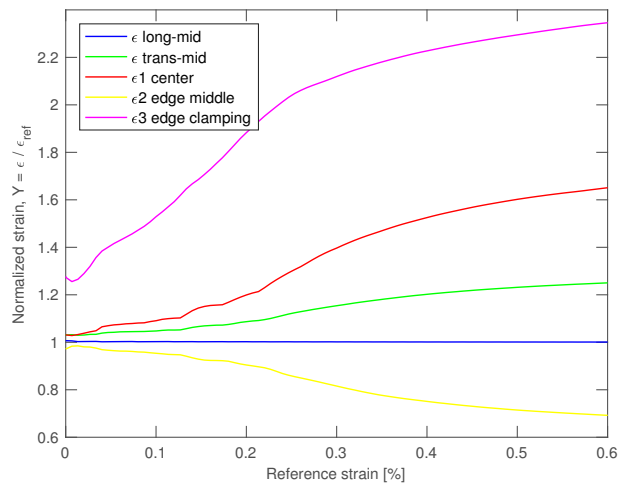
Figure C.4: Specimen A straight, normalized strain in the TSG.

C.2   Specimen B

Specimen B have the highest strain peak at the edge of the narrowing curvature, point (3), see figure C.5. On the curved specimen the edge middle, point (2), have the highest strain peak after the reference strain passes $0.3\,\%$, see figure C.6. Also $\epsilon_{long-mid}$ is below 1, which indicates the reference strain could be too high. The normalized strain would then be too low when comparing with other specimens. On the straight specimen the edge middle, point (2), have a very low strain, see figure C.8.
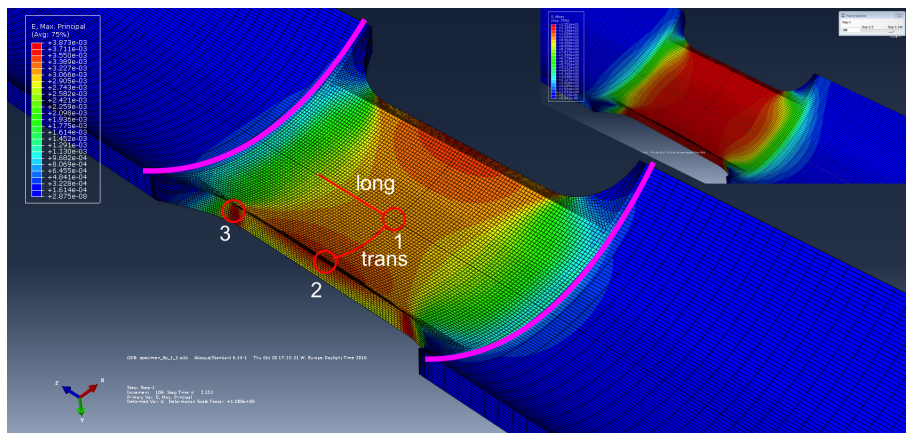
Figure C.5: FEM model of specimen B curved, data extraction points and clamping indicated in figure: (1) center, (2) edge middle, (3) edge curvature, avg longitudinal, avg transverse. Stress field is displayed in top right corner.
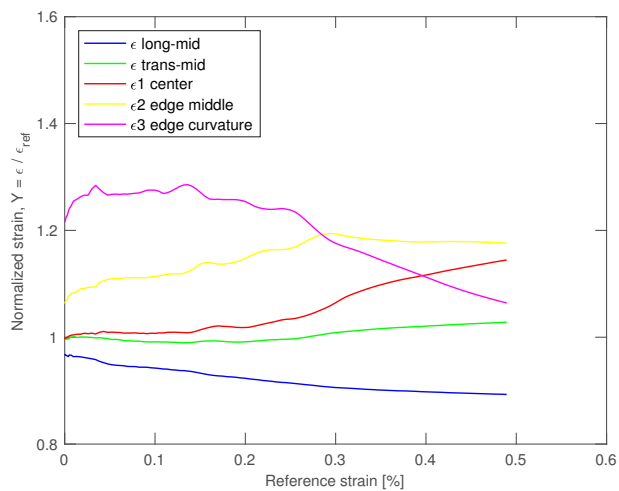
Figure C.6: Specimen B curved, normalized strain in the TSG.
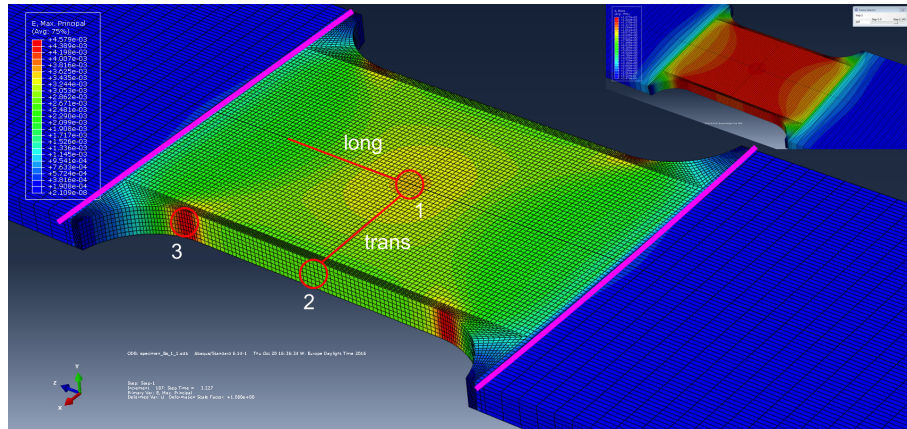
Figure C.7: FEM model of specimen B straight, data extraction points and clamping indicated in figure: (1) center, (2) edge middle, (3) edge curvature, avg longitudinal, avg transverse. Stress field is displayed in top right corner.
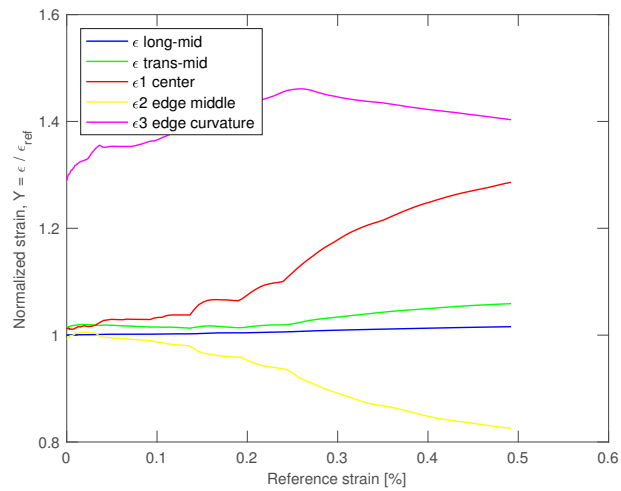
Figure C.8: Specimen B straight, normalized strain in the TSG.

C.3 Specimen C

Specimen C have the highest strain peak along the edge of the inner curvature, point (2), see figure C.9. This is significantly higher than the center. Both the curved and the straight show the same tendency, but the normalized strain is significantly lower in the straight.
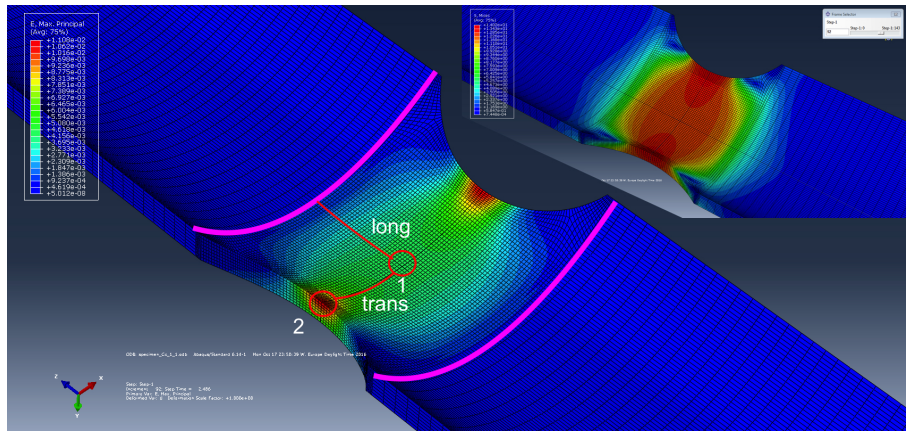
Figure C.9: FEM model of specimen C curved, data extraction points and clamping indicated in figure: (1) center, (2) edge middle, avg longitudinal, avg transverse. Stress field is displayed in top right corner.
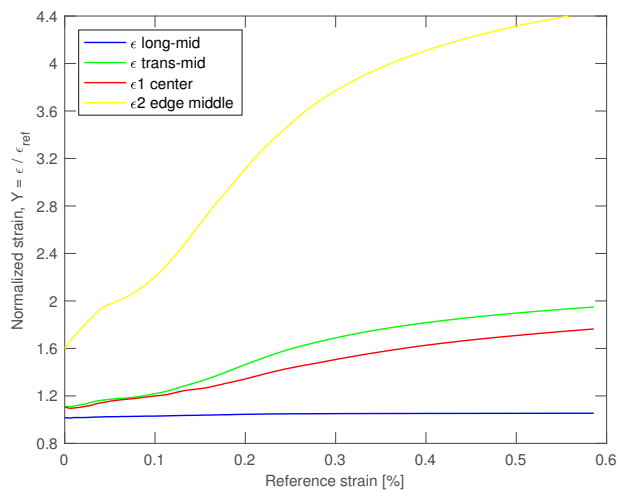
Figure C.10: Specimen C curved, normalized strain in the TSG.
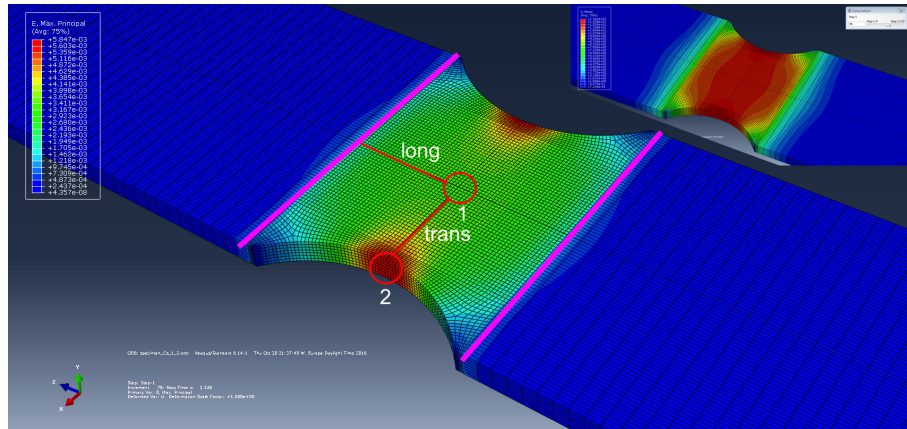
Figure C.11: FEM model of specimen C Stress straight, data extraction points and clamping indicated in figure: (1) center, (2) edge middle, avg longitudinal, avg transverse. Stress field is displayed in top right corner.
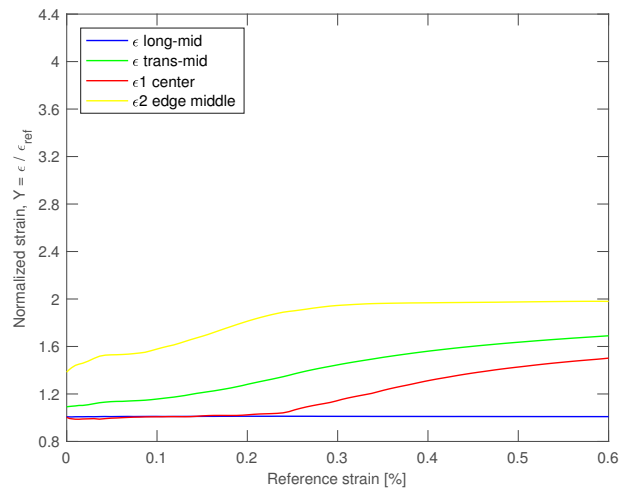
Figure C.12: Specimen C straight, normalized strain in the TSG.

C.4 Specimen D

Specimen D have the highest strain peak by the corner of the clamping, point (3), see figure C.13. In the straightened specimen point (5) has the highest strain peak after the reference strain passes 0.3%, see figure C.16. Besides the clamping, point (5) is the most strained. FEM analysis are not trust worthy at sharp edges, therefore specimen D seems promising. Verification has to be done in the laboratory. $\epsilon_{long-mid}$ is just below 1, which indicates the reference strain could be too high. The normalized strain would then be too low when comparing with other specimens.
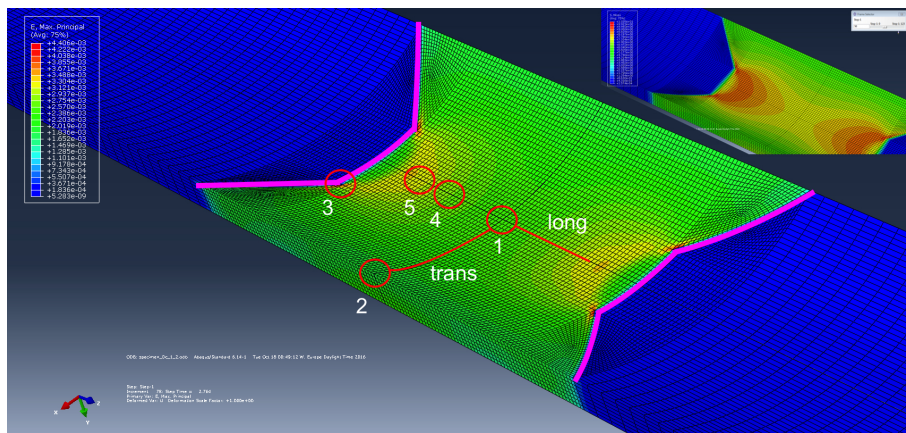
Figure C.13: FEM model of specimen D curved, data extraction points and clamping indicated in figure: (1) center, (2) edge middle, (3) corner of clamping, (4) $9\,\mathrm{mm}$ offset from middle, (5) $14\,\mathrm{mm}$ offset from middle, avg longitudinal, avg transverse. Stress field is displayed in top right corner.
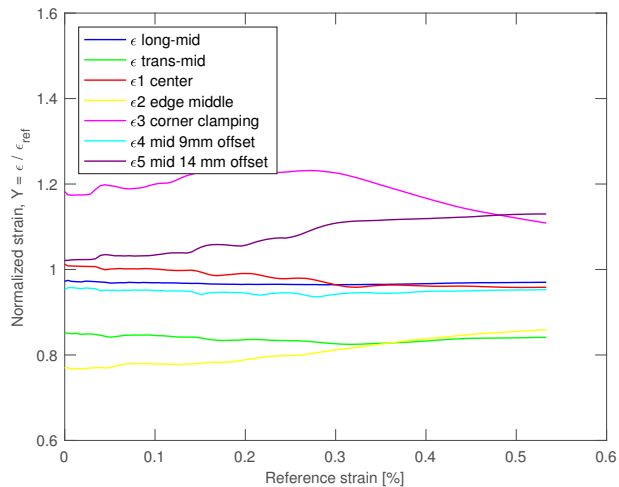
Figure C.14: Specimen D curved, normalized strain in the TSG.
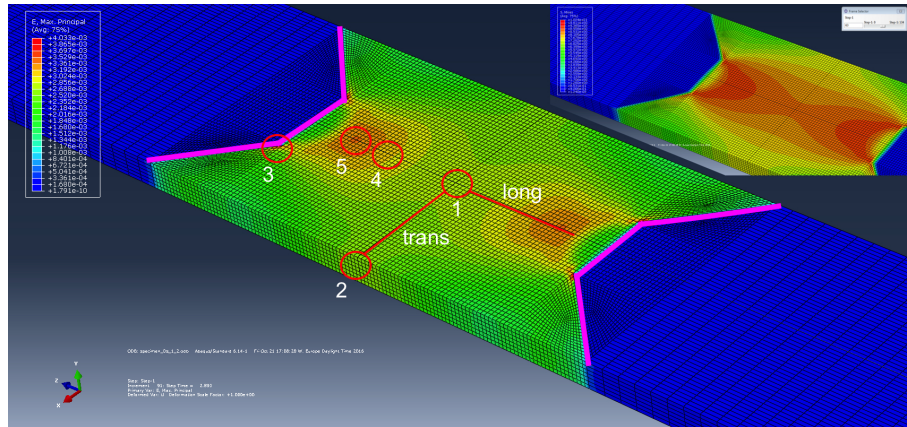
Figure C.15: FEM model of specimen D straight, data extraction points and clamping indicated in figure: (1) center, (2) edge middle, (3) corner of clamping, (4) $9\,\text{mm}$ offset from middle, (5) $14\,\text{mm}$ offset from middle, avg longitudinal, avg transverse. Stress field is displayed in top right corner.
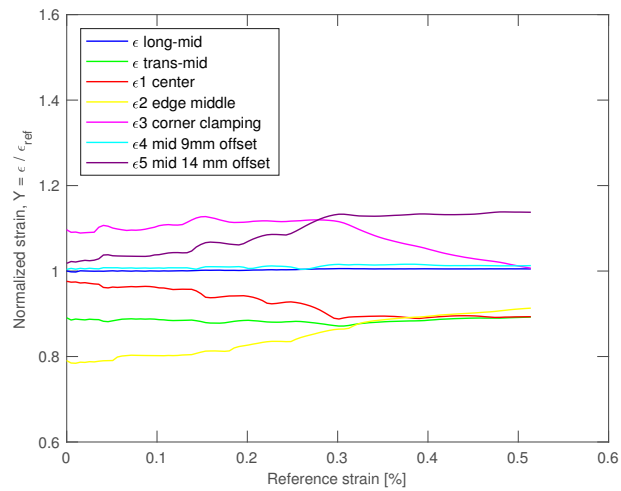
Figure C.16: Specimen D straight, normalized strain in the TSG.

Laboratory Setup - Morphology Table

Morphology table				
Grips	Sandblasting, coarse sand	-	Untreated	Sandblasting, fine sand
End of specimens	Sandpaper	Narrowing / Stress concentatraion	Untreated	Cast
Fastening method	Screws	-	Springs	Pneumatic
Strain measurement	Clip extensometer	DIC	Stain gauge	Laser extensometer
Specles for DIC	Mosquito net as stencil	Spray, custom nozzle	Brush squirt	Pen, one by one
Lights for DIC	LED lights	-	Roof light only	Glow lamp

Figure D.1: The morphology table presents different options considered as setup to perform laboratory experiments of testing in tension configuration on lead. The green fields indicates method used, while the grey fiedls indicates methods discontinued.

- **Concerning the choice of grips** If the grips were roughened by sandblasting there would be more friction against the specimen, see figure D.2.

- **Concerning the choice of end of specimens** If sandpaper were glued to the specimen the friction against the grips would increase. This was not necessary for specimens with narrowing, see figure D.3b. To cast the ends are time consuming, difficult and can easily introduce torsion and bending in the specimens when testing.

- **Concerning the choice of fastening method** Pneumatic constant pressure of $5\,\mathrm{MPa}$, even if volume of specimen would change. Specimens without narrowing are most susceptible for this to be a problem. When the specimens are pulled, the thickness could change due to isovolumetric behavior in the material. This would lead to less friction between specimen and grip and a pull out would occur, see section 5.2.9. The pneumatic clamps available did not have possibilities for custom grips. Stiff springs were tested to see if that would allow the grip to self adjust, when thickness changed. The springs were not stiff enough. Regular screws were used to fasten the grips. Springs are presented in figure D.3a.

- **Concerning the choice of strain measurement** DIC would allow for non contact strain measurement. Strain gauge is difficult to place. Clip extensometer could introduce strain concentration and cracks, see figure D.3c. Laser extensometer was not available in the laboratory, but could be a good solution if it can be used for strain control.

- **Concerning the choice of DIC speckles** To use a spray can with a custom nozzle was the simplest and easiest way to get a good speckle pattern, displayed in figure D.2.

- **Concerning the choice of DIC lights** LED lights was the best alternative, as it would provide enough light for a good depth of field also it would not heat up the test specimen like the glow lamp did.
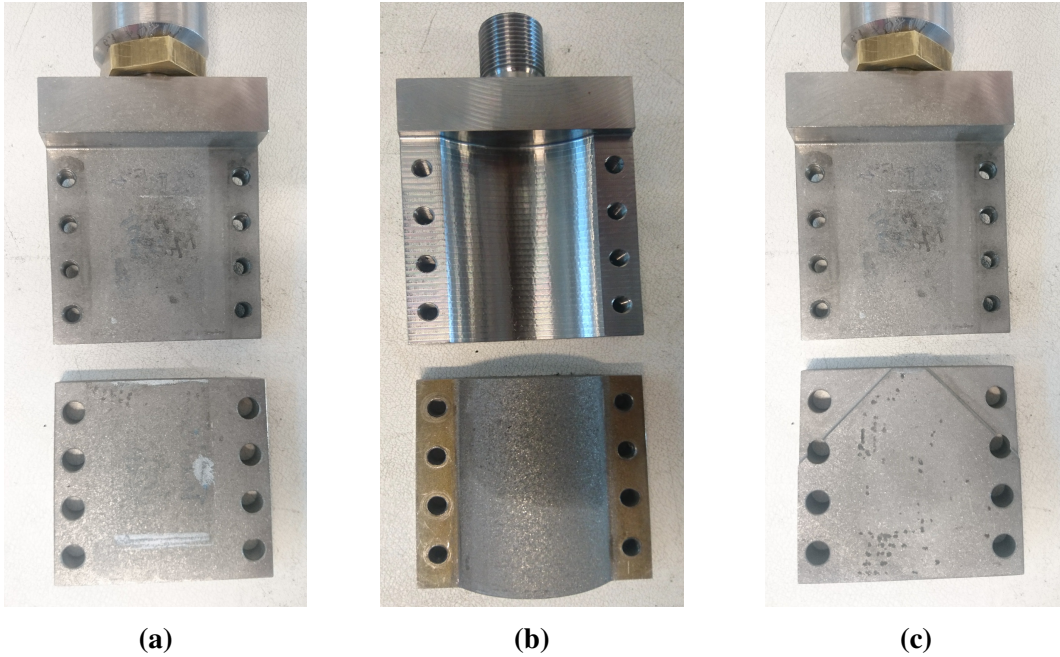
Figure D.2: Grips used for laboratory testing. All the grips has been sandblasted for better friction. (a) straight specimens, (b) curved specimens, and (c) grip with $45°$ for specimen D straight.
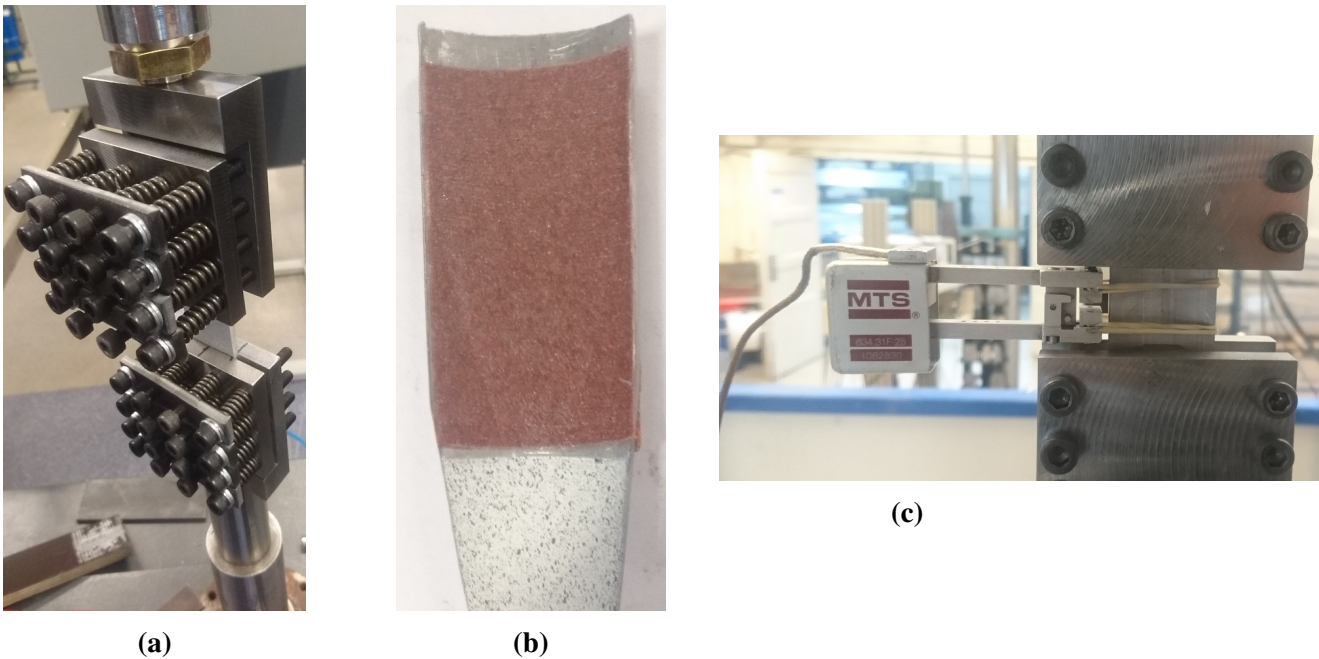
Figure D.3: (a) Stiff springs were tested to make self adjusting grips, (b) sandpaper glued to the specimen for more friction to the grip, and a speckle pattern made by spray can with custom nozzle, and (c) a regular clip extensometer.

Laboratory Tests - Results

E.1 Localization in TSGs

E.1.1 Specimen B
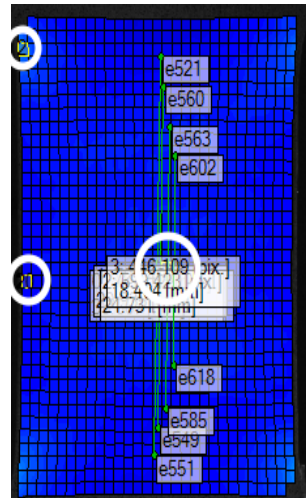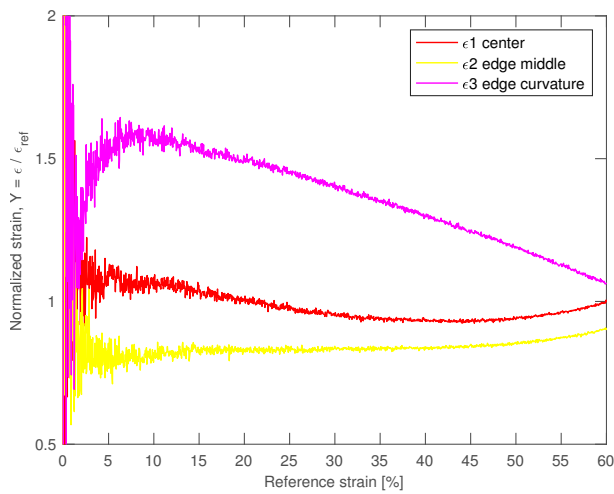
Figure E.1: Specimen B curved, $\epsilon = 60\,\%$ in tension, $\dot{\epsilon} = 1\text{E-4 s}^{-1}$, ϵ/ϵ_{ref}.
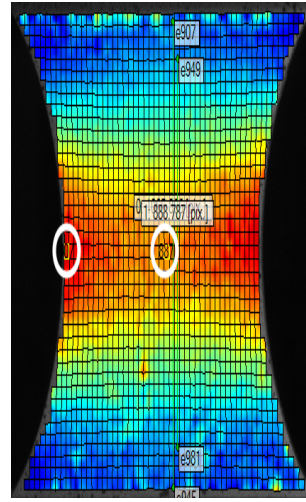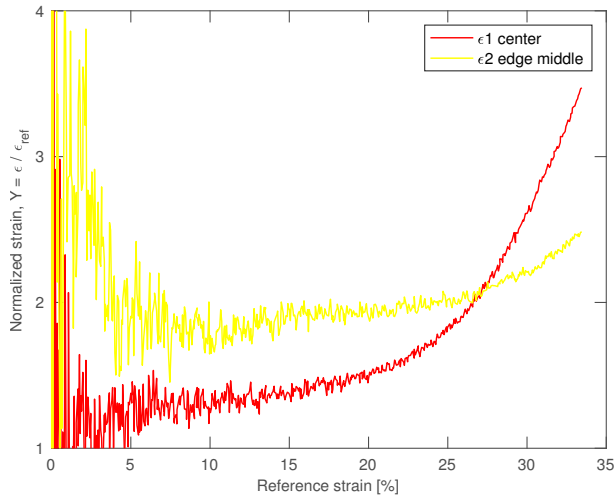
E.1.2 Specimen C

Figure E.2: Specimen C straight, $\epsilon = 30\,\%$ in tension, $\dot{\epsilon} = 1\text{E-}4\ \text{s}^{-1}$, ϵ/ϵ_{ref}.
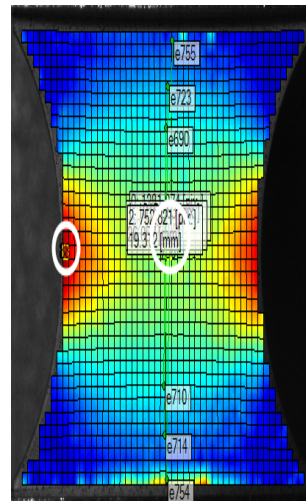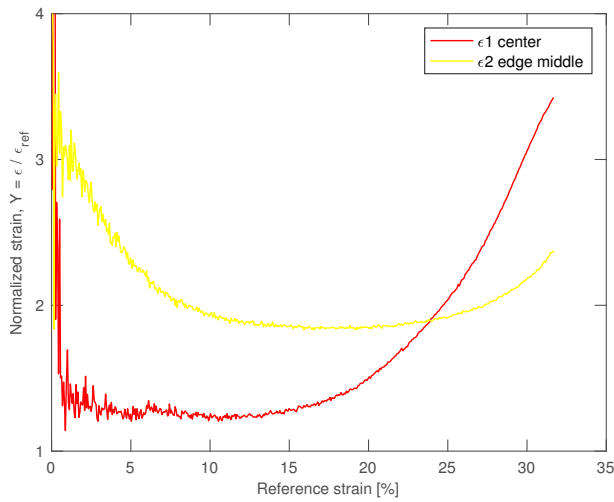
Figure E.3: Specimen C curved, $\epsilon = 30\,\%$ in tension, $\dot{\epsilon} = 1\text{E-}4\ \text{s}^{-1}$, ϵ/ϵ_{ref}.
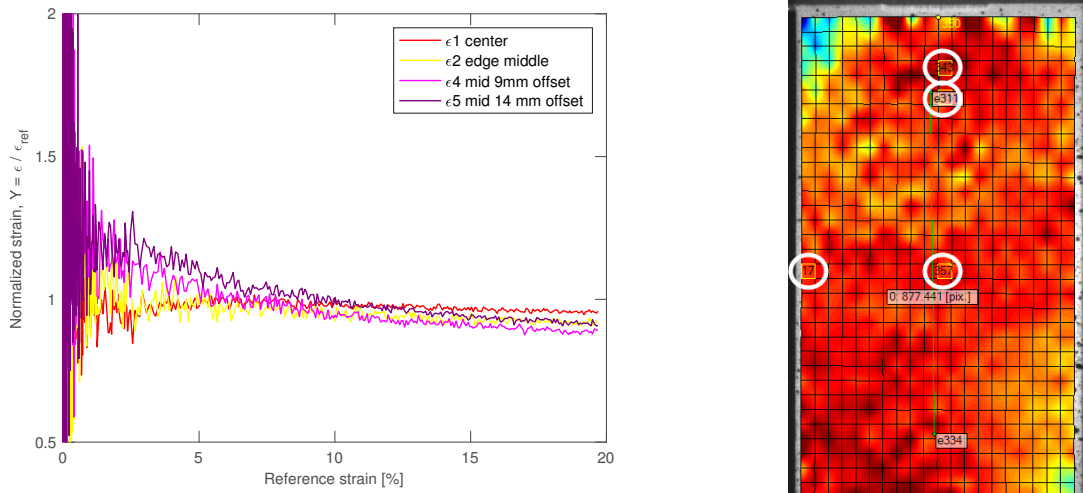
E.1.3 Specimen D

Figure E.4: Specimen D straight, $\epsilon = 20\,\%$ in tension, $\dot{\epsilon} = $ 1E-4 s^{-1}, ϵ/ϵ_{ref}.

E.2 Tension Tests

E.2.1 DIC Data Check
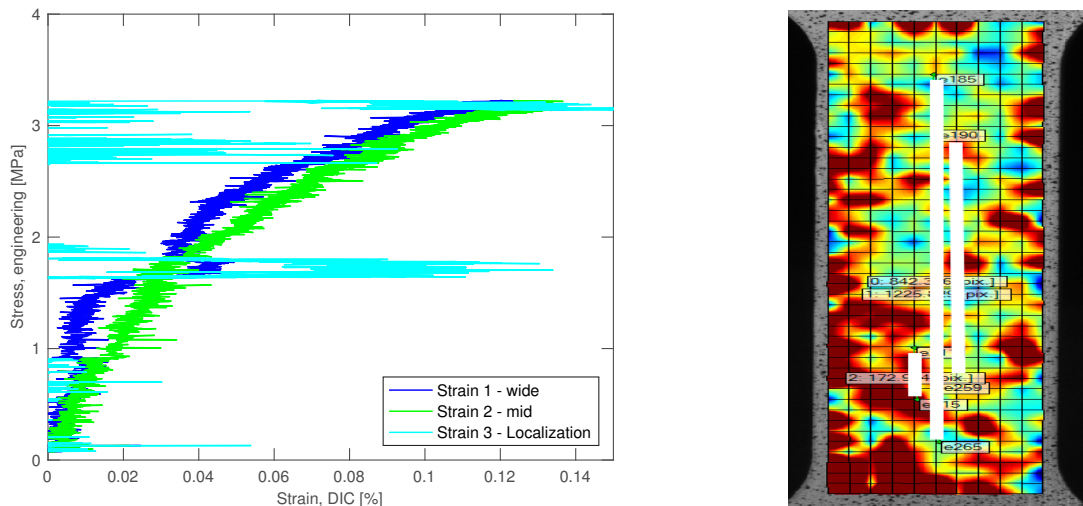
Figure E.5: Tension test: t $= 3.3\,\text{mm}$, $\dot{\epsilon} = $ 1E-8 s^{-1}. Strain 2 mid were used as strain from DIC.

E.2.2 Constant Thickness
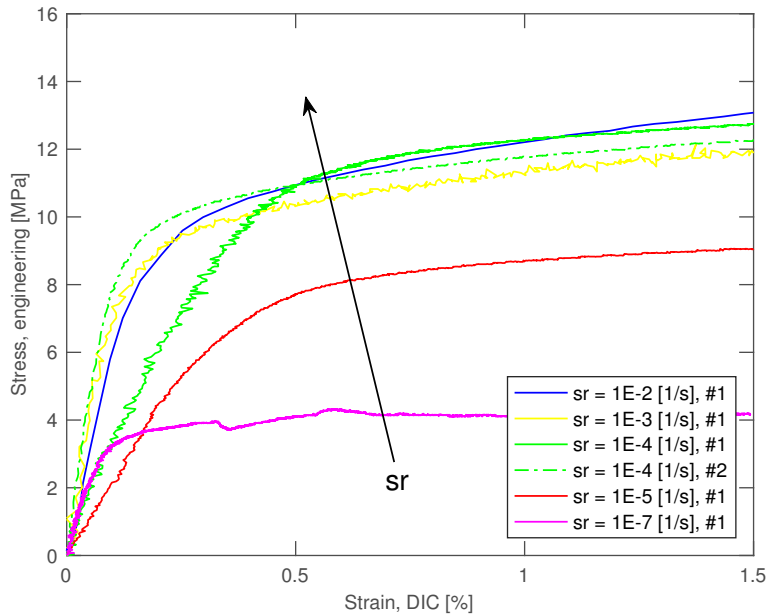
Figure E.6: Tension test: t = 1.0 mm, arrow indicates increasing strain rate, where # specify the specimen number in each series.
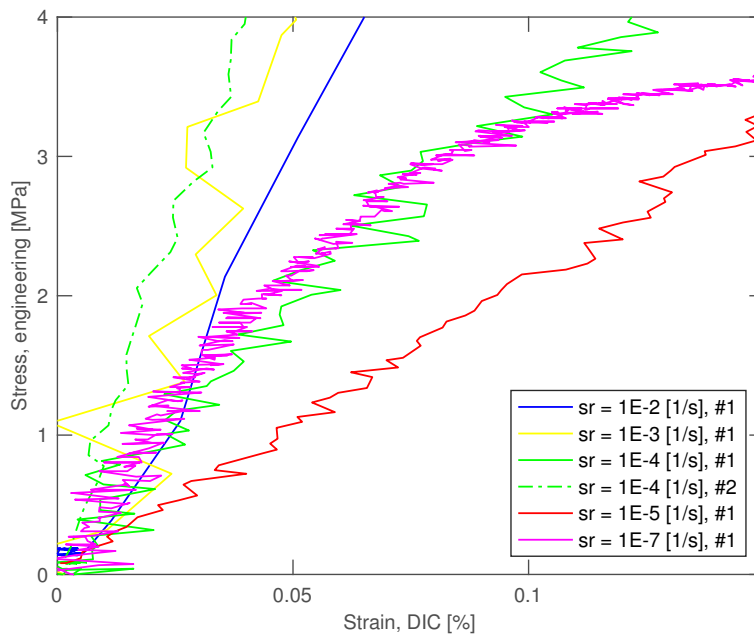
Figure E.7: Tension test: t = 1.0 mm, arrow indicates increasing strain rate, where # specify the specimen number in each series.
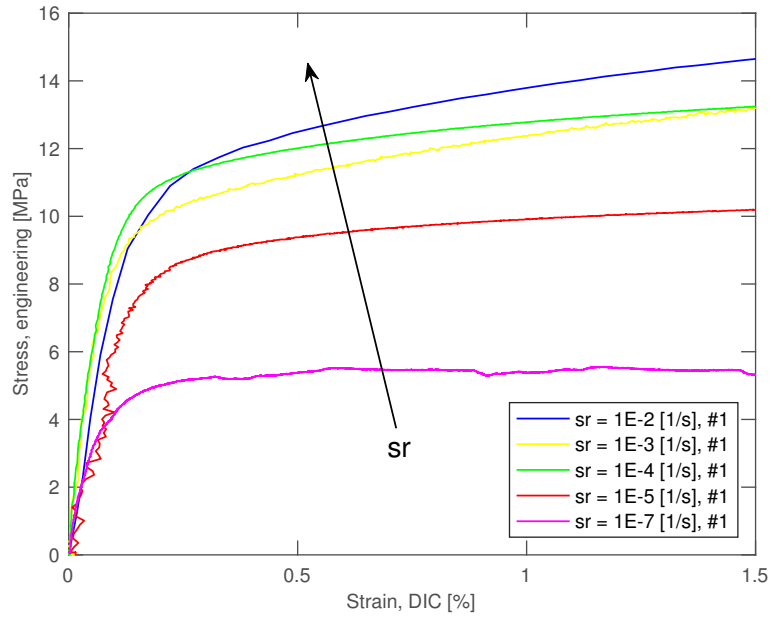
Figure E.8: Tension test: t = 1.8 mm, arrow indicates increasing strain rate, where # specify the specimen number in each series.
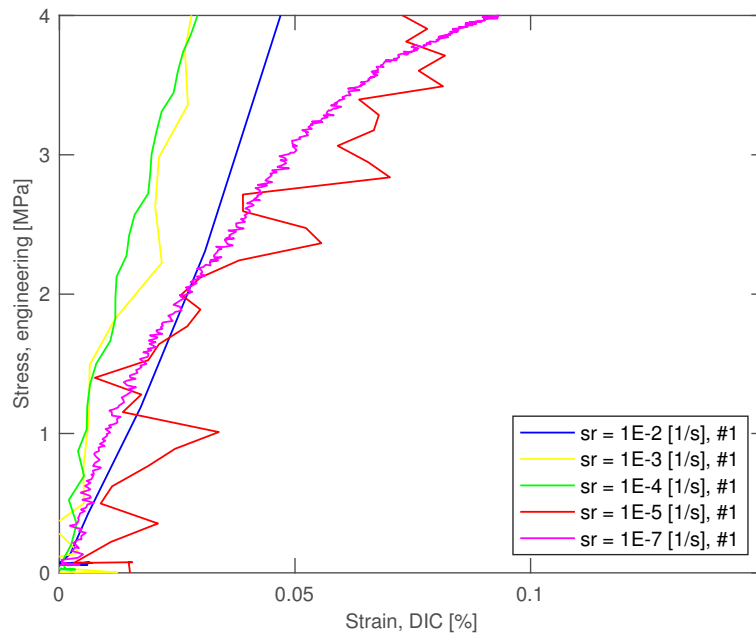
Figure E.9: Tension test: t = 1.8 mm, arrow indicates increasing strain rate, where # specify the specimen number in each series.
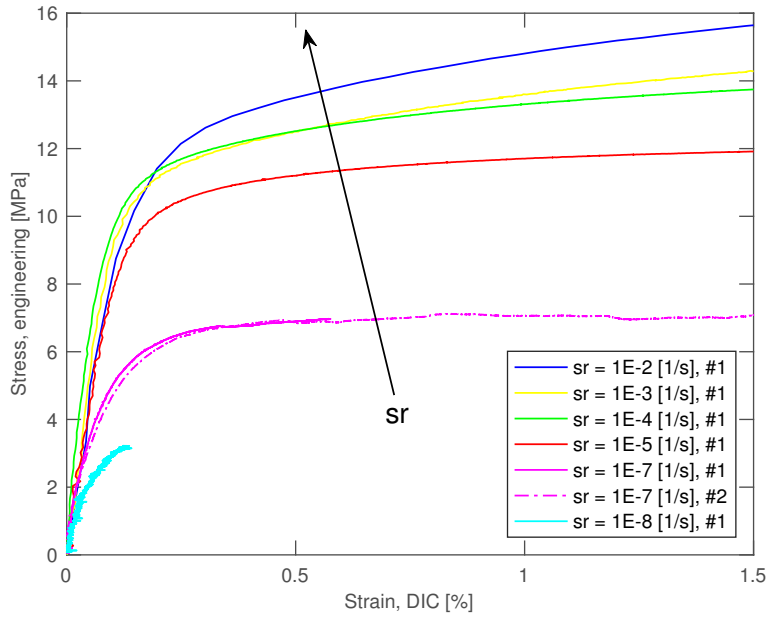
Figure E.10: Tension test: t = 3.3 mm, arrow indicates increasing strain rate, where # specify the specimen number in each series.
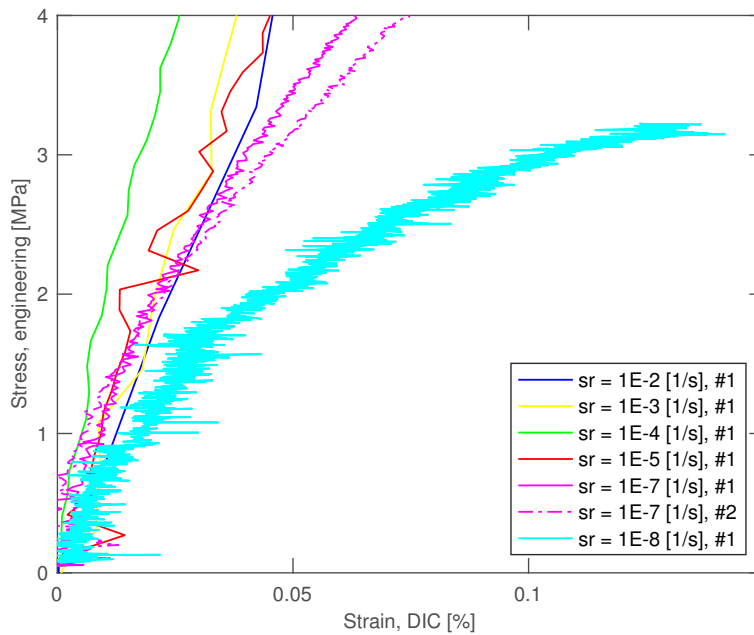
Figure E.11: Tension test: t = 3.3 mm, arrow indicates increasing strain rate, where # specify the specimen number in each series.
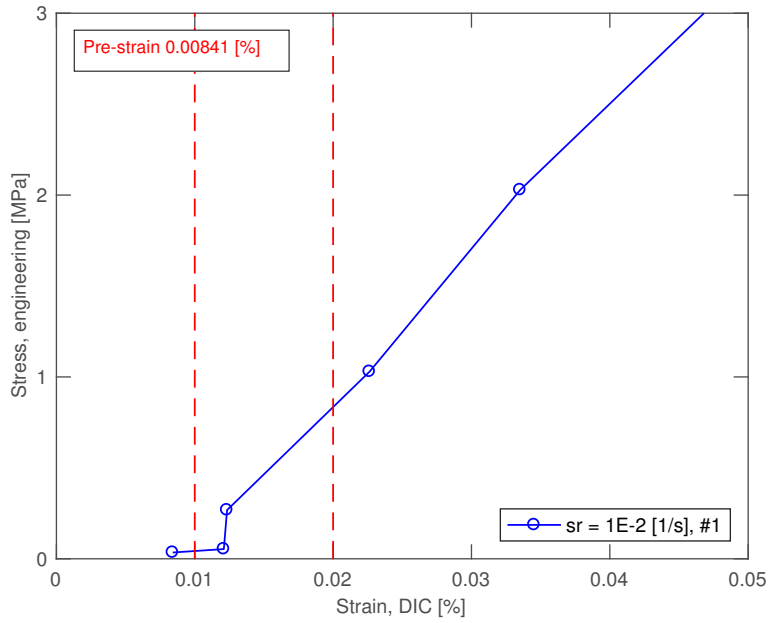
Figure E.12: Tension test: t = 3.3 mm, $\dot{\epsilon}$ = 1E-2 s^{-1}, #1, where # specify the specimen number in each series.
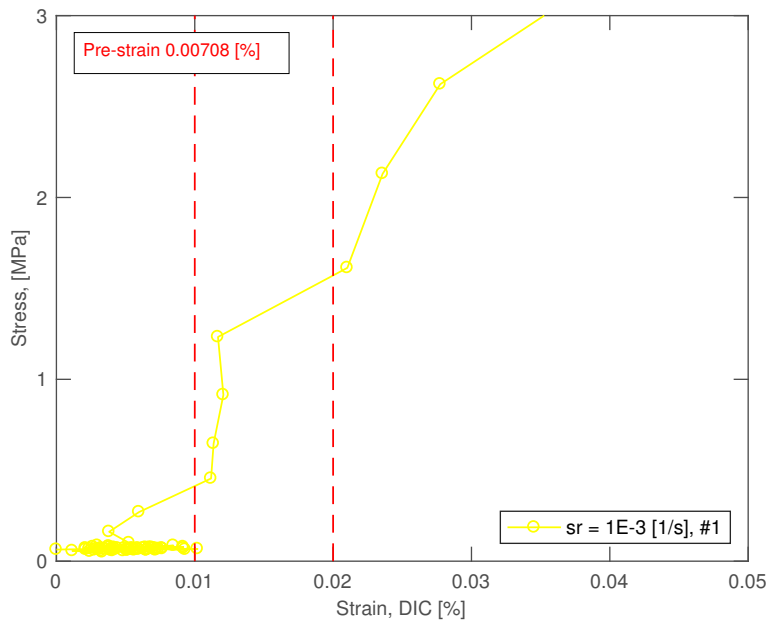
Figure E.13: Tension test: t = 3.3 mm, $\dot{\epsilon}$ = 1E-3 s^{-1}, #1, where # specify the specimen number in each series.
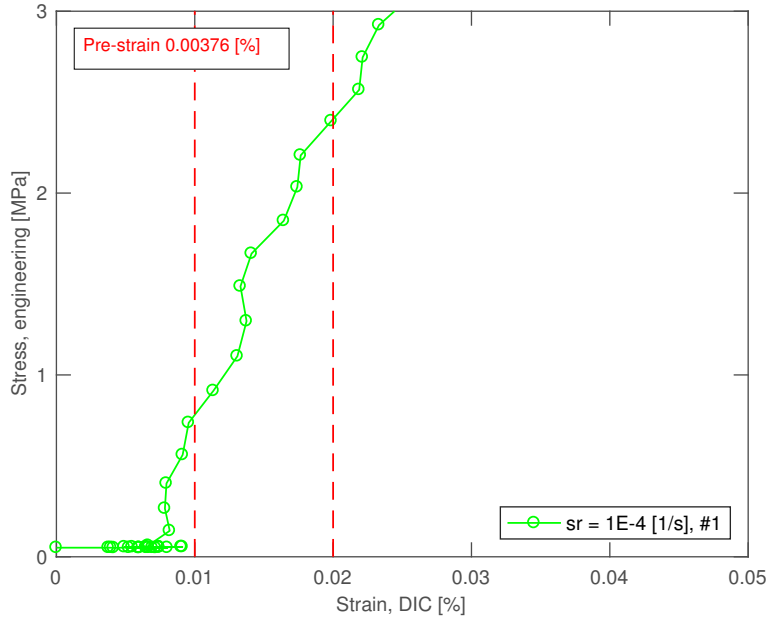
Figure E.14: Tension test: t = 3.3 mm, $\dot{\epsilon}$ = 1E-4 s^{-1}, #1, where # specify the specimen number in each series.
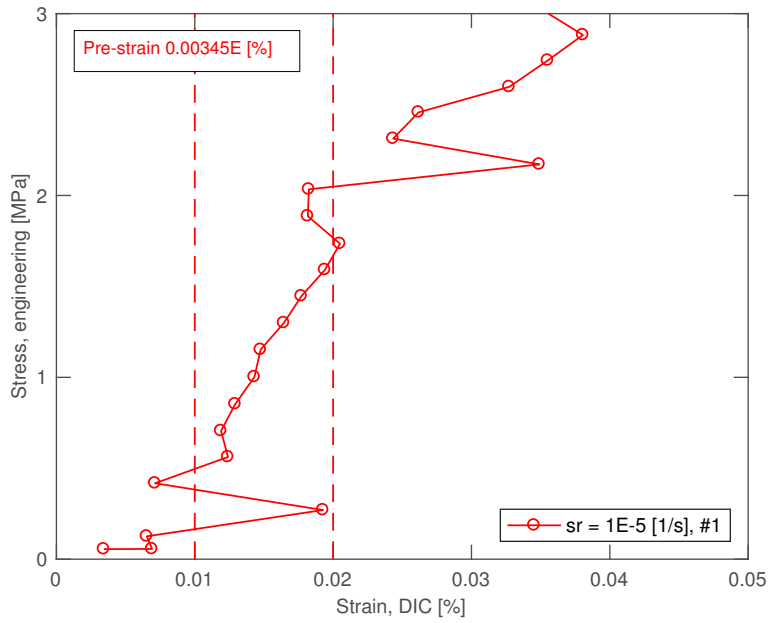
Figure E.15: Tension test: t = 3.3 mm, $\dot{\epsilon}$ = 1E-5 s^{-1}, #1, where # specify the specimen number in each series.
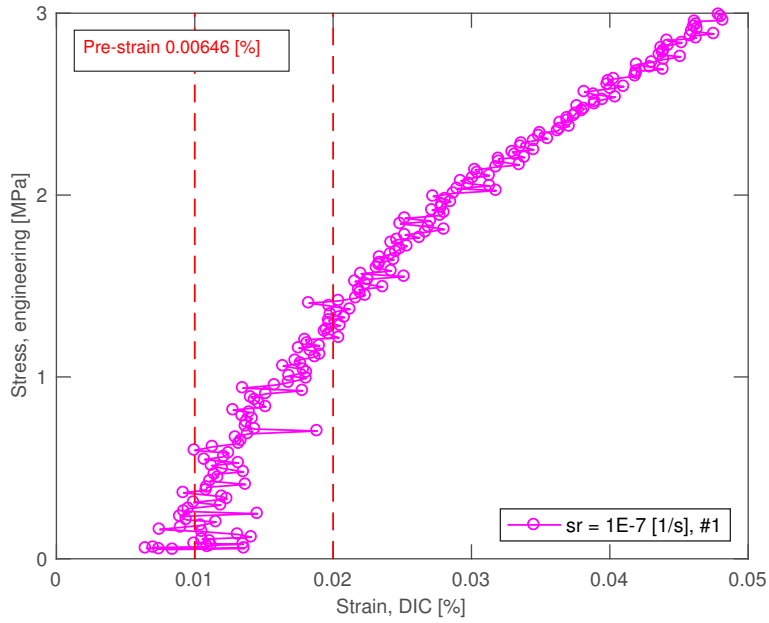
Figure E.16: Tension test: t = 3.3 mm, $\dot{\epsilon}$ = 1E-7 s^{-1}, #1, where # specify the specimen number in each series.
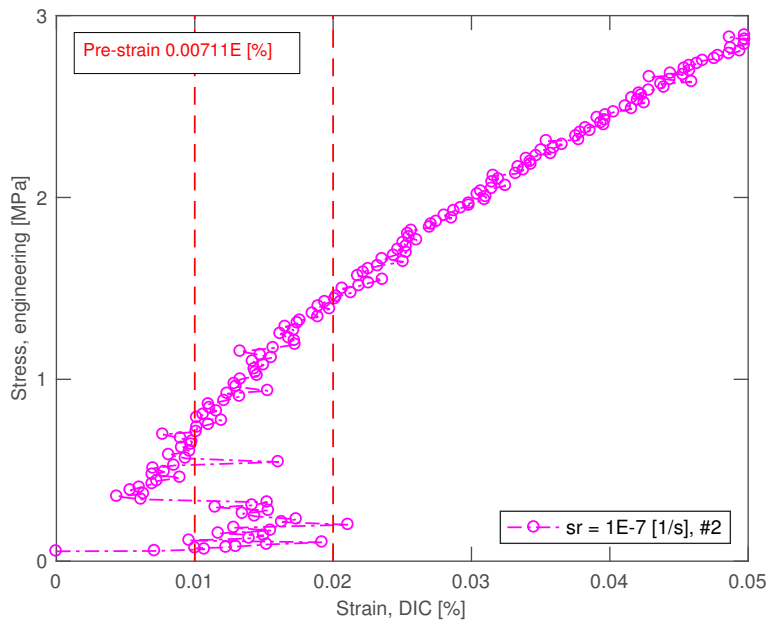
Figure E.17: Tension test: t = 3.3 mm, $\dot{\epsilon}$ = 1E-7 s^{-1}, #2, where # specify the specimen number in each series.
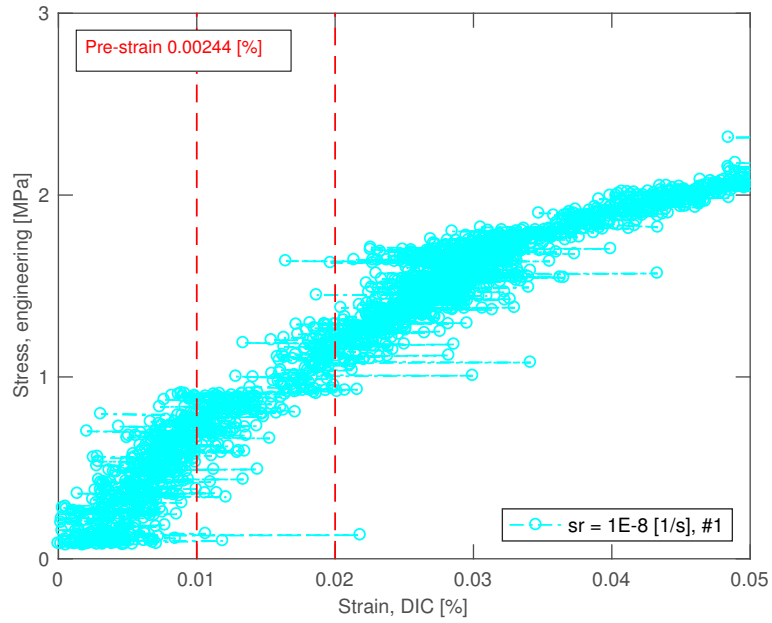
Figure E.18: Tension test: t = 3.3 mm, $\dot{\epsilon}$ = 1E-8 s^{-1}, #1, where # specify the specimen number in each series.

E.2.3 Constant Strain Rate
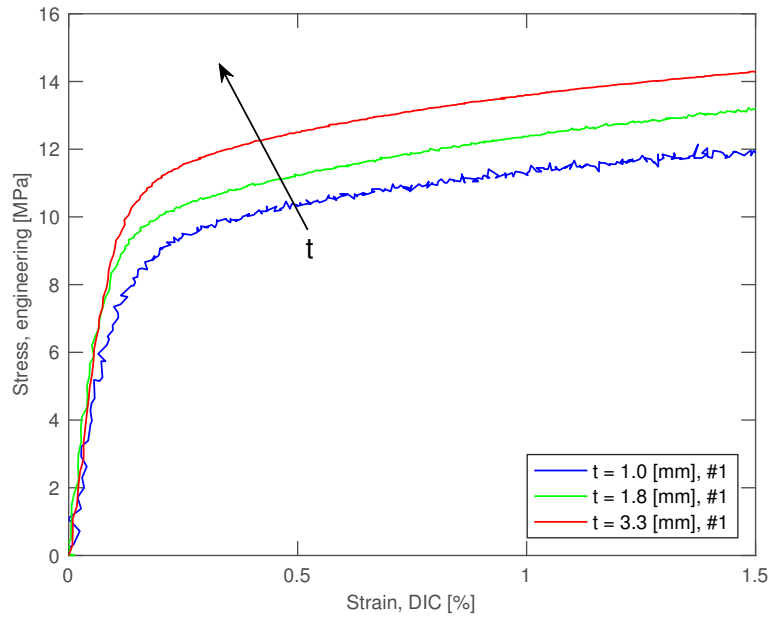
Figure E.19: Tension test: $\dot{\epsilon} = $ 1E-3 s^{-1}, arrow indicates increasing thickness, where # specify the specimen number in each series.
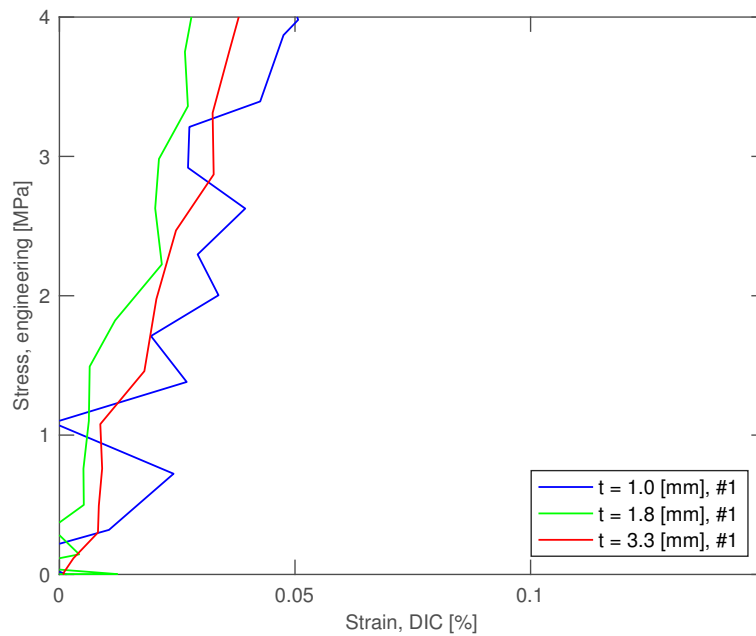

**Figure E.20:** Tension test: $\dot{\epsilon} = $ 1E-3 s^{-1}, arrow indicates increasing thickness, where # specify the specimen number in each series.
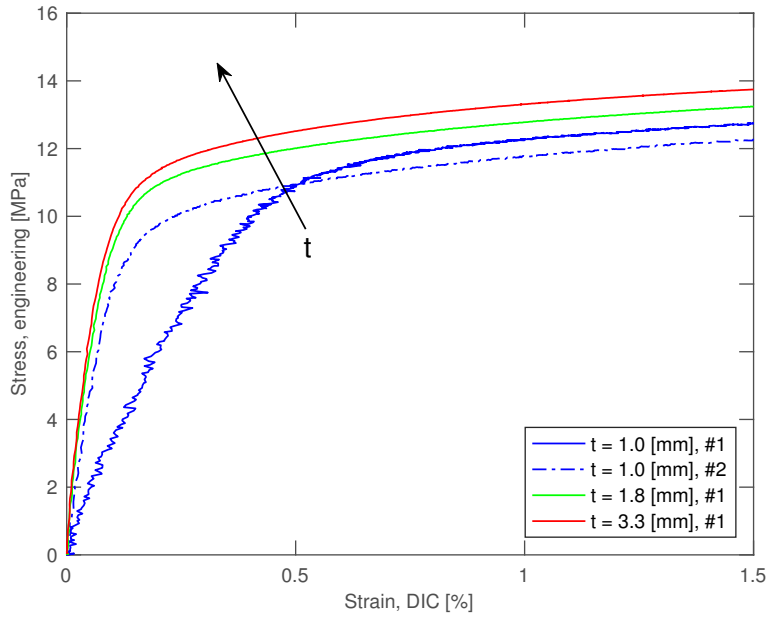
Figure E.21: Tension test: $\dot{\epsilon} = $ 1E-4 s^{-1}, arrow indicates increasing thickness, where # specify the specimen number in each series.
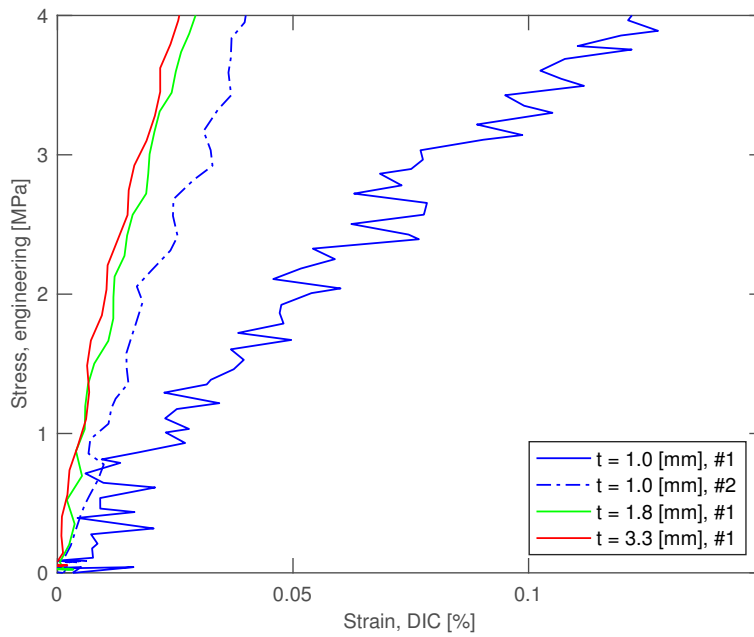
Figure E.22: Tension test: $\dot{\epsilon} = $ 1E-4 s^{-1}, arrow indicates increasing thickness, where # specify the specimen number in each series.
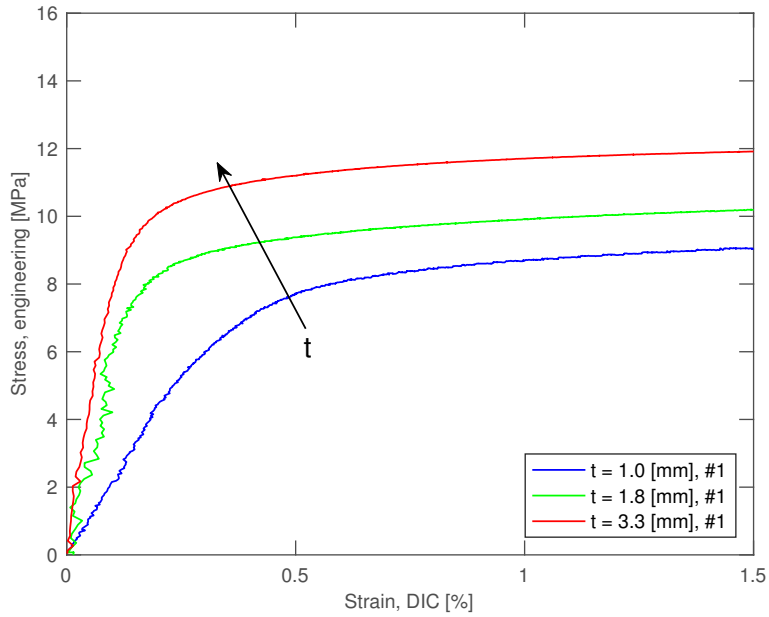
Figure E.23: Tension test: $\dot{\epsilon}$ = 1E-5 s^{-1}, arrow indicates increasing thickness, where # specify the specimen number in each series.
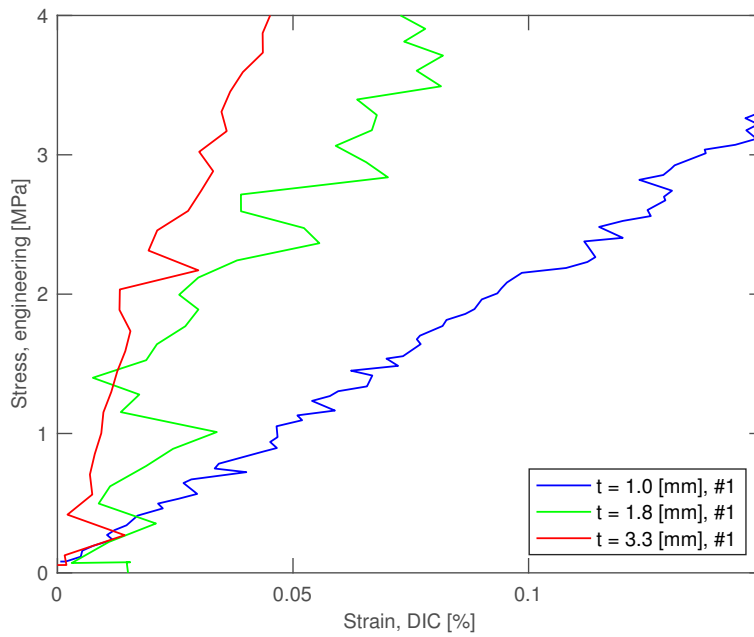
Figure E.24: Tension test: $\dot{\epsilon}$ = 1E-5 s^{-1}, arrow indicates increasing thickness, where # specify the specimen number in each series.
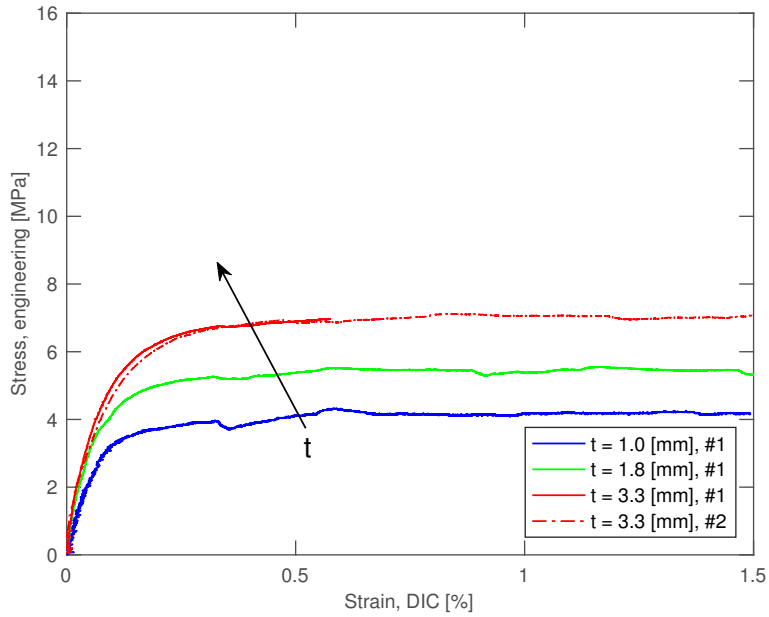
Figure E.25: Tension test: $\dot{\epsilon}$ = 1E-7 s^{-1}, arrow indicates increasing thickness, where # specify the specimen number in each series.
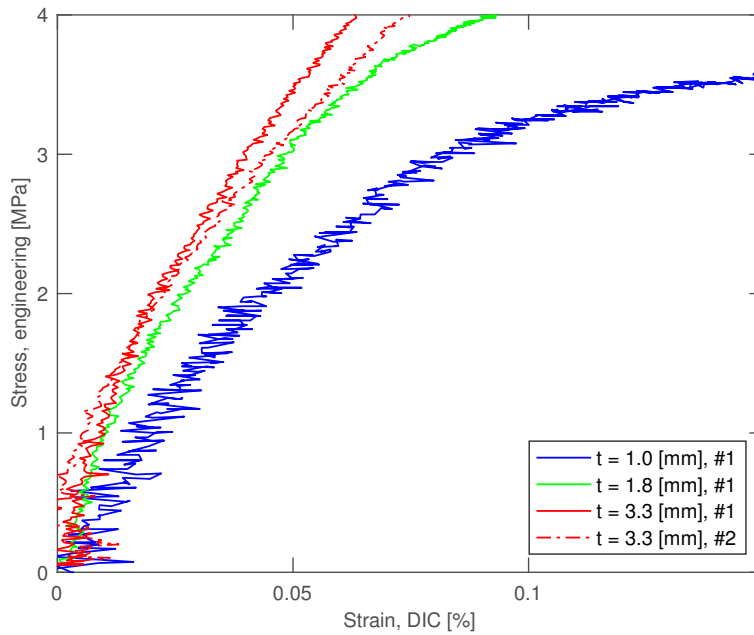
Figure E.26: Tension test: $\dot{\epsilon}$ = 1E-7 s^{-1}, arrow indicates increasing thickness, where # specify the specimen number in each series.

E.2.4   Comparison of strain rates from DIC
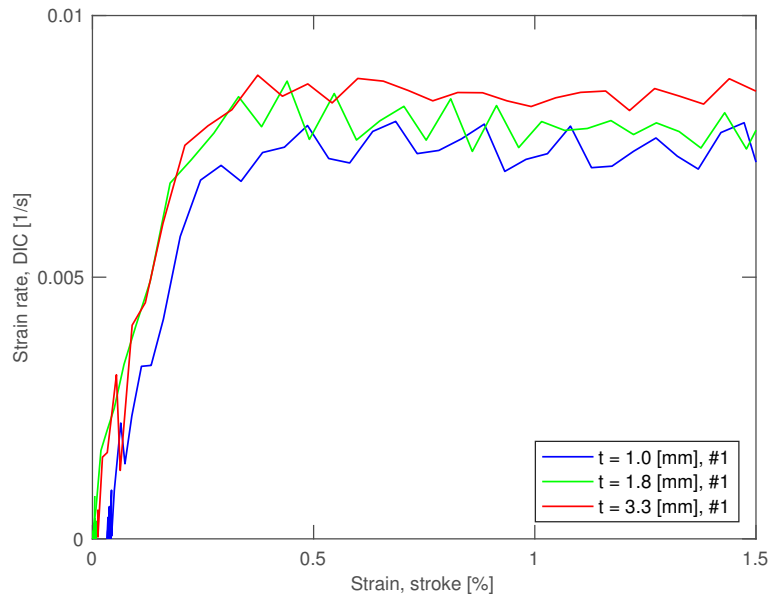
Figure E.27: Tension test: Comparison of strain rates calculated from DIC for $\dot{\epsilon} =$ 1E-2 s^{-1}, where # specify the specimen number in each series.
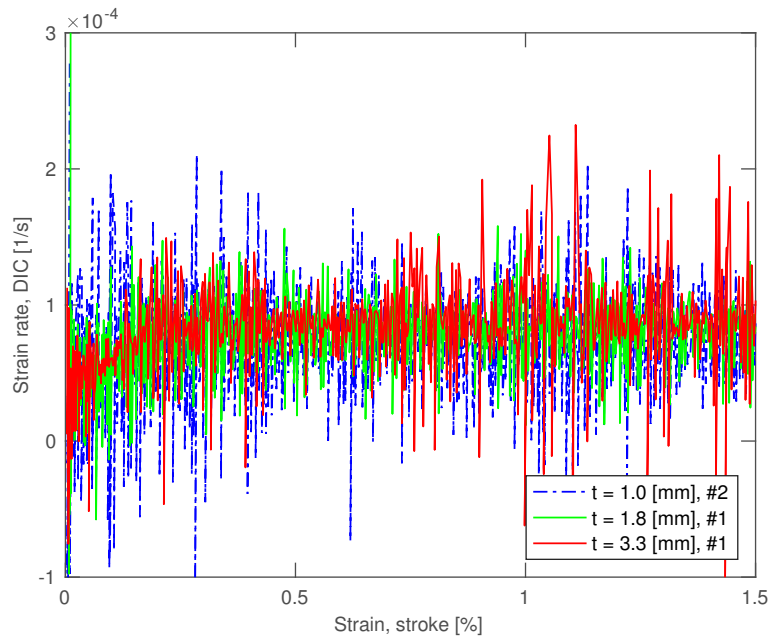

Figure E.28: Tension test: Comparison of strain rates calculated from DIC for $\dot{\epsilon} =$ 1E-4 s^{-1}, where # specify the specimen number in each series.
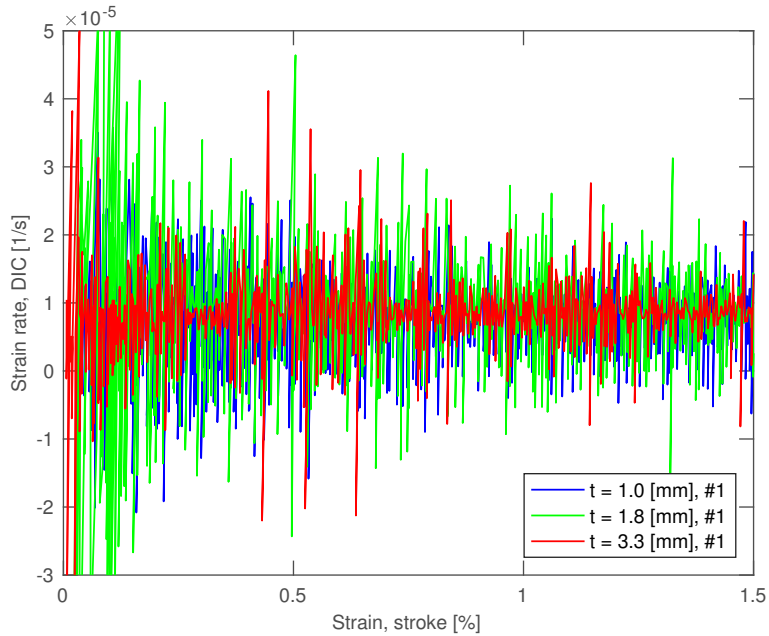
Figure E.29: Tension test: Comparison of strain rates calculated from DIC for $\dot{\epsilon} =$ 1E-5 s^{-1}, where # specify the specimen number in each series.
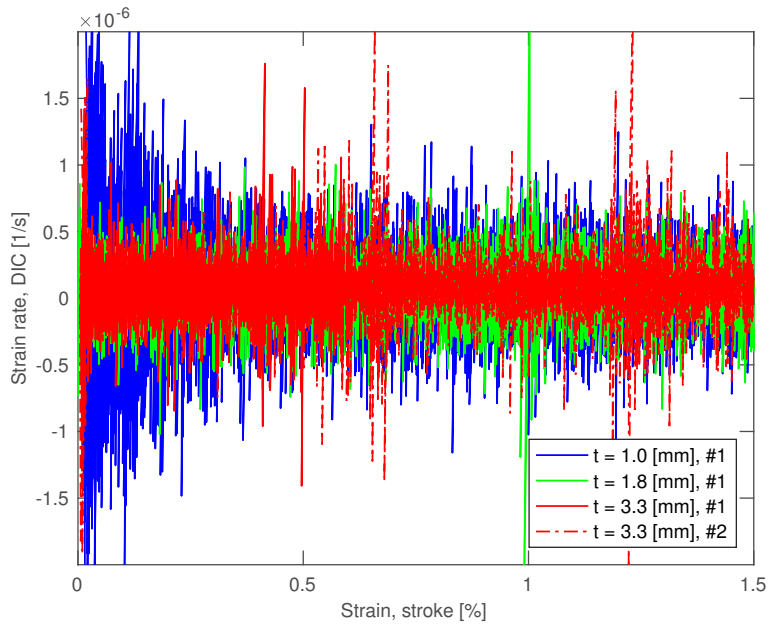
Figure E.30: Tension test: Comparison of strain rates calculated from DIC for $\dot{\epsilon} =$ 1E-7 s^{-1}, where # specify the specimen number in each series.

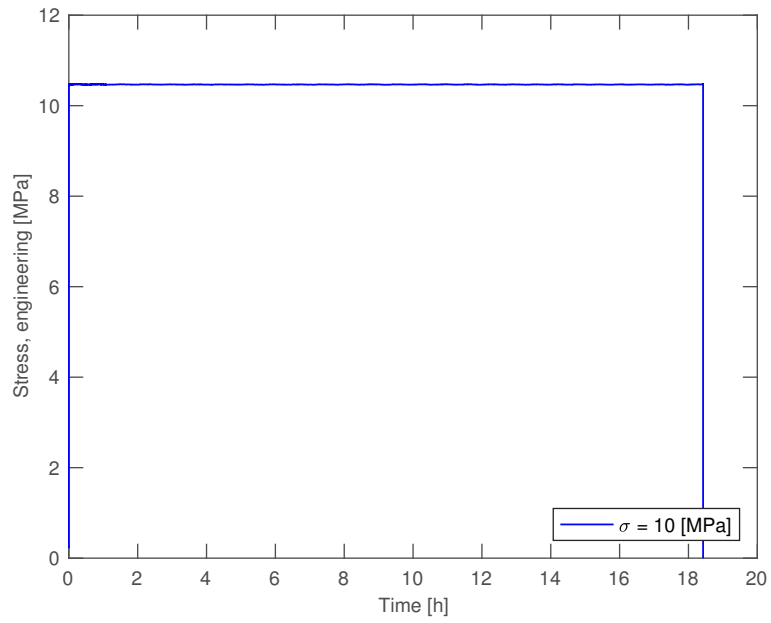# E.3 Creep Test
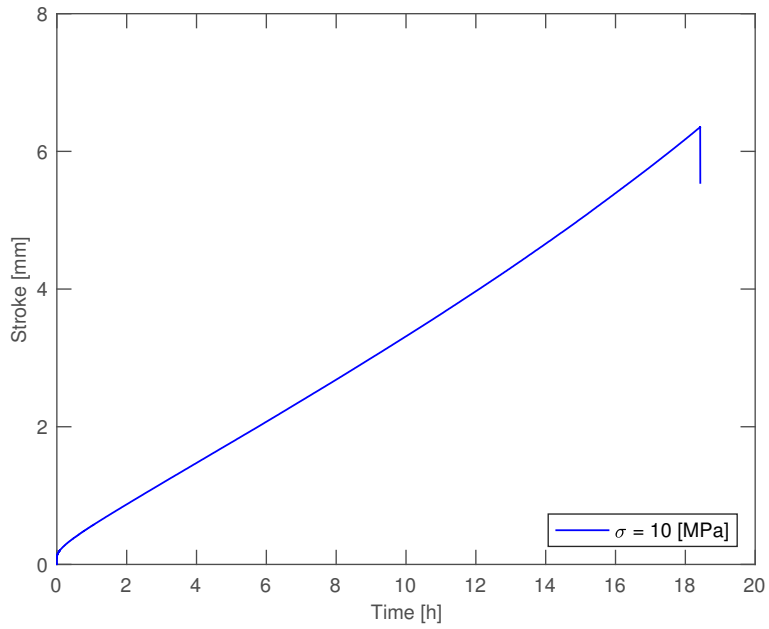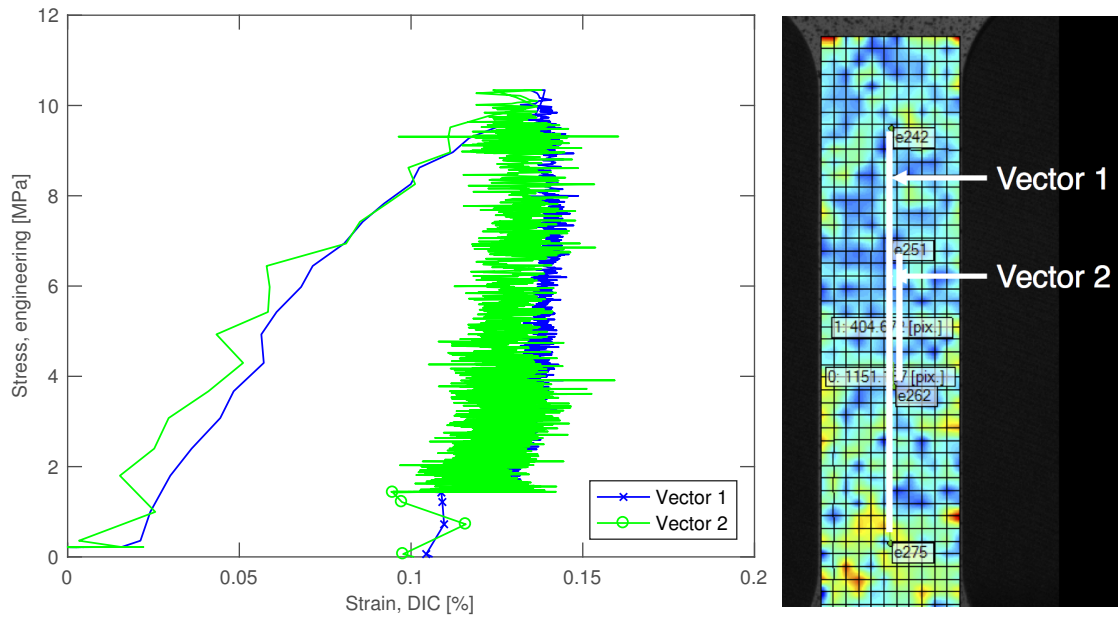

Figure E.31: Creep test: stroke vs time.
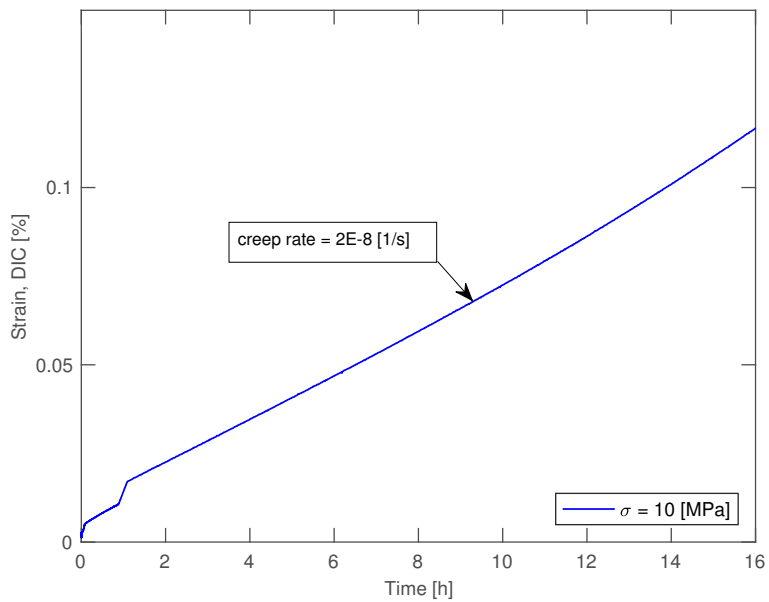
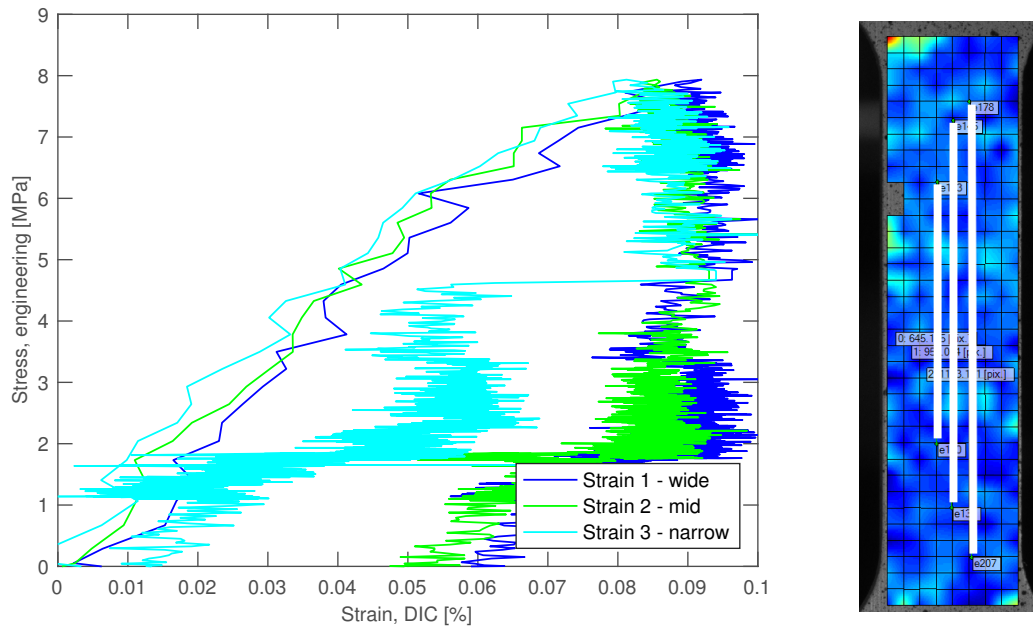**Figure E.32:** Creep test: strain vs time, creep rate $\epsilon_{cr} =$ 2E-8 [1/s].
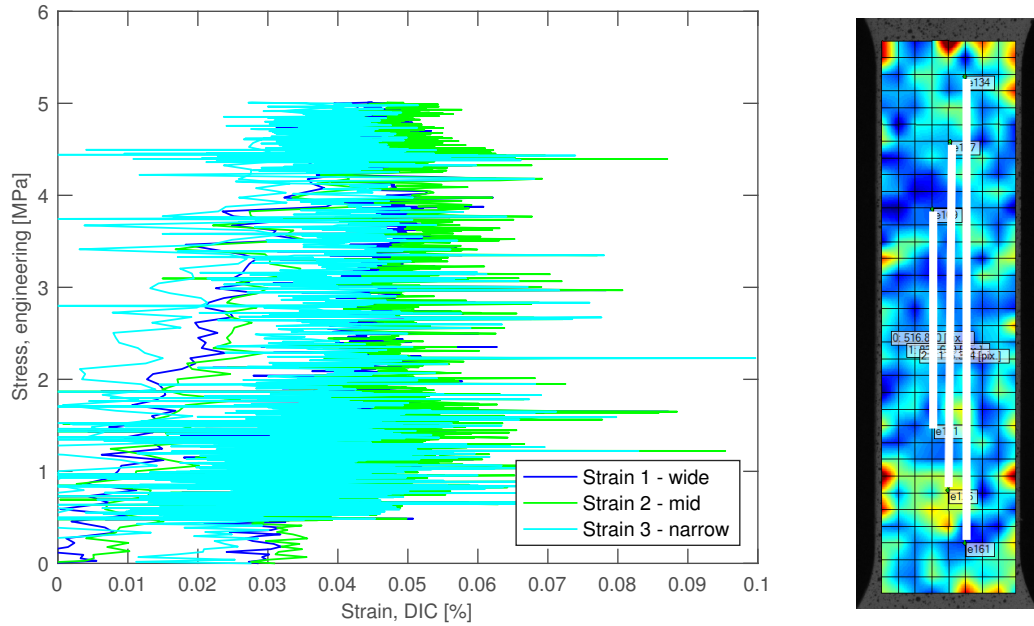
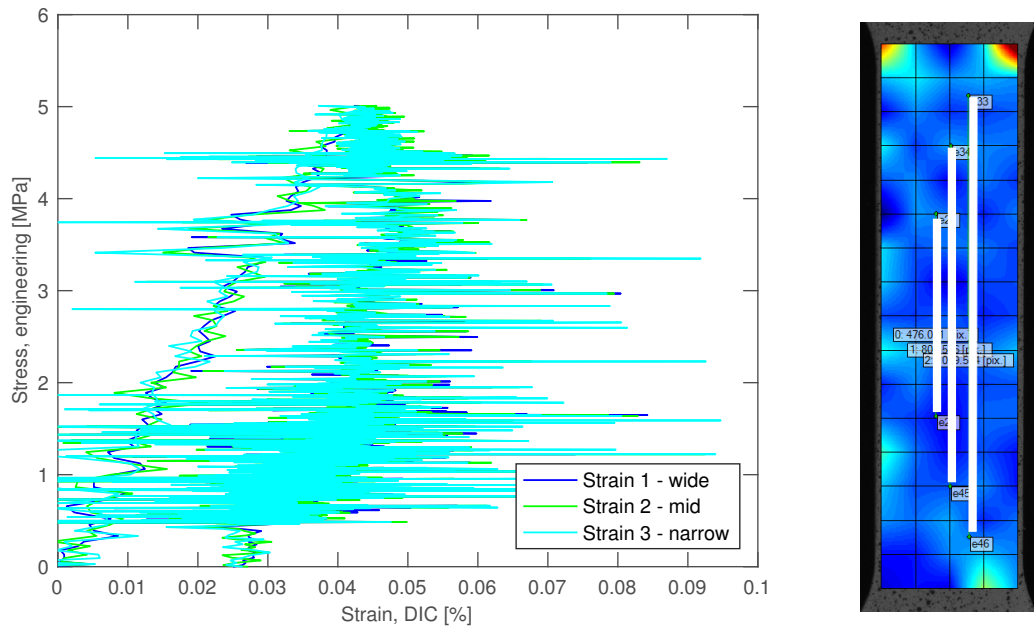**Figure E.33:** Creep test: stress vs time.

E.4 Relaxation Tests

Figure E.34: Relaxation test: $\sigma = 10\,\text{MPa}$, $\dot{\epsilon}$ = 1E-3 s^{-1}. Vector 1 wide were used as strain from DIC. Too few data points from unloading to obtain E-modulus.

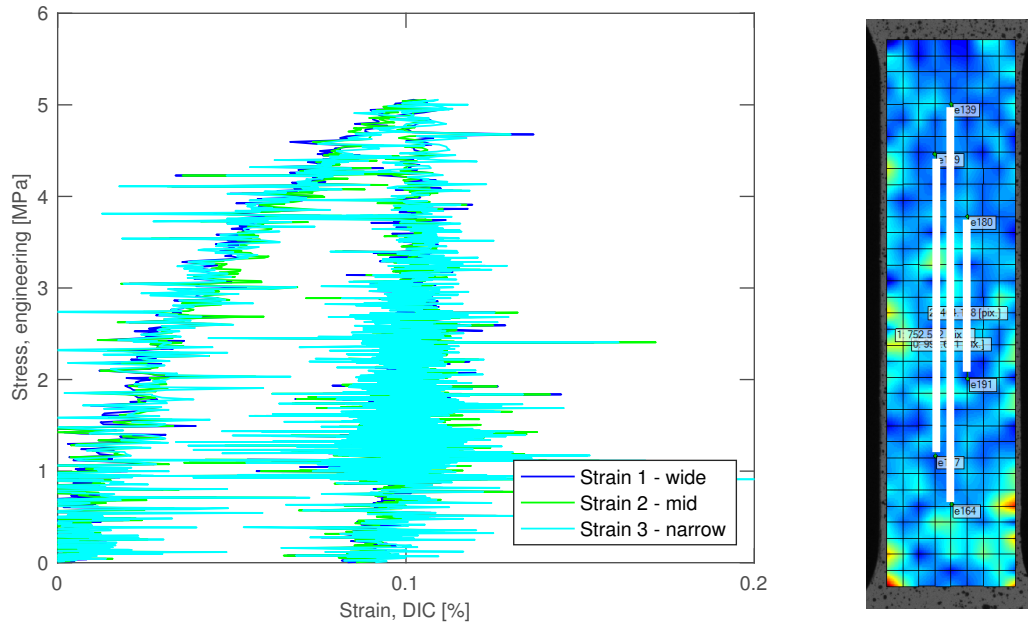**Figure E.35:** Relaxation test: $\sigma = 8\,\text{MPa}$, $\dot{\epsilon}$ = 1E-4 s^{-1}. Strain 2 - mid were used as strain from DIC.
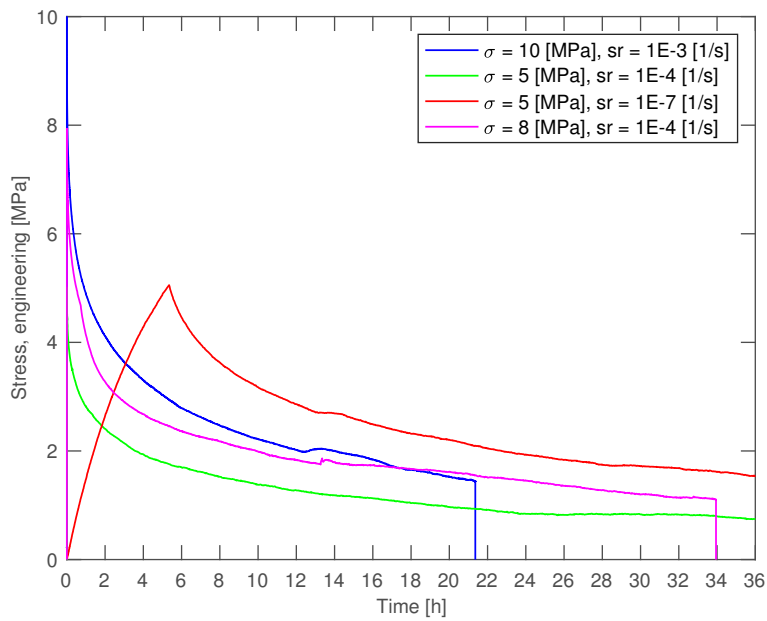
Figure E.36: Relaxation test: $\sigma = 5\,\text{MPa}$, $\dot{\epsilon} = 1\text{E-4 s}^{-1}$. Strain 1 - wide from figure E.37 were used as strain from DIC.
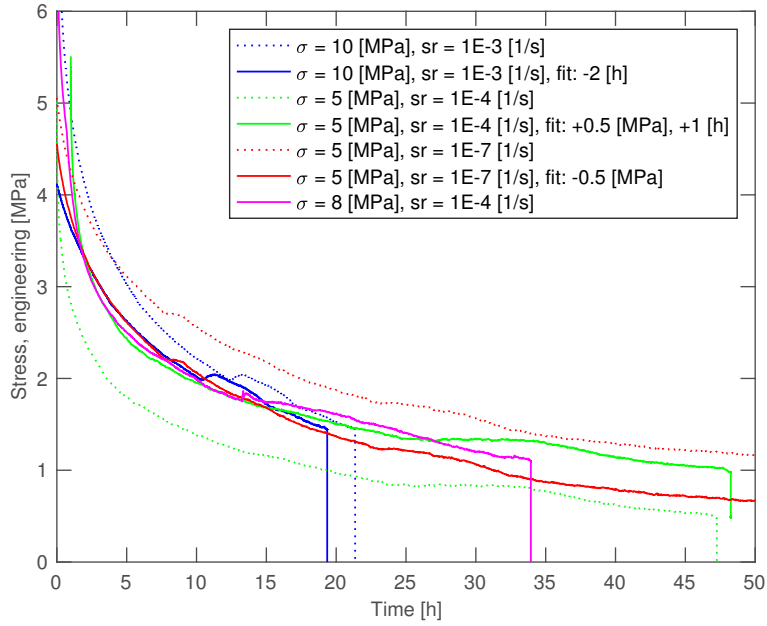

Figure E.37: Relaxation test: $\sigma = 5\,\text{MPa}$, $\dot{\epsilon} = 1\text{E-4 s}^{-1}$, large elements. Strain 1 - wide were used as strain from DIC.

Figure E.38: Relaxation test: $\sigma = 5\,\mathrm{MPa}$, $\dot{\epsilon} = 1\text{E-}7\,\mathrm{s}^{-1}$. Strain 1 - wide were used as strain from DIC.

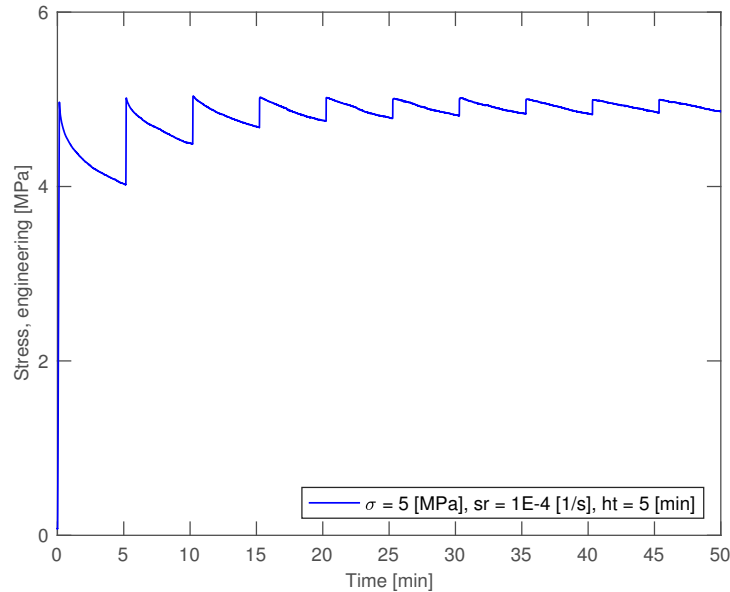**Figure E.39:** Relaxation test: Stress vs time, with preloading.

Figure E.40: Relaxation test: Stress vs time. Stippled line indicates the measured data, full line is the attempt of fitting to the $\sigma = 8\,\mathrm{MPa}$, $\dot{\epsilon} = 1\mathrm{E}\text{-}4\,\mathrm{s}^{-1}$ curve.

Relaxation tests show strong dependency on loading history. An attempt to find a trend and a general rule for how strain rate and loading impact the test was made in figure E.40. For this to be confirmed, several tests would have to be performed.
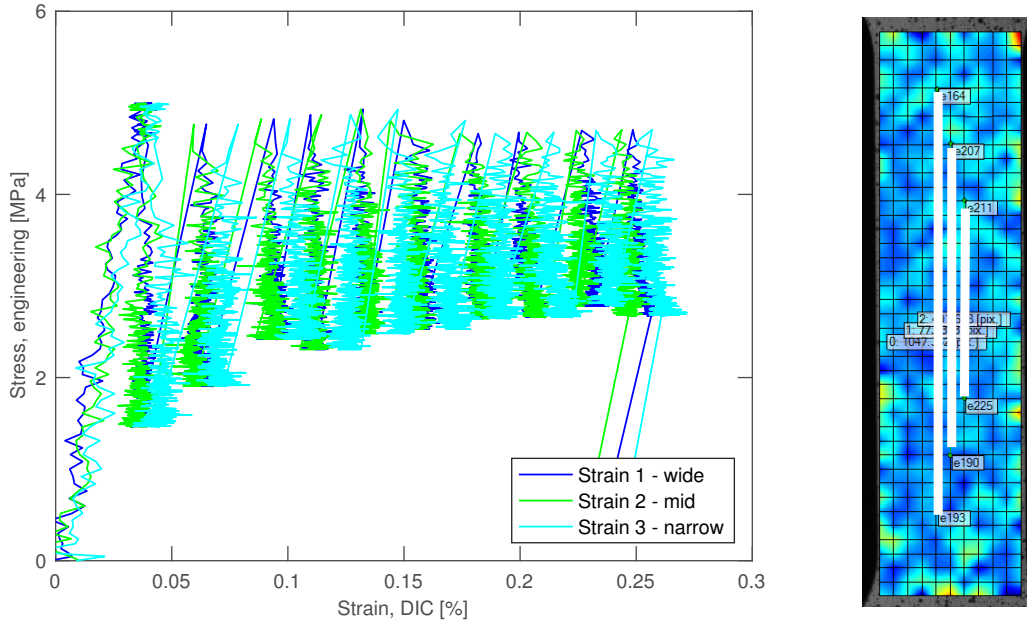
E.5 Cyclic Relaxation Tests

Unfortunately it was not possible to obtain strain from DIC due to error in the data output.

Figure E.41: Cyclic relaxation test: Stress vs time. $\sigma = 5\,\text{MPa}$, $\dot{\epsilon} = $ 1E-4 s^{-1}, ht = 5 min.
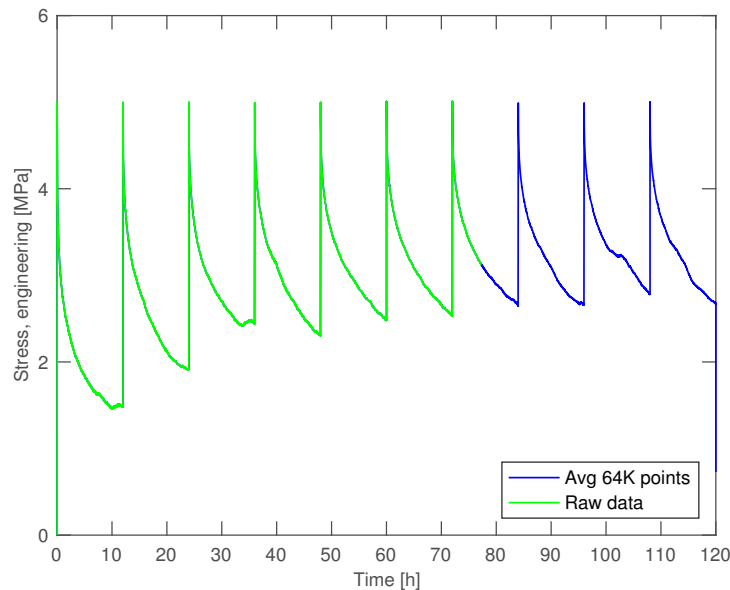
Figure E.42: Cyclic relaxation test: Stress vs time. $\sigma = 5\,\text{MPa}$, $\dot{\epsilon} = $ 1E-4 s^{-1}, ht = 12. 72500 data points were registered in the test machine, but it could only write 64000 to Excel. Therefore Excel made an average out of the data points. This did not affect the results.

Figure E.43: Cyclic relaxation test: Stress vs strain. $\sigma = 5\,\mathrm{MPa}$, $\dot{\epsilon} = $ 1E-4 s^{-1}, ht = 12. Strain 2 - mid was used for further comparison.

Figure E.44: Cyclic relaxation test: Stress vs strain. $\sigma = 5\,\mathrm{MPa}$, $\dot{\epsilon} = $ 1E-4 s^{-1}, ht = 12. eCorr and VIC compared, where VIC has much less noise in the results than eCorr vectors.
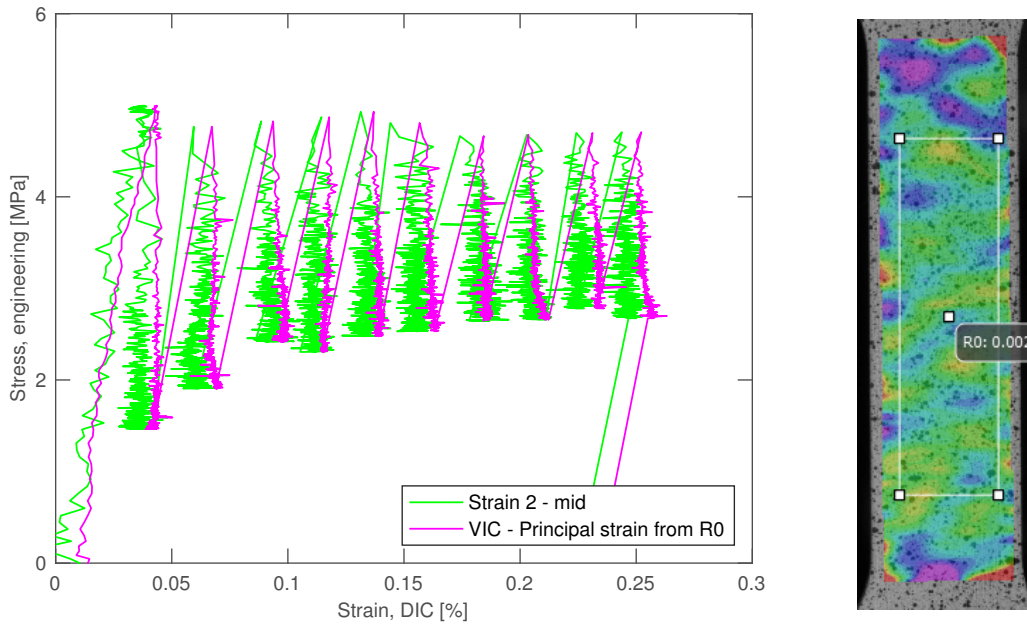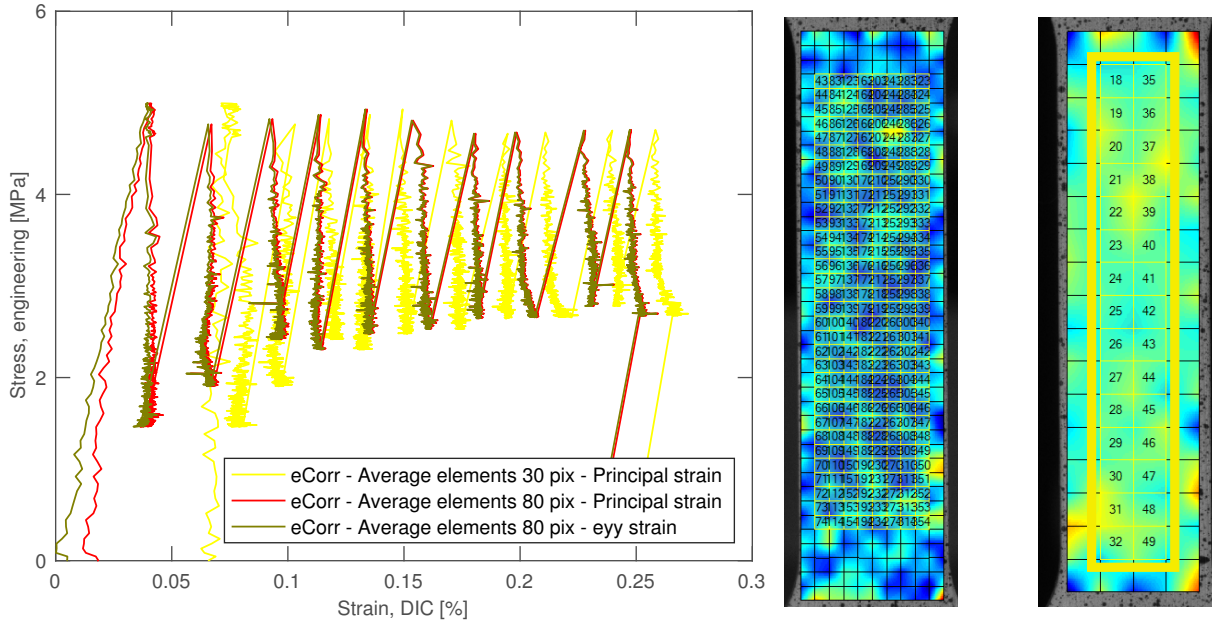
Figure E.45: Cyclic relaxation test: Stress vs strain. $\sigma = 5\,\text{MPa}$, $\dot{\epsilon} = 1\text{E-4 s}^{-1}$, ht = 12. An average of elements with 30 pixels and 80 pixels were compared. 80 pix logarithmic are used for further comparison.

Figure E.46: Cyclic relaxation test: Stress vs strain. $\sigma = 5\,\text{MPa}$, $\dot{\epsilon} = 1\text{E-4 s}^{-1}$, ht = 12. Average of longitudinal strain 80 pix elements were used as strain from DIC.
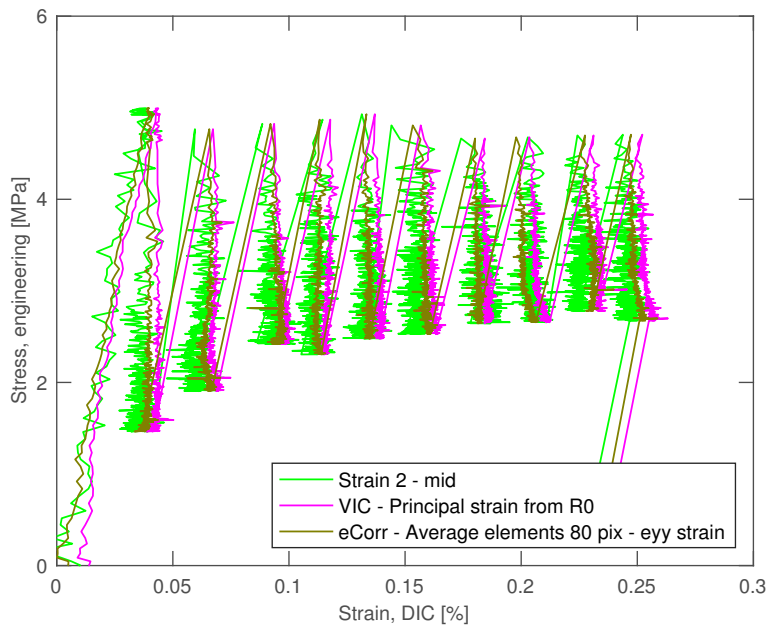
Figure E.47: Cyclic relaxation test: Stress vs strain. $\sigma = 5\,\text{MPa}$, $\dot{\epsilon} = $ 1E-4 s^{-1}, ht = 12. Stroke is scaled down with 0.6 due to geometry factor in the dog bone specimen (0.6 is found by trial and error).
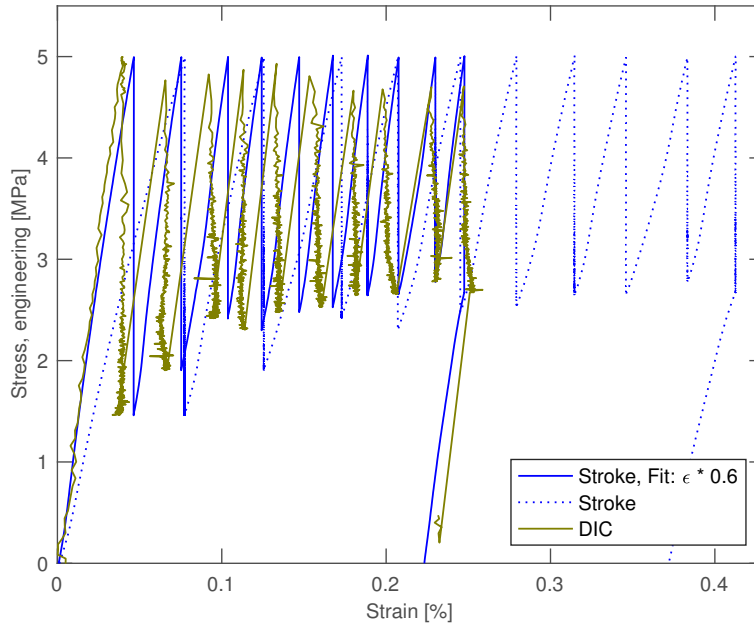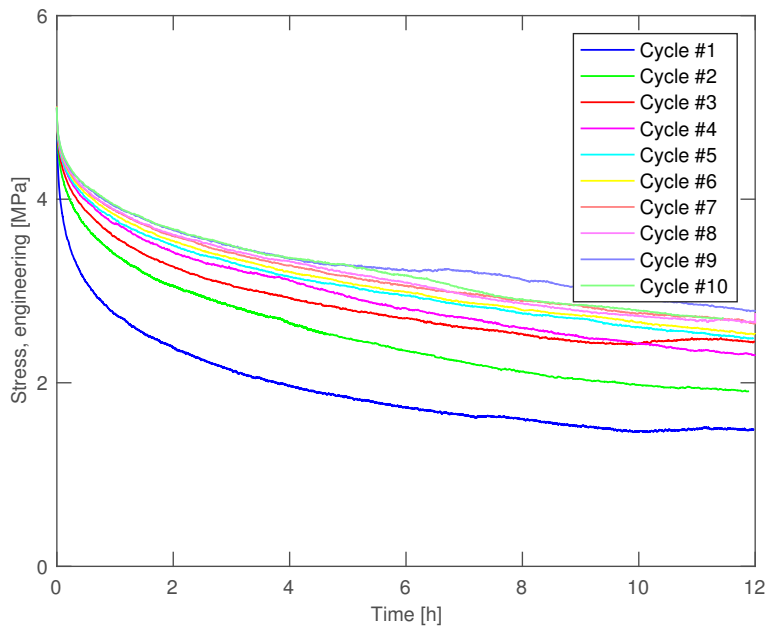

Figure E.48: Cyclic relaxation test: Stress vs time. $\sigma = 5\,\text{MPa}$, $\dot{\epsilon} = $ 1E-4 s^{-1}, ht = 12. Zeroed for each cycle.

E.6 Alternating Cyclic Relaxation Test

Figure E.49: Alternating cyclic relaxation test: Strain vs time. $\pm\sigma = 5\,\mathrm{MPa}$, $\dot{\epsilon} = 1\mathrm{E}\text{-}4\ \mathrm{s}^{-1}$, ht = 5 min. Average of longitudinal strain 50 pix elements were used as strain from DIC.
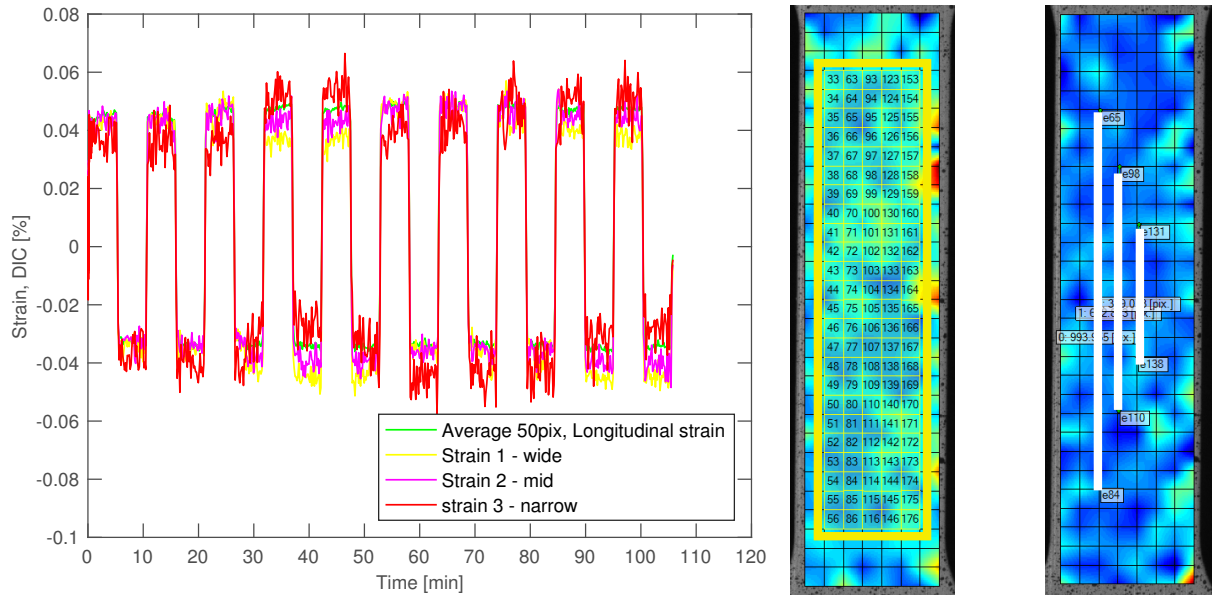

Figure E.50: Alternating cyclic relaxation test: Stress vs time. $\pm\sigma = 5\,\mathrm{MPa}$, $\dot{\epsilon} = 1\mathrm{E}\text{-}4\ \mathrm{s}^{-1}$, ht = 5 min.

Figure E.51: Alternating cyclic relaxation test: Strain vs time. $\pm\sigma = 5\,\mathrm{MPa}$, $\dot{\epsilon} = $ 1E-4 s^{-1}, ht = 5 min. Stroke is scaled down with 0.6 due to geometry factor in the dog bone specimen (0.6 is found by trial and error).

Figure E.52: Alternating cyclic relaxation test: Stress vs strain. $\pm\sigma = 5\,\mathrm{MPa}$, $\dot{\epsilon} = $ 1E-4 s^{-1}, ht = 5 min. Stroke is scaled down with 0.6 due to geometry factor in the dog bone specimen (0.6 is found by trial and error).
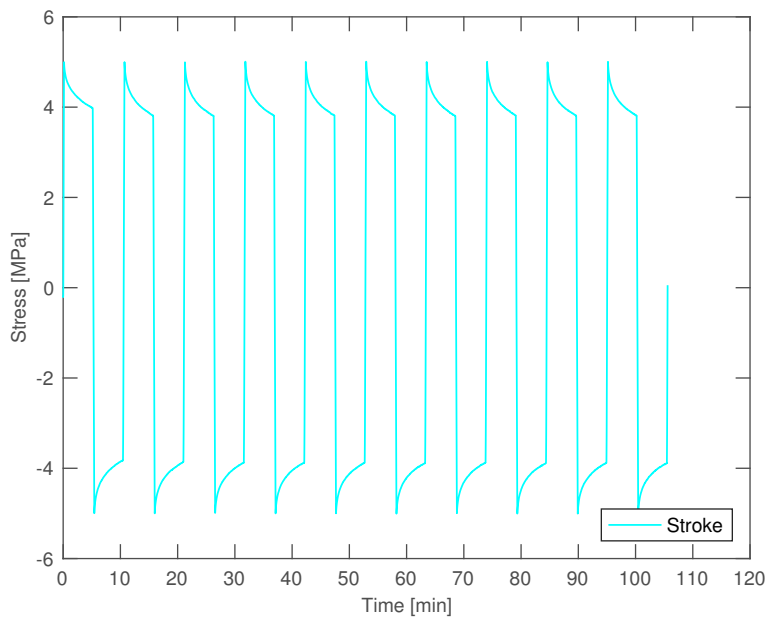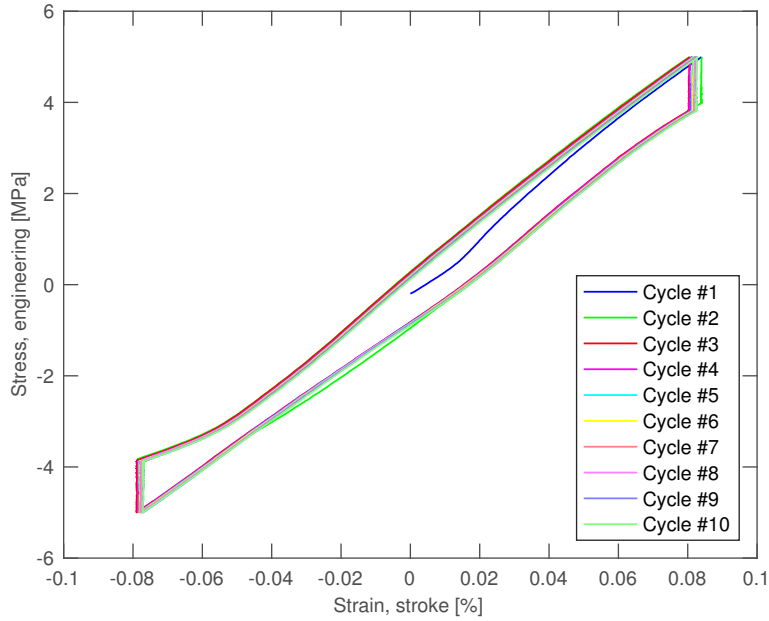
Figure E.53: Alternating cyclic relaxation test: Stress vs stroke. $\pm\sigma = 5\,\text{MPa}$, $\dot{\epsilon} = $ 1E-4 s^{-1}, ht = 5 min.
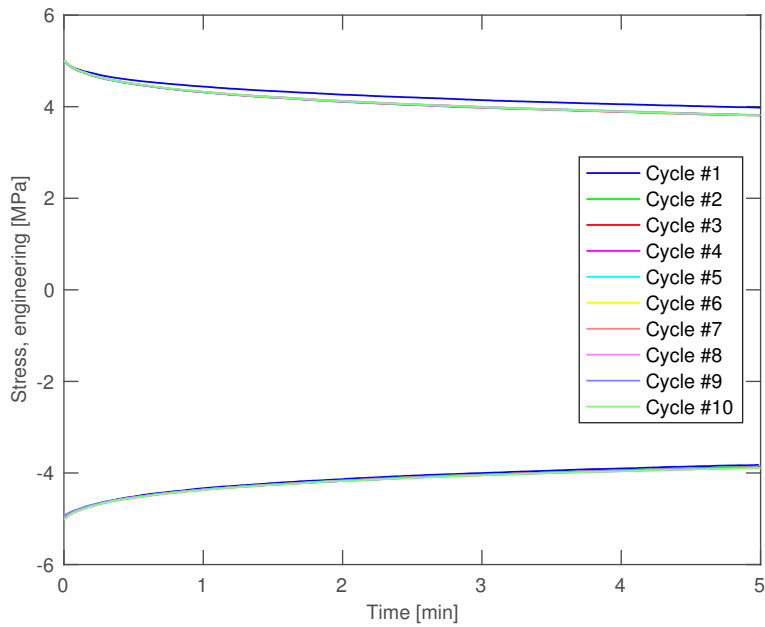
Figure E.54: Alternating cyclic relaxation test: Strain vs time. $\pm\sigma = 5\,\text{MPa}$, $\dot{\epsilon} = $ 1E-4 s^{-1}, ht = 5 min. Zeroed for each cycle.
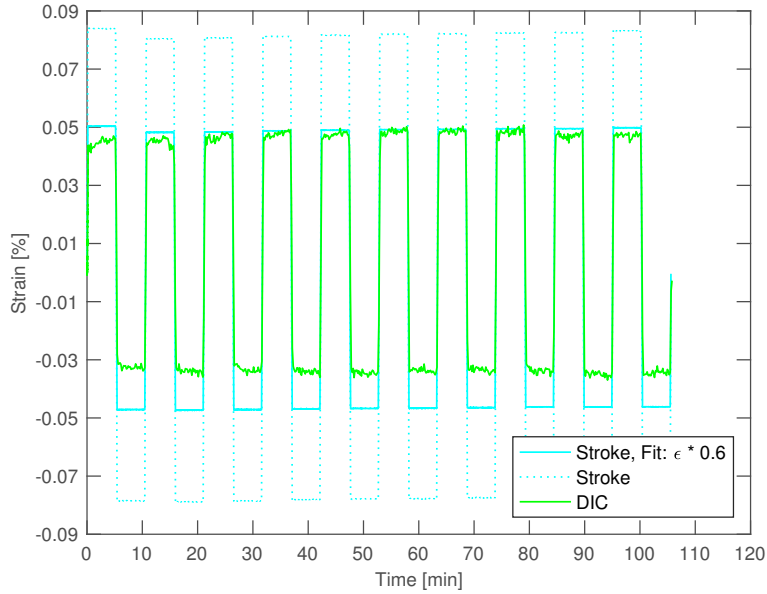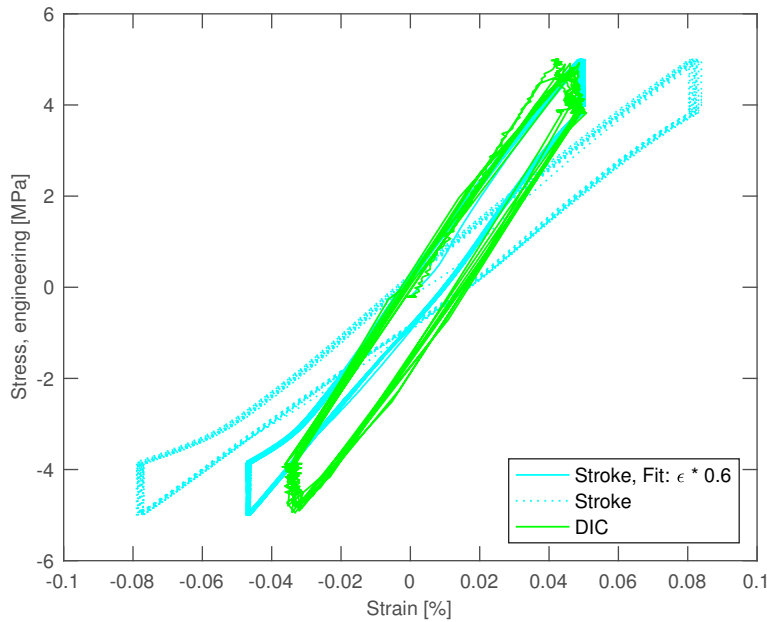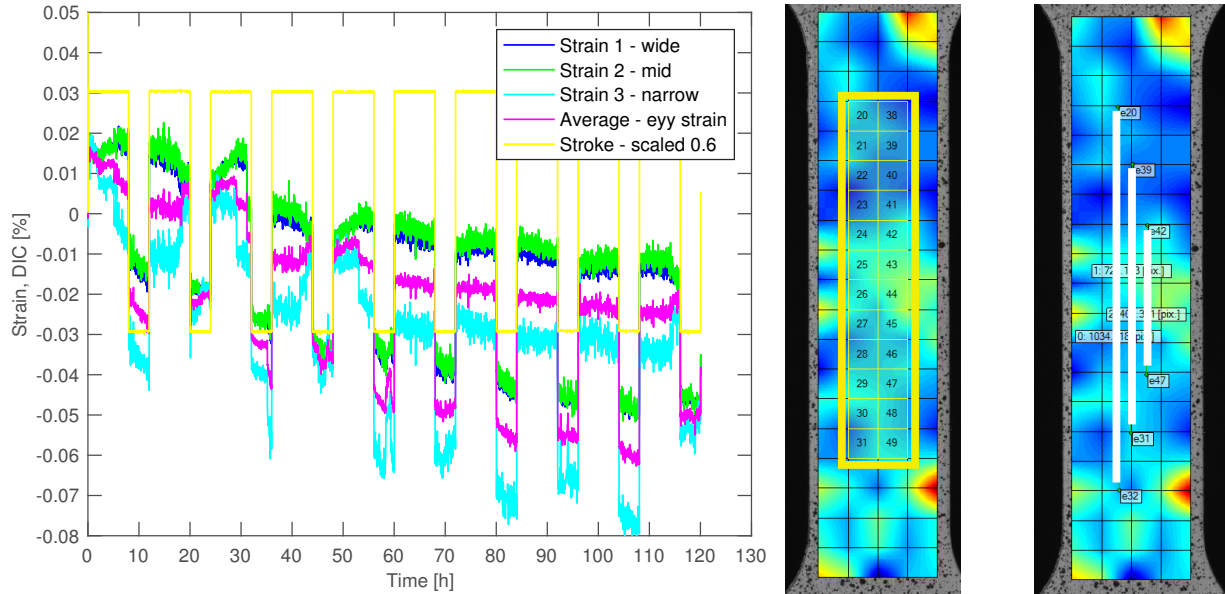
Figure E.55: Alternating cyclic relaxation test: Strain vs time. $\pm\epsilon_{stroke}$ = 0.03 %, $\dot{\epsilon}$ = 1E-4 s^{-1}, ht = 8 - 4. No greyscale correction. The drops in strain observed at 29 h, 35 h, 54 h etc. is due to lights switched off in the laboratory.
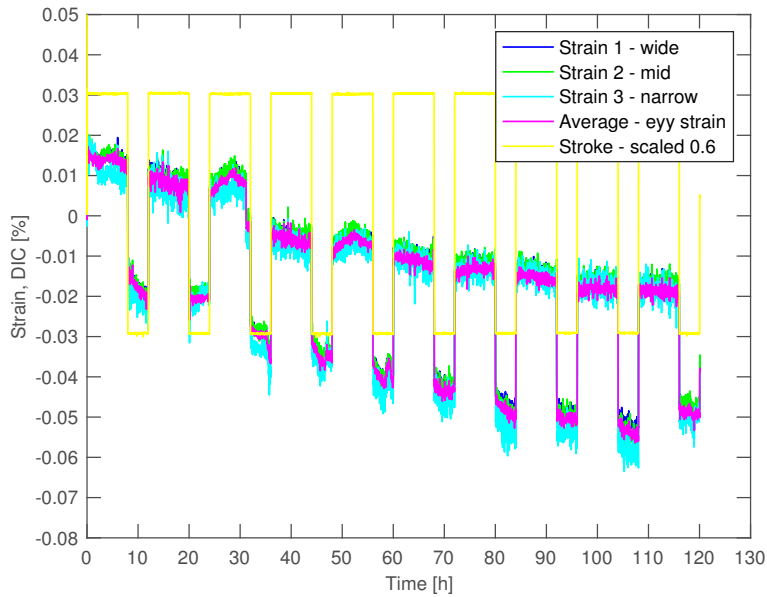
Figure E.56: Alternating cyclic relaxation test: Strain vs time. $\pm\epsilon_{stroke}$ = 0.03 %, $\dot{\epsilon}$ = 1E-4 s^{-1}, ht = 8 - 4. With greyscale correction. Longitudinal logarithmic are used as strain from DIC.
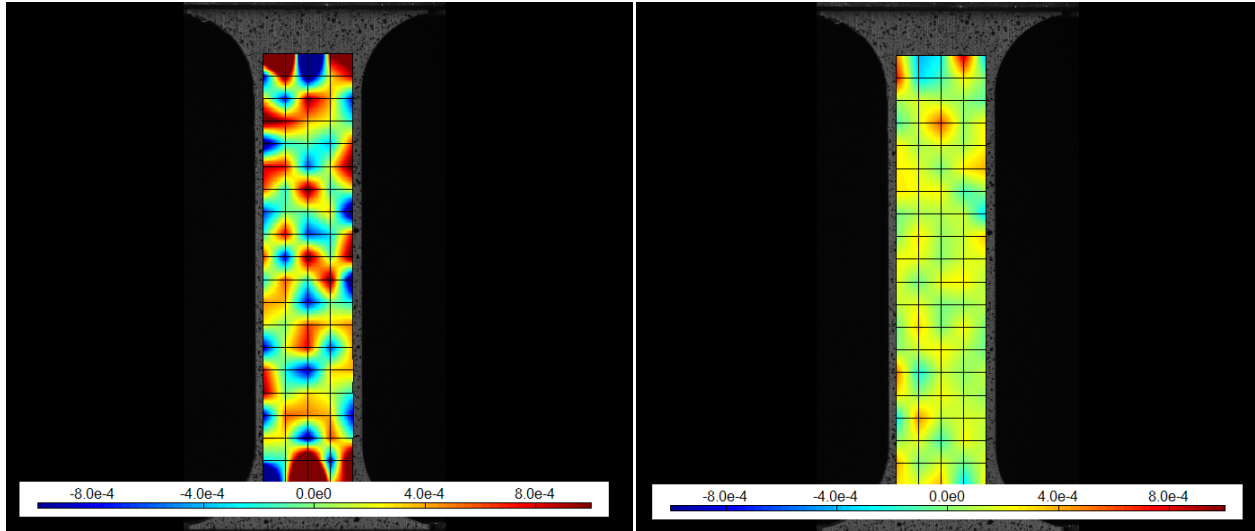
Figure E.57: Alternating cyclic relaxation test: Strain vs time. $\pm\epsilon_{stroke}$ = 0.03 %, $\dot{\epsilon}$ = 1E-4 s^{-1}, ht = 8 - 4. Localization after 6.5 h, greyscale ON to the left and OFF to the right. The hot spots are the same, but they have been smoothed out. Further investigation should reveal if this is due to errors in the DIC or actual behavior in the material.
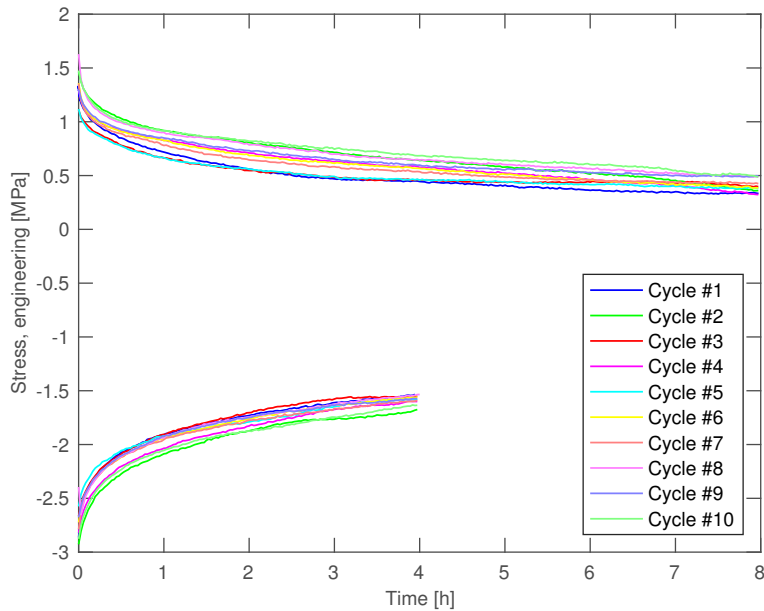
Figure E.58: Alternating cyclic relaxation test: Stress vs time. $\pm\epsilon_{stroke}$ = 0.03 %, $\dot{\epsilon}$ = 1E-4 s^{-1}, ht = 8 - 4. Zeroed for each cycle.
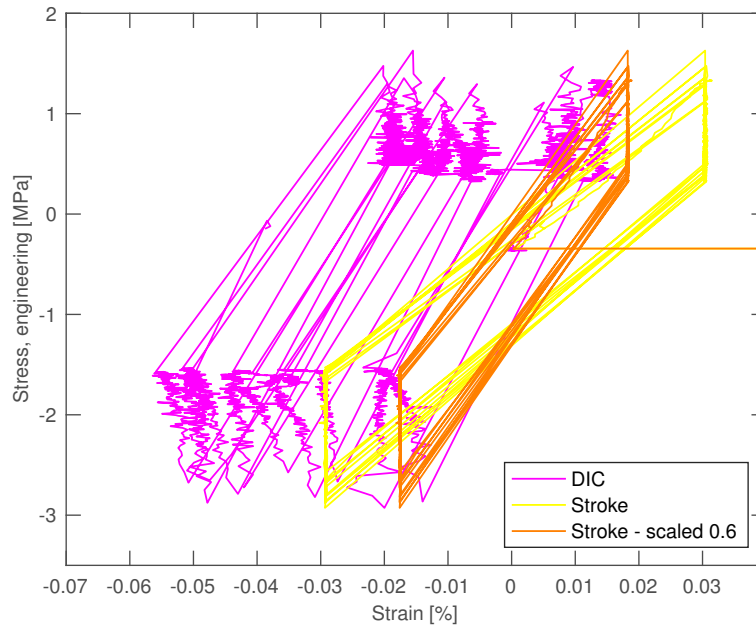
Figure E.59: Alternating cyclic relaxation test: Stress vs strain. $\pm\epsilon_{stroke} = 0.03\,\%$, $\dot{\epsilon} = $ 1E-4 s^{-1}, ht = 8 - 4.

E.7 Hysteresis Loops
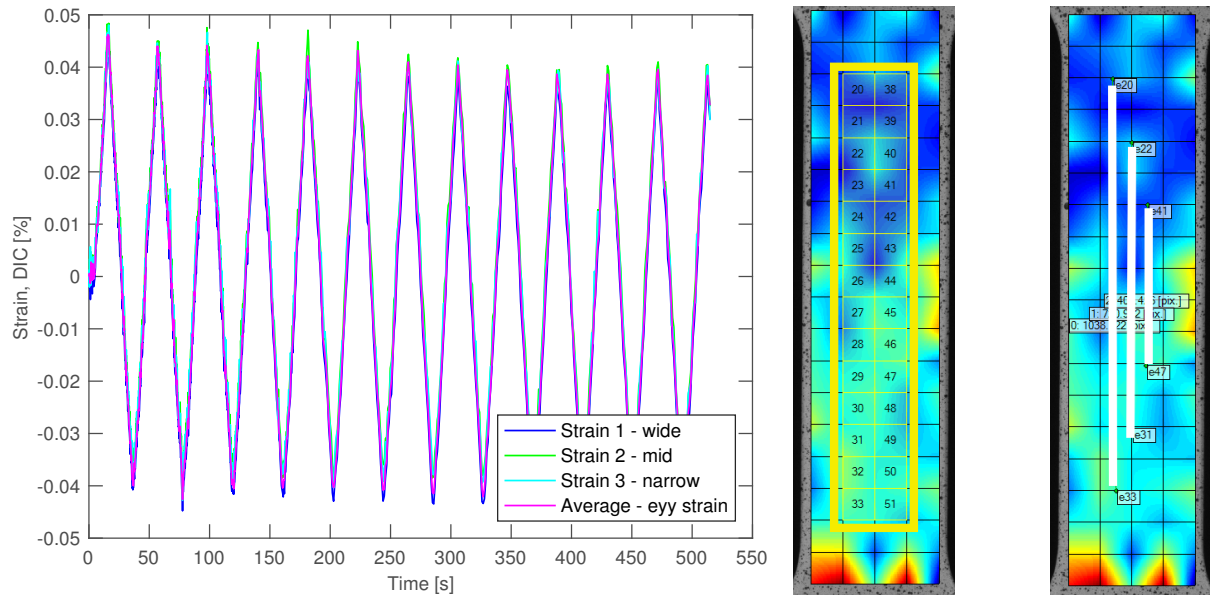
Figure E.60: Hysteresis loop: Strain vs time. $\pm\sigma = 5\,\text{MPa}$, $\dot{\epsilon} = \text{1E-4 s}^{-1}$. Average of longitudinal strain were used as strain from DIC.
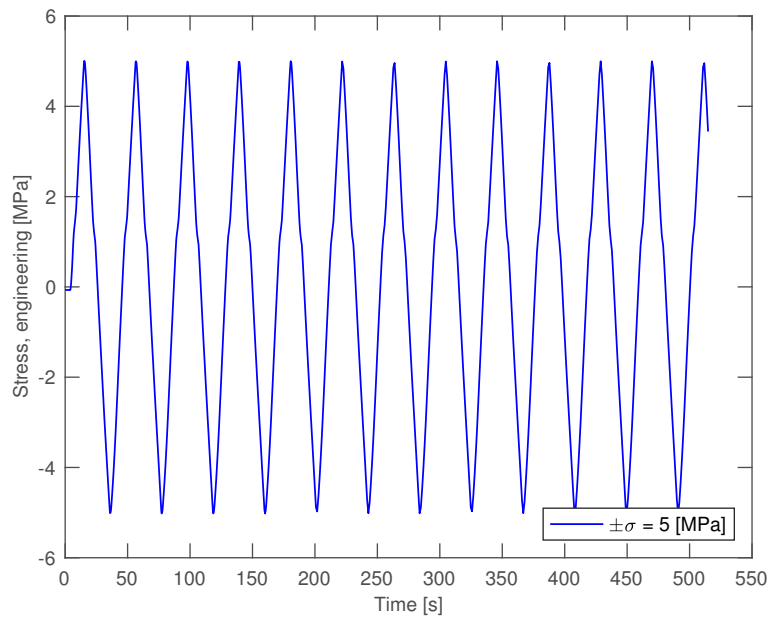
Figure E.61: Hysteresis loop: Stress vs time. $\pm\sigma = 5\,\text{MPa}$, $\dot{\epsilon} = \text{1E-4 s}^{-1}$.
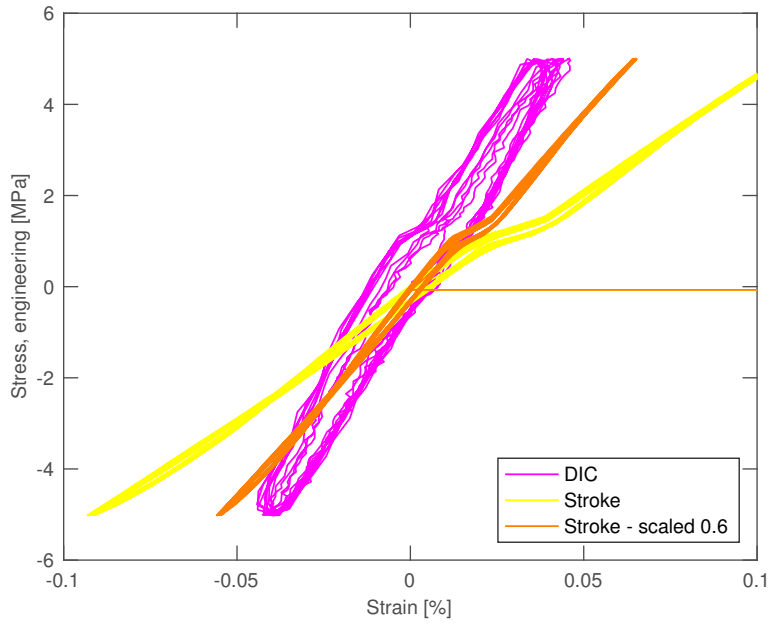
Figure E.62: Hysteresis loop: Strain vs strain. $\pm\sigma = 5\,\mathrm{MPa}$, $\dot{\epsilon} = 1\mathrm{E}\text{-}4\,\mathrm{s}^{-1}$. Average of longitudinal strain were used as strain from DIC.
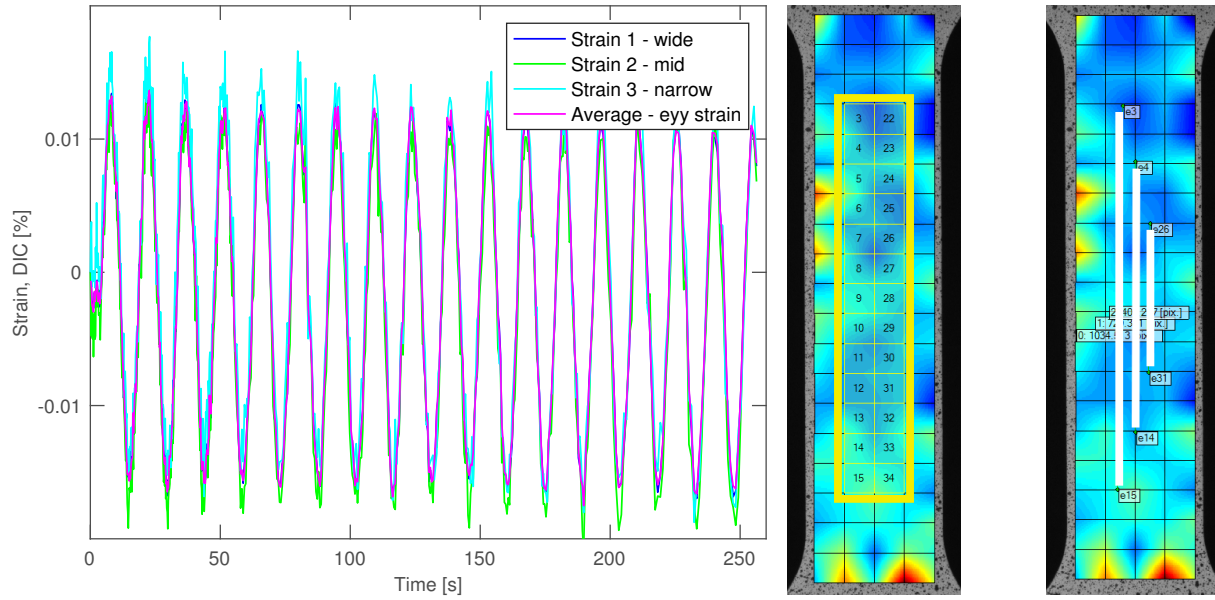
Figure E.63: Hysteresis loop: Strain vs time. $\pm\epsilon = 0.03\,\%$, $\dot{\epsilon} = $ 1E-4 s^{-1}. Average of longitudinal strain were used as strain from DIC.
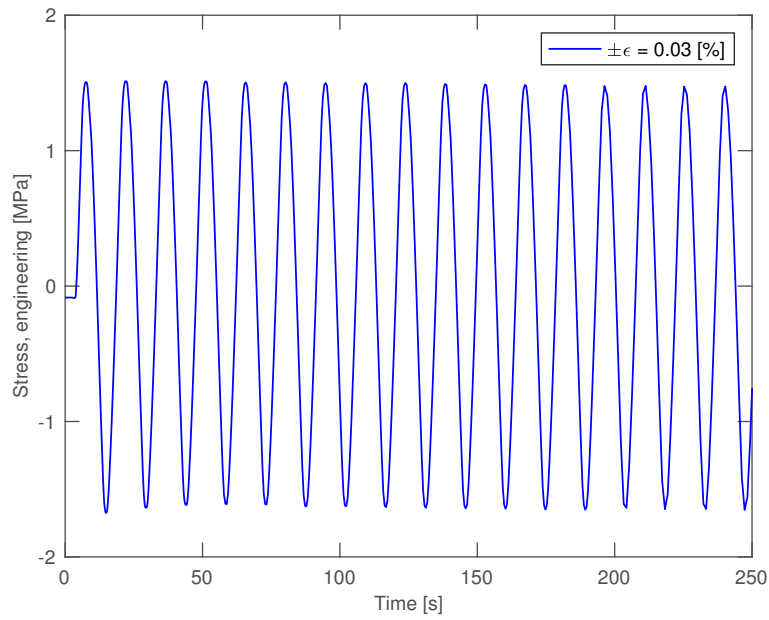
Figure E.64: Hysteresis loop: Stress vs time. $\pm\epsilon = 0.03\,\%$, $\dot{\epsilon} = $ 1E-4 s^{-1}. Average of longitudinal strain were used as strain from DIC.
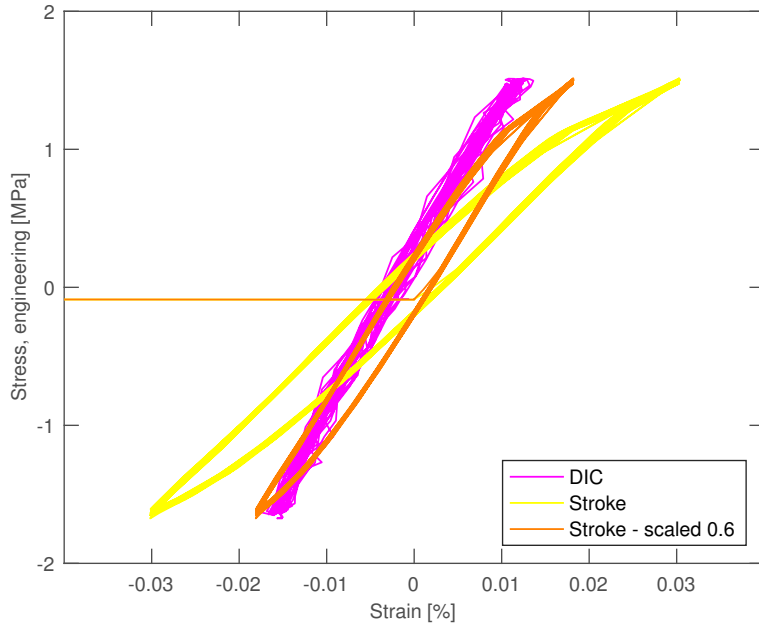
Figure E.65: Hysteresis loop: Stress vs strain. $\pm\epsilon = 0.03\,\%$, $\dot{\epsilon} = 1\text{E-4 s}^{-1}$. Average of longitudinal strain were used as strain from DIC.

APPENDIX F

Risk Analysis

This page is intentionally left blank.

NTNU ▢ HMS	Kartlegging av risikofylt aktivitet		Dato:	25.01.17	Utarbeidet av HMS-avd.	Nummer HMSRV2601	Dato 22.03.2011	
					Godkjent av Rektor	Erstatter	01.12.2006	

Enhet: MTP, Verksted MTI/Lab – SINTEF

Linjeleder: Torgeir Welo

Deltakere ved kartleggingen (m/ funksjon): Gaute Fotland (Student),
(Ansv. veileder, student, evt. medveiledere, evt. andre m. kompetanse Vidar Hjelmen (Lab ansvarlig)
Odd Magne Akselsen (Veileder)
Antonio Alvaro (Medveileder)

Kort beskrivelse av hovedaktivitet/hovedprosess: Strekkprøving av bly

Er oppgaven rent teoretisk? (JA/NEI): NEI «JA» betyr at veileder innestår for at oppgaven ikke inneholder noen aktiviteter som krever
risikovurdering. Dersom «JA»: Beskriv kort aktiviteten i kartleggingskjemaet under. Risikovurdering trenger ikke å fylles ut.

Signaturer: *Ansvarlig veileder:* [signature] *Student:* [signature]

ID nr.	Aktivitet/prosess	Ansvarlig	Eksisterende dokumentasjon	Eksisterende sikringstiltak	Lov, forskrift o.l.	Kommentar
01	Strekkprøving og utmattingstesting av bly	Vidar Hjelmen	Instruks for arbeid med blylegering - SINTEF, Risikovurdering arbeid med bly - SINTEF	Avgrense soner, verneutstyr	-	-
02	Strekkprøving og utmattingstesting av bly	Vidar Hjelmen	Instruks for arbeid med blylegering - SINTEF, Risikovurdering arbeid med bly - SINTEF	Avgrense soner, verneutstyr	-	-
03	Strekkprøving og utmattingstesting av bly	Vidar Hjelmen	Instruks for arbeid med blylegering - SINTEF, Risikovurdering arbeid med bly - SINTEF	Avgrense soner, verneutstyr	-	-
04	Strekkprøving og utmattingstesting av bly	Vidar Hjelmen	Instruks for arbeid med blylegering - SINTEF, Risikovurdering arbeid med bly - SINTEF	Avgrense soner, verneutstyr	-	-

138

	Utarbeidet av	Nummer	Dato
	HMS-avd.	HMSRV2601	22.03.2011
	Godkjent av		Erstatter
	Rektor		01.12.2006

Risikovurdering

Enhet: MTP, Verksted MTI/Lab – SINTEF
Linjeleder: Torgeir Welo

Dato: 25.01.17

Deltakere ved kartleggingen (m/ funksjon):
(Ansv. veileder, student, evt. medveiledere, evt. andre m. kompetanse

Gaute Fotland (Student),
Vidar Hjelmen (Lab ansvarlig)
Odd Magne Akselsen (Veileder)
Antonio Alvaro (Medveileder)

Risikovurderingen gjelder hovedaktivitet: Masteroppgave, student Gaute Fotland.

Signaturer: *Ansvarlig veileder:* _____ *Student:* Gaute Fotland

ID nr	Aktivitet fra kartleggings-skjemaet	Mulig uønsket hendelse/belastning	Vurdering av sannsynlighet (1-5)	Vurdering av konsekvens: Menneske (A-E)	Ytre miljø (A-E)	Øk/materiell (A-E)	Om-dømme (A-E)	Risiko-Verdi (menneske)	Kommentarer/status Forslag til tiltak
01	Strekkprøving og utmattingstesting av bly	Eksponering over lengre tid.	2	D2			C1	D2	Benytt briller og hansker ved håndtering, hold blyprøvene innenfor soner
02	Strekkprøving og utmattingstesting av bly	Akutt forgiftning	2	E2			D1	E1	Benytt verneutstyr, soner, merking, forbud mat/drikke/snus
03	Strekkprøving og utmattingstesting av bly	Utilsiktet eksponering via hud eller svelg	2	D2			D1	D2	Soner, rengjøring av arbeidspersonell etter fullført jobb, merking.
04	Strekkprøving og utmattingstesting av bly	Utslipp av bly til ytre miljø	3	A1	A1	A1	A4	A1	Benytt briller og hansker ved håndtering, hold blyprøvene innenfor soner

NTNU		Risikovurdering	Utarbeidet av	Nummer	Dato
HMS			HMS-avd.	HMSRV2601	22.03.2011
			Godkjent av		Erstatter
			Rektor		01.12.2006

Sannsynlighet vurderes etter følgende kriterier:

Svært liten 1	Liten 2	Middels 3	Stor 4	Svært stor 5
1 gang pr 50 år eller sjeldnere	1 gang pr 10 år eller sjeldnere	1 gang pr år eller sjeldnere	1 gang pr måned eller sjeldnere	Skjer ukentlig

Konsekvens vurderes etter følgende kriterier:

Gradering	Menneske	Ytre miljø Vann, jord og luft	Øk/materiell	Omdømme
E Svært Alvorlig	Død	Svært langvarig og ikke reversibel skade	Drifts- eller aktivitetsstans >1 år.	Troverdighet og respekt betydelig og varig svekket
D Alvorlig	Alvorlig personskade. Mulig uførhet.	Langvarig skade. Lang restitusjonstid	Driftsstans > ½ år Aktivitetsstans i opp til 1 år	Troverdighet og respekt betydelig svekket
C Moderat	Alvorlig personskade.	Mindre skade og lang restitusjonstid	Drifts- eller aktivitetsstans < 1 mnd	Troverdighet og respekt svekket
B Liten	Skade som krever medisinsk behandling	Mindre skade og kort restitusjonstid	Drifts- eller aktivitetsstans < 1uke	Negativ påvirkning på troverdighet og respekt
A Svært liten	Skade som krever førstehjelp	Ubetydelig skade og kort restitusjonstid	Drifts- eller aktivitetsstans < 1dag	Liten påvirkning på troverdighet og respekt

Risikoverdi = Sannsynlighet x Konsekvens

Beregn risikoverdi for Menneske. Enheten vurderer selv om de i tillegg vil beregne risikoverdi for Ytre miljø, Økonomi/materiell og Omdømme. I så fall beregnes disse hver for seg.

Til kolonnen "Kommentarer/status, forslag til forebyggende og korrigerende tiltak":

Tiltak kan påvirke både sannsynlighet og konsekvens. Prioriter tiltak som kan forhindre at hendelsen inntreffer, dvs. sannsynlighetsreduserende tiltak foran skjerpet beredskap, dvs. konsekvensreduserende tiltak.

Risikomatrise

	utarbeidet av	Nummer	Dato
	HMS-avd.	HMSRV2604	08.03.2010
	godkjent av		Erstatter
	Rektor		09.02.2010

MATRISE FOR RISIKOVURDERINGER ved NTNU

KONSEKVENS	Svært liten	Liten	Middels	Stor	Svært stor
Svært alvorlig	E1	E2	E3	E4	E5
Alvorlig	D1	D2	D3	D4	D5
Moderat	C1	C2	C3	C4	C5
Liten	B1	B2	B3	B4	B5
Svært liten	A1	A2	A3	A4	A5

SANNSYNLIGHET

Prinsipp over akseptkriterium. Forklaring av fargene som er brukt i risikomatrisen.

Farge	Beskrivelse
Rød	Uakseptabel risiko. Tiltak skal gjennomføres for å redusere risikoen.
Gul	Vurderingsområde. Tiltak skal vurderes.
Grønn	Akseptabel risiko. Tiltak kan vurderes ut fra andre hensyn.

INSTRUKS FOR ARBEID MED BLYLEGERING

Krav	Tiltak/vurdering
- Hvis mulig skal det benyttes lukkede systemer for prosesser der kreftfremkallende eller arvestoffskadelige kjemikalier brukes	Det forventes minimal støving fra maskineringen av prøvene, og ingen fra testingen. Det lar seg også vanskelig gjøre å benytte lukkede systemer. En velger derfor heller å operere med tydelig avgrensede soner.
- En skal alltid sørge for at eksponeringen blir så lav som overhode mulig	Det involveres ikke flere i arbeidet enn nødvendig og en forsøker etter beste evne å sette av sammenhengende perioder for arbeidet.
- Det skal utarbeides rutiner for: 1. Arbeidsmetode 2. Oppbevaring, merking, håndtering og transport 3. Behandling av søl og avfall 4. Renhold av arbeidslokalet 5. Bruk av arbeidstøy og PVU 6. Spesielle krav til innredning av arbeidssted	1. Arbeidsmetode følger arbeidsprosedyre men med ekstra fokus på HMS mtp. bly, kadmium og tellurium. 2. Eget, avgrenset og merket område for oppbevaring av prøver og materiale. Av merkingen skal det komme tydelig frem hva prøvene/materialet består av, faremomenter og påkrevd verneutstyr ved håndtering. Transport utføres av informert og opplært personell. 3. Søl og avfall håndteres av arbeidspersonell, og avhendes til avfallsdunk (med lokk) dedikert til avfall med bly-rester. Avfall leveres videre til Børstad. 4. Renhold av arbeidslokalet gjøres av arbeidspersonell etter endt arbeid. Utstyr som brukes til rengjøring av kontaminert område skal merkes og oppbevares i "bly-sonen". Utstyr skal ikke brukes utenfor området. Det er ikke tillatt å bruke støvsuger til rengjøring, og heller ikke væsker. Avfall kastes i egen avfallsdunk. Rengjøringsutstyr kastes i egen avfallsdunk dersom det må byttes og alltid når blyarbeidet er avsluttet (når kontaminert sone er rengjort og før det er åpnet for ordinært arbeid) NTNUs driftspersonell skal ikke rengjøre i "bly-sonene". 5. Det skal i tillegg til ordinært verneutstyr benyttes laboratoriefrakk/kjeledress, skotrekk og hansker – som ikke under noen omstendigheter skal benyttes utenfor "bly-sonen". Laboratoriefrakk/kjeledress oppbevares i "bly-sonen", skotrekk og hansker kastes i egen avfallsdunk etter bruk. Laboratoriefrakk/kjeledress kastes når blyarbeidet er avsluttet (når kontaminert sone er rengjort og før det er åpnet for ordinært arbeid) 6. Arbeidsstedet, "bly-sonen", skal tydelig merkes opp med gulvteip eller sperrebånd og skilting. Kun nødvendig utstyr skal oppbevares i arbeidsområdet.
- Arbeidstaker skal lese sikkerhetsdatablad før et kjemikalie tas i bruk	Det holdes et obligatorisk informasjonsmøte med fokus på HMS hvor en gjennomgår faremomenter, bruken av verneutstyr og lignende.

- Registrere eksponering i et eksponeringsregister	Med eksponering menes alt arbeid med. Prosjektleder sørger for at hver enkelt arbeidstaker registrerer eksponering i sitt eksponeringsregister, og sender dette inn til HR for oppbevaring.
- Krav til risikovurdering ivaretas	Se risikovurdering.
- Kunne dokumentere at arbeidsatmosfæren er på et fult forsvarlig nivå	Arbeidsatmosfæren overvåkes, kartlegges og dokumenteres med regelmessige målinger av kyndig personell.
- Arbeidstakere som er utsatt for farlige kjemikalier skal gjennomgå helseundersøkelser - Arbeidstakere som skal arbeide med bly skal gjennomgå helseundersøkelser jevnlig	Arbeidstakere gjennomgår klinisk helseundersøkelse og blodprøvetaking jfr. Forskrift om utførelse av arbeid.
- Kun nødvendig personell får tilgang til lokaler der det benyttes kreftfremkallende og arvestoffskadelige stoffer - Lokalet er tydelig merket med advarsel- og sikkerhetsskilting	Arbeidsstedet, "bly-sonen", skal tydelig merkes opp med gulvteip, sperringer og skilting. Kun nødvendig personell får lov til å oppholde seg her – dette kommer tydelig frem av merking. Romkort revideres slik at de informerer om bruken av kreftfremkallende og arvestoffskadelige materialer.
- Nødvendig verneutstyr er tilgjengelig	Hver enkelt får utdelt egen laboratoriefrakk/kjeledress. Skotrekk og hansker står tilgjengelig ved inngang til "bly-sonen".
- Det er tilgjengelige skap slik at privat tøy og personlig verneutstyr blir oppbevart atskilt	Laboratoriefrakker/kjeledresser oppbevares på personlig knagg i "bly-sonen".
- Det skal ikke benyttes resirkulering av luft i lokaler der kreftfremkallende kjemikalier benyttes	Det benyttes ikke resirkulering av luft.

Enhet: Materialers Integritet og Sveising
Aktivitet: Arbeid med blylegering
Sted / bygning / rom / rigg / utstyr: Verksted MTl/Lab

Dato: 2016-04-11
Deltagere: Bård Nyhus, Benedicte Adelheide, Elise Midthun
Linjeleder: Magnus Eriksson

Id	Delaktivitet	Mulig uønsket hendelse	Eksisterende barrierer	Risikoverdi med eksisterende tiltak				Nye barrierer / risikoreduserende tiltak (handlingsplan)	Risikoverdi med nye tiltak				Ansvarlig Frist	Status
				Menneske	Ytre miljø	Omdømme	Økonomi / materiell		Menneske	Ytre miljø	Omdømme	Økonomi / materiell		
1	Maskinering og testing av ekstruderte blyrør	Arbeidspersonell blir overeksponert for lengre tid over for bly, kadmium eller tellurium						Jfr. *Forskrift om utførelse av arbeid* tas det blodprøver og luftprøver jevnlig for å overvåke den enkeltes eksponering.Eksponering registreres i eksponeringsregister. Arbeidspersonell og øvrig personale informeres om aktiviteten og dens faremomenter. Det innføres avgrensede soner for arbeidet, med krav egne krav til bekledning, avfallshåndtering, rengjøring og hygiene. Soner, områder og prøver merkes tydelig. Det innføres forbud mot mat/drikke/snus i aktuelle soner.	D2		C1			
2	Maskinering og testing av ekstruderte blyrør	Arbeidspersonell eller annet personell blir akutt forgiftet av bly, kadmium eller tellurium						Arbeidspersonell og øvrig personale informeres om aktiviteten og dens faremomenter. Det innføres soner med klare HMS-krav. Prøver og materiale merkes tydelig og med info og advarsel. Obligatorisk informasjonsmøte angående HMS for arbeidspersonell. Det innføres forbud mot mat/drikke/snus. Renhold foretas av arbeidspersonell, ikke renholdspersonal.	E1		D1			
3	Maskinering og testing av ekstruderte blyrør	Utilsiktet eksponering via hud eller svelg						Arbeid begrenses til avgrensede soner. Arbeidsområde skal rengjøres av arbeidspersonell etter endt arbeid. Prøver og soner merkes tydelig med advarsel. Krav om å bruke hansker ved håndtering, og å vaske hendene etterpå.	D2		D1			
4	Maskinering og testing av ekstruderte blyrør	Utslipp av bly til ytre miljø						Avfall samles i egne avfallsduker og leveres til Børsta. Dette gjelder også kontaminert kjølevæske dersom det må benyttes.	A1	A1	A4	A1		
5	Maskinering og testing av ekstruderte blyrør							Se også instruks for arbeid med bly.						

144